The Dissertation Committee for Enrico Rossi

certifies that this is the approved version of the following dissertation:

Fluctuations and Dissipation of Collective Dynamics in Spin and Pseudospin Ferromagnets

Committee:

Allan H. MacDonald, Supervisor

Richard Fitzpatrick

John T. Markert

Jack B. Swift

Brian A. Korgel

Fluctuations and Dissipation of Collective Dynamics in Spin and Pseudospin Ferromagnets

by

Enrico Rossi, B.A.; M.S.

Dissertation

Presented to the Faculty of the Graduate School of

The University of Texas at Austin

in Partial Fulfillment

of the Requirements

for the Degree of

Doctor of Philosophy

The University of Texas at Austin

August 2005

Acknowledgments

The last three and half years have been the most intellectually fulfilling years of my career as a physics student. In this short period I learned more about physics than in all the years before. For this I will always be grateful to my adviser, Professor Allan MacDonald. In him a profound knowledge of physics and intuition are complemented by extreme patience and tolerance that make working with him a wonderful experience.

I have also been very lucky to have worked during my first two years in graduate school with Professor Richard Fitzpatrick. His deep knowledge of physics and integrity set an example. I am extremely grateful for his continuous support regardless of where my interests led me.

I am grateful to Professors John Markert, Jack Swift and Brian Korgel for serving on my research committee and for carefully reading this thesis.

I would like to thank Dr. Olle Heinonen for all the things that he taught me about magnetism, for his support and with whom the work presented in chapter 6 has been done.

I also would like to thank Anton Burkov, for the many times he helped me to better understand the subtleties of quantum Hall bilayers and with whom I started working on these fascinating systems. Some of the results presented in chapter 5 have been obtained in collaboration with him. I also have to thank Yogesh Joglekar for sharing with me his insights on quantum Hall systems.

Special thanks to Alvaro Núñez. The discussions with him in the last three years about physics and other subjects have been constant source of inspiration. Also his great sense of humor and optimism always helped me to keep things in the right perspective.

I would like to thank Chris Crabtree for the many conversations about physics and so many other things, and for very patiently leading me through my first years in graduate school.

I am very grateful to Becky Drake. Her wonderful attitude and constant willingness to help with the administrative tasks made the life as a graduate student much more pleasant.

I also have to thank all the other friends and colleagues with whom I had the luck to interact during these years: Ramin Abolfath, Sergey Cheskhov, Raj Desikan, Gergana Drandova, Rembert Duine, Evstati Evstatiev, Joaquín Fernández-Rossier, Ion Garate, Paul Haney, Emiliano Papa, Nikola Petrov and many others.

I would like to thank my undergraduate adviser Professor Franco Porcelli for introducing me to physics research.

Finally, for everything, I would like to thank my wife Margarita.

Enrico Rossi

The University of Texas at Austin

August 2005

Fluctuations and Dissipation of Collective Dynamics in Spin and Pseudospin Ferromagnets

Publication No. _____

Enrico Rossi, Ph.D.
The University of Texas at Austin, 2005

Supervisor: Allan H. MacDonald

In this thesis a careful study of the equilibrium and transport properties of $\nu = 1$ quantum Hall bilayers is presented. Our approach is based on the pseudospin analogy in which the layer degree of freedom for the electrons is treated as a spin degree of freedom. This treatment reveals the many analogies between these systems and spin systems. After briefly reviewing the basic physics of the quantum Hall effect in chapter 2, in chapter 3 we introduce the quantum Hall bilayer systems and define the pseuduspin model used in the following chapters to study their properties. In chapter 4 we present our results on the equilibrium properties of quantum Hall bilayers in presence of strong disorder. In particular we calculate the critical disorder strength above which the interlayer phase coherence is lost, and the Kosterlitz-Thouless tem-

perature goes to zero. In chapter 5 we develop a theory for the tunneling transport in these systems. In contrast to most previous theoretical work our theory predicts that the zero bias conductance is finite even in a perfect disorder free bilayer at zero temperature and accounts, within an order of magnitude, for the width of the anomaly observed in experiments. Also the theory correctly predicts the suppression of the tunneling conductance in presence of a magnetic field in the plane of the 2DEG. Using the results of chapter 4 the theory can also quantify the suppression of the tunneling conductance due to disorder.

In chapter 6 we study the dynamics of the magnetization when coupled to a thermal bath of elastic modes. We derive explicit expressions for the memory friction kernel and the spectral density of the fluctuations starting from a realistic form of the coupling of the magnetization to the elastic modes.

Finally in chapter 7 we study the dynamics of a particularly interesting class of collective modes in magnetized plasmas: tearing modes. We develop a rigorous approach to describe the evolution of these modes beyond the linear approximation. Using this approach we then consider nonlinear effects due to the coupling of the fundamental mode to higher harmonics and external perturbations.

Contents

List of Figures

Chapter 1

Introduction

One of the most general idea of condensed matter physics is the concept of *condensate*. Using this concept new remarkable phenomena have been discovered and theoretically explained in strongly interacting systems. In these systems the strong interactions may cause the interacting single particles to *condense* in new states that spontaneously break the symmetries of the quantum Hamiltonian. When this happens the quantum behavior becomes manifest on macroscopic scales and extremely interesting effects can be observed. This is the case for example for magnetism in which the ground state spontaneously breaks the rotational symmetry. Another example is superconductivity in which the gauge symmetry is spontaneously broken.

The fractional quantum Hall effect is the most striking recent example of another phenomenon due to the condensation of strongly interacting electrons. It was discovered in 1982 by Tsui, Störmer and Gossard [3] only two years after the discovery by von Klitzing of the integer quantum Hall effect [4]. The quantum Hall effect is only one of the remarkable effects that can be observed in two dimensional gases (2DEG) in the quantum Hall regime. In this regime the energy levels are macroscopically degenerate and their mixing due to disorder or interactions may be considered a weak perturbation. It quickly became clear that the two effects were

just a small part of a vast new subfield of condensed matter physics [5], [6],[7].

Quantum Hall bilayers are systems in the quantum Hall regime that in recent years have attracted a lot of attention [8]. In a quantum Hall bilayer two 2DEG separated by a distance d are created. When the distance d is small enough that the interlayer Coulomb interactions are comparable to the intralayer ones we have a broken symmetry ground state characterized by interlayer coherence. What is notable is that in this situation the coherence may be spontaneous, i.e. it may be present even in the limit of zero tunneling between the layers. Of all the quantum Hall bilayer systems, bilayers with total filling factor $\nu = 1$ have been the most studied. The filling factor is the ratio between the number of particles in the 2DEG and the number of degenerate states per energy level. In these systems the number of particles in each layer is then equal to $1/2$ the total number of degenerate states in the lowest energy band. A very effective way to describe these systems is to treat the layer degree of freedom as a spin degree of freedom: *pseudospin*. This approach makes evident the many analogies between quantum Hall bilayers and spin systems. The broken symmetry state of a $\nu = 1$ quantum Hall bilayers is equivalent to an easy-plane ferromagnetic state.

One of the main motivations for this thesis was to try to better understand in general the interplay between a condensate and external degrees of freedom, in particular non equilibrium transport quasiparticles. This is a very interesting problem because in most of the experiments the probing and or manipulations of the condensate can be achieved by driving a current of quasiparticles through the system. A recent remarkable example is the *spin-transfer* effect in which the magnetization of a ferromagnet is manipulated via a spin current. Spin-transfer is one of the effects studied by the growing field of spintronics in which the goal is to use the electron spin degree of freedom to carry and store information. Quantum Hall bilayers with $\nu = 1$ in many respects are ideal systems to test theoretical models for such phenomena.

In this thesis a careful study of the transport properties of $\nu = 1$ quantum Hall bilayers is presented. The first step in this effort was to better characterize the broken symmetry ground state taking into account the presence of disorder. The effect of disorder had been considered in previous work but almost always in a perturbative way. Our effort focused on including disorder effects non perturbatively (Chapter 4). We then developed a theory for the tunneling transport experiments (Chapter 5). In contrast to most previous theoretical work our theory predicts that the zero bias conductance is finite even in a perfect disorder free bilayer at zero temperature and accounts, within an order of magnitude, for the width of the anomaly observed in experiments. Also, the theory correctly predicts the suppression of the tunneling conductance in presence of a magnetic field in the plane of the 2DEG. Using the results of Chapter 4 the theory can also quantify the suppression of the tunneling conductance due to disorder.

A very important element in the dynamics of quantum Hall bilayers is damping. Previous work, [9], carefully calculated the damping of collective modes in $\nu = 1$ quantum Hall bilayers. As mentioned before these systems are very analogous to easy-plane ferromagnets and, it turns out, Josephson junctions. One aspect in which these three systems differ is in the form of the damping. The damping terms used in the dynamical equation for ferromagnets and Josephson junctions are not fully justified from microscopic models and often rely on phenomenological approaches. To try to improve our understanding of the damping in these systems, we derived the damping terms in the equation of motion of the magnetization for the case when the main source of dissipation is the coupling of the magnetization to elastic modes (Chapter 6). Previous studies of this problem used the Fermi golden rule to derive a relaxation constant and were limited to infinite systems. In our analysis we use a Caldeira-Leggett approach [10] that allows us to overcome some of the limitations of relaxation theories based on the Fermi golden rule, and we do not impose any

restriction on the size or shape of the system.

Finally in Chapter 7 we study the dynamics of a particularly interesting class of collective modes in magnetized plasmas: tearing modes. These modes have the remarkable effect of changing the topology of the magnetic flux surfaces through the phenomenon of *magnetic reconnection*. We develop a rigorous approach to describe the evolution of these modes beyond the linear approximation. Our approach in particular allows us to to consider nonlinear effects due to the coupling of the fundamental mode to higher harmonics and external perturbations.

Chapter 2

Quantum Hall effect

2.1 Introduction

In the classical Hall effect [11] when a current flows in the plane of a thin conducting material a voltage drop develops between the sides of the Hall bar, Fig. 2.1, parallel to the direction of the current when a magnetic field perpendicular to the conducting sheet is applied. The classical effect can be explained using the Drude theory [12] of magnetotransport in two dimensions. In Drude's theory the external force **F** acting

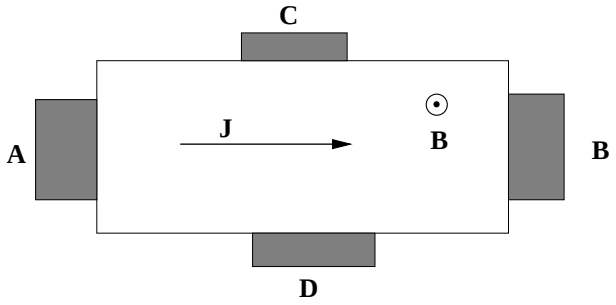

Figure 2.1: Hall bar geometry. A current I flows between the terminals A and B of thin conducting sample. A magnetic field along the perpendicular to the plane of the conducting sheet (direction out of the page in the picture) is applied. Once the stationary state is reached a potential difference is measured between the terminals C and D.

on the electrons in a conductor is compensated, in stationary state, by scattering processes until a constant drift velocity, $\mathbf{v}_D$, is reached:

$$\mathbf{v}_D = \frac{\mathbf{F}\tau}{m^*}$$

where τ is the average time between scattering events and m^* is the effective mass of the carriers. For the Hall bar geometry the force will be given by:

$$\mathbf{F} = e\mathbf{E} + \frac{e}{c}B\mathbf{v}_D \times \hat{\mathbf{z}}.$$

so that

$$\mathbf{v}_D = \frac{e\tau}{m^*}\left[\mathbf{E} + \frac{1}{c}B\mathbf{v}_D \times \hat{\mathbf{z}}\right]. \tag{2.1}$$

According to Drude's theory the current density is simply given by $\mathbf{j} = ne\mathbf{v}_D$. Using this expression for the current and (2.1) can write:

$$\mathbf{E} = \frac{m^*}{ne^2\tau}\mathbf{j} + \frac{B}{nec}\hat{\mathbf{z}} \times \mathbf{j}. \tag{2.2}$$

By definition the components of the resistivity tensor are given by the ratio of the components of $\mathbf{E}$ over the components of $\mathbf{j}$. From (2.2) we then find:

$$\rho = \begin{pmatrix} \frac{m^*}{ne^2\tau} & -\frac{B}{nec} \\ \frac{B}{nec} & \frac{m^*}{ne^2\tau} \end{pmatrix}. \tag{2.3}$$

The off diagonal part of ρ is called the Hall resistivity and the corresponding resistance, Hall resistance. From (2.3) we see that the Hall resistivity grows linearly with the intensity of the applied magnetic field and inversely with the carrier density.

In 1980 Klaus Von Klitzing and collaborators [4] while measuring the transport properties of a two dimensional electron gas, 2DEG, in presence of a strong perpendicular magnetic field discovered something quite unusual. For certain car-

rier concentrations the Hall resistance had fixed values depending only on the fine-structure constant and the speed of light, independent of the geometry of the sample. What's more, for the same concentration values, the longitudinal resistance was almost zero. Von Klitizing and collaborators had discovered the quantum Hall effect, one of the most remarkable condensed matter phenomena discovered in the 20th century.

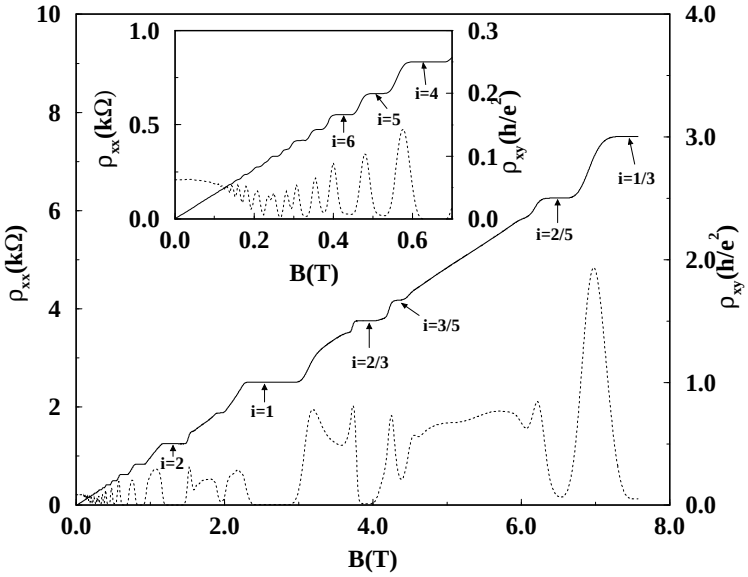

Figure 2.2: Typical transport data for a quantum Hall sample: The Hall resistivity has plateaus at $\rho_{xy} = h/\nu e^2$, accompanied by deep minima in the transverse resistivity ρ_{xx}. The inset shows Shubnikov-de Haas oscillations in ρ_{xx} and linear Hall resistivity at small magnetic fields. The areal density is $n_e = 6.3 \times 10^{10}$ cm^{-2} and the mobility is $\mu = 5 \times 10^5$ cm^2/Vs (courtesy: Dr. Edmond Chow).

What is remarkable about the quantum Hall effect is that, as in superconductivity, the quantum mechanical laws that govern the microscopic world become manifest on a macroscopic scale. What Von Klitzing and collaborators discovered is what is now called the *integer quantum Hall effect*. Two years later, in 1982, Tsui, Stormer and Gossard, [3] discovered the *fractional quatnum Hall effect*. For a

general introduction to the quantum Hall effect, see [13], [7], [6].

Von Klitzing and collaborators did their experiments on a silicon metal-oxide-semiconductor field effect transistor (MOSFET) whereas Tsui, Stormer and Gossard did their experiment on a 2DEG formed at the interface of a $GaAs - AlGaAs$ heterojunction for which the mobility is much higher. $GaAs - AlGaAs$ heterojunctions have since become the standard system on which quantum Hall effects experiments are performed.

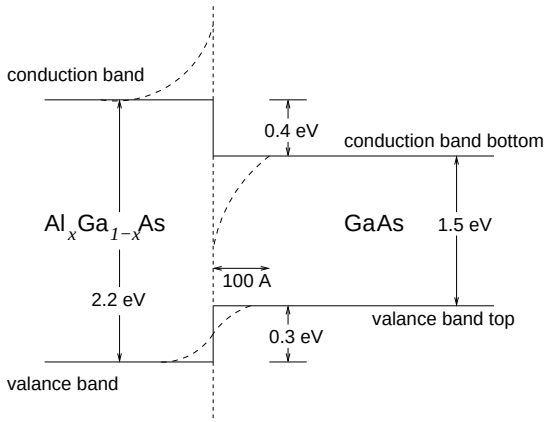

Figure 2.3: Schematic profile of the band structure at the interface of a $GaAs - AlGaAs$ heterojunction.

In $GaAs$ the band gap is $1.5eV$, $Al_xGa_{1-x}As$ has a larger gap that depends on the concentration, x, of aluminum. In a modulation-doped heterojunction

$Al_xGa_{1-x}As$ is $n-$doped with silicon away from the interface to minimize the disorder potential caused by the donor ions. Because of the band mismatch electrons move from the $Al_xGa_{1-x}As$ to $GaAs$. Once in $GaAs$ the electrons feel the Coulomb attraction due to the positive ions left behind and as a consequence we have bending of the bands near the interface as shown in Fig.2.3. Once equilibrium is reached the electron at the interface will occupy the narrow quantum well created by the bent bands. Here they are free to move in the direction parallel to the junction but see a random potential that has contributions from the remote ionized donors and imperfections in the interface. If the subband spacing due to the confinement in the direction perpendicular at the interface is much bigger than all relevant energy scales the electron gas in the quantum well is, for all practical purposes, a 2DEG.

For hypercube systems of lateral size L the resistance and the resistivity are related by

$$R = \rho L^{(2-d)}$$

where d is the number of dimensions of the hypercube. We then see that $d = 2$ is special because in this case $R = \rho$, i.e. the resistance of the sample is scale invariant. This is crucial for the universality of the quantum Hall effect, its independence on the specific geometry of the sample, and the incredibly high accuracy with which the quantized Hall resistance can be measured.

2.2 2D free electron gas in a perpendicular magnetic field

Let us consider a gas of free electrons confined in the XY plane in presence of a perpendicular magnetic field B. Neglecting the spin degree of freedom the Hamiltonian

for every electron, of charge $-e$ and mass m, is

$$H = \frac{1}{2m}\left(\mathbf{p} + \frac{e}{c}\mathbf{A}\right)^2 \tag{2.4}$$

In our case a convenient gauge for the vector potential is the Landau gauge for which we have:

$$\mathbf{A} = xB\hat{\mathbf{y}}.$$

In this gauge the Hamiltonian (2.4) takes the form:

$$H = \frac{1}{2m}\left[p_x^2 + \left(p_y + \frac{eB}{c}x\right)^2\right].$$

The Hamiltonian is invariant with respect to translations along the y direction. Without loss of generality we can then assume the eigenstates $\psi_k(x, y)$ to have the form:

$$\psi_k(x, y) = e^{iky}u_k(x).$$

Using this expression we find the effective Schrödienger equation for $u_k(x)$:

$$\frac{1}{2m}\left[p_x^2 + \left(\hbar k + \frac{eB}{c}x\right)^2\right]u_k(x) = \epsilon_k u_k(x). \tag{2.5}$$

Let's define the cyclotron frequency

$$\omega_c \equiv \frac{eB}{mc};$$

and the magnetic length

$$l \equiv \sqrt{\frac{\hbar c}{eB}}.$$

Using these definitions we can rewrite (2.5) in the form:

$$\frac{1}{2m}p_x^2 + \frac{1}{2}m\omega_c^2(x + kl^2)^2 = \epsilon_k u_k(x). \tag{2.6}$$

Equation (2.5)/(2.6) is simply the Schrödienger equation for a harmonic oscillator whose center is displaced by kl^2 from the origin. The eigenvalues of (2.6) are then:

$$\epsilon_k = \hbar\omega_c\left(n + \frac{1}{2}\right); \qquad n = 0, 1, 2, ... \tag{2.7}$$

independent of k, the value of the momentum along the y direction. We then see that for any integer n we have a macroscopic degeneracy given by all the values allowed for k by the boundary conditions along y. The degenerate energy levels given by (2.7) are called Landau levels. Let's now assume for definiteness that the 2DEG is confined in a rectangular region of size $L_x \times L_y$. Then the minimum and maximum position for the center of the harmonic oscillator along x will be 0 and L_x respectively, so that we must have $k \in [0; L_x/l^2]$. The total number of states, N_ϕ, in each Landau level will then be

$$\begin{aligned} N_\phi &= \frac{L_y}{2\pi}\int_0^{L_x/l^2} dk \\ &= \frac{L_x L_y}{2\pi l^2} \\ &= \frac{BL_xL_y}{\Phi_0} \end{aligned} \tag{2.8}$$

where $\Phi_0 \equiv hc/e$ is the quantum of magnetic flux. The last line of (2.8) is particularly intuitive: it tells us that the number of degenerate states in each Landau level is simply given by the total number of magnetic quantum fluxes piercing the system. The higher the magnetic field the higher the degeneracy. It is this macroscopic degeneracy that creates the opportunity for unique physical phenomena. We define the filling factor ν as the ratio between the number of electrons N in the 2DEG and

the number of degenerate states

$$\nu \equiv \frac{N}{N_\phi} \tag{2.9}$$

When ν is an integer we have the integer quantum Hall effect.

When the perpendicular magnetic field is strong enough to make the degeneracy of the Landau levels macroscopic (of the same order of the number of particles in the system) and their spacing, $\hbar\omega_c$, high enough so that their mixing due to disorder *or* interactions can be seen as a small perturbation we are in the so called *quantum Hall regime*. Notice that for a gas of electrons all in the same Landau level there is no energy scale associated with a one-body term in the Hamiltonian that can be used as basis for a perturbative approach. As a consequence neither the interactions or the disorder can be treated perturbatively. When the interactions can be considered as a small perturbation with respect to the disorder terms we are in the integer quantum Hall regime , in the opposite case we are in the fractional quantum Hall regime.

2.3 Quantum Hall effect

The quantum Hall effect can be explained qualitatively using a very general thermodynamic argument based on the concept that at particular filling factors the 2DEG becomes incompressible, [14], [13].

For a two dimensional system with N particles the compressibility κ is defined as the relative change of the area A due to a change of the pressure P:

$$\kappa \equiv -\frac{1}{A}\left.\frac{\partial A}{\partial P}\right|_N .$$

In terms of the energy of the system we can write:

$$\frac{1}{\kappa} = -A\left.\frac{\partial P}{\partial A}\right|_N = A\left.\frac{\partial^2 E}{\partial A^2}\right|_N .$$

On the other hand E is an extensive quantity and then we can always write $E = N\epsilon(n)$, where $n = N/A$ is the particle density. Using this fact and the expression for $1/\kappa$ in terms of E we find:

$$\frac{1}{\kappa} = n^2 \left[2\frac{d\epsilon}{dn} + \frac{d^2\epsilon}{dn^2} \right]. \tag{2.10}$$

By definition the chemical potential μ is:

$$\mu = \left. \frac{\partial E}{\partial N} \right|_A = \frac{d(n\epsilon(n))}{dn}.$$

From the definition of μ and (2.10) we find:

$$\frac{1}{\kappa} = n^2 \frac{d\mu}{dn} \tag{2.11}$$

Equation (2.11) tells us that when the system is incompressible, $\kappa = 0$, the chemical potential as a function of the density n must be discontinuous. This means that it takes different energies to add or remove a particle from the system. In particular for an electron gas it takes a finite amount of energy to create unbound particle-hole pairs which are able to carry current: an incompressible 2DEG has a charge gap.

We have so far shown that incompressibility implies a charge gap. Let's now see what are the consequences of this connection for quantum Hall systems. To do this let's calculate the change δI of the equilibrium currents, always present because the time reversal symmetry is broken by the magnetic field, when we make an infinitesimal change $\delta\mu$ of the chemical potential for an incompressible 2DEG. Assuming that there is no disorder, because $\kappa = 0$ the change in the orbital current can only happen at the edge of the system; only at the edge can there be states close to the chemical potential, Fig.2.4. By continuity the edge current must be a circulating current. We can then relate δI to a change of the total orbital magnetic

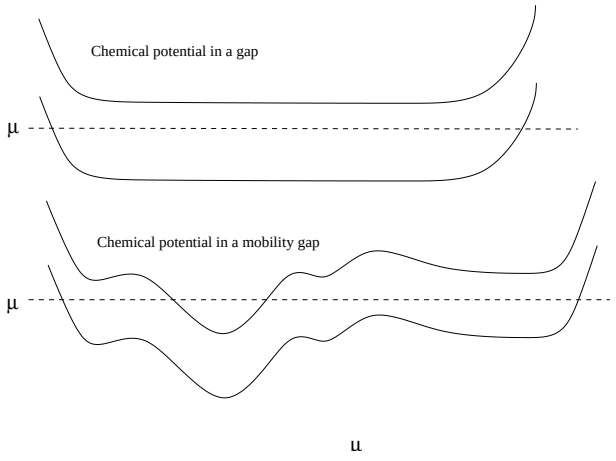

Figure 2.4: Illustration of the situation when the chemical potential of a 2DEG is in a charge gap and mobility gap.

moment of the 2DEG:

$$\delta I = \frac{c}{A}\delta M. \tag{2.12}$$

On the other hand:

$$\delta M = \left(\frac{\partial M}{\partial \mu}\right)_B \delta\mu$$

From the identity:

$$\left[\frac{\partial}{\partial \mu}\left(\frac{\partial F}{\partial B}\right)_\mu\right]_B = \left[\frac{\partial}{\partial B}\left(\frac{\partial F}{\partial \mu}\right)_B\right]_\mu.$$

we have the Maxwell relation

$$\left(\frac{\partial M}{\partial \mu}\right)_B = \left(\frac{\partial N}{\partial B}\right)_\mu$$

so that we can write:

$$\delta M = \left(\frac{\partial N}{\partial B}\right)_\mu \delta\mu.$$

Using this expression of δM from (2.12) we find:

$$\frac{\delta I}{\delta \mu} = c \left(\frac{\partial n}{\partial B} \right)_{\mu} \tag{2.13}$$

In the quantum Hall regime we know that, because of the quantization of the orbital motion of the electrons, the 2DEG has a gap whenever the filling factor is equal to an integer. Therefore whenever ν is an integer we have edge currents for which (2.13) applies. Considering that

$$n = \nu \frac{B}{\Phi_0}$$

from (2.13) we find:

$$\frac{\delta I}{\delta \mu} = \nu \frac{e}{h}; \qquad \text{for } \nu = 1, 2, ...$$

If we have a chemical potential difference, eV_H, between the two edges a net current can be carried given by:

$$I = \nu \frac{e^2}{h} V_H \qquad \text{for } \nu = 1, 2, ...$$

We then recover the experimentally observed quantization of the Hall conductivity $\sigma_H = \nu e^2/h$. The result is still valid also in presence of disorder. In this case a change of chemical potential creates orbital currents also in the bulk along the internal closed shorelines created by the disorder. However as long as these currents are localized away from the edges, they will not give any contribution to the net current. On the other hand the disorder is instrumental to make the range of values of B, (n) over which the Hall conductance is quantized, finite. For example as we increase n to values slightly bigger than the value for which we have $\nu = 1$ we will only fill localized states in the bulk that don't affect the edge current. Only when n is big enough that the we have percolation between opposite edges the quantization of the Hall conductance will be lost and the longitudinal resistivity be different from

zero.

The argument used here, based on the incompressibility of the state for which we have the quantization of the Hall resistivity is quite general and can be used also to explain the fractional quantum Hall effect. In the fractional quantum Hall effect the incompressibility is due to the strong electron-electron interactions that can produce a charge gap even when the noninteracting system would otherwise be compressible.

Chapter 3

Quantum Hall bilayers

3.1 Introduction

A quantum Hall bilayer consists of two 2DEG layers separated by a distance d in a strong perpendicular magnetic field so that the system is in the quantum Hall regime. Using modern molecular beam epitaxy techniques, a double quantum well structure (Fig. 3.1) is realized by sandwiching a thin layer of $Al_xGa_{1-x}As$ between $GaAs$. In a quantum Hall bilayer in presence of strong perpendicular magnetic field the electrons in a Landau level besides the orbital degree of freedom (and the spin) have one additional degree of freedom, the one that specifies in which of the two layers, top (T), or bottom (B), they are localized. In the remainder of this thesis we will assume the spin degree of freedom to be frozen out on account of the Zeeman energy due to the strong perpendicular magnetic field. In reality, because of the very small effective mass and strong spin-orbit interaction of electrons in $GaAs$ the Zeeman energy is much smaller (about 60 times) than the cyclotron energy. However for the typical experimental conditions we are interested in (with magnetic fields of the order 5 Tesla) the Zeeman energy is of the order of 1 K, much bigger than the other energy scales that characterize the system and the normal temperature (50

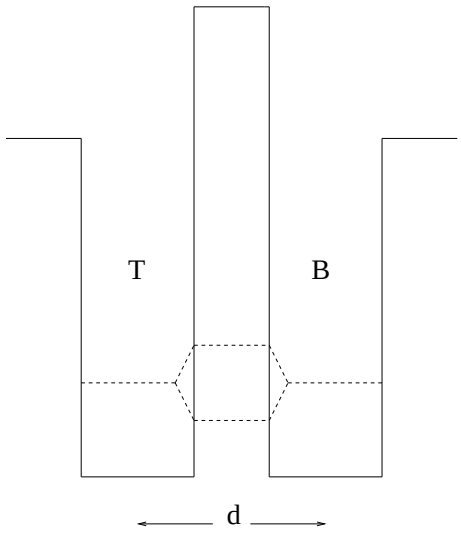

Figure 3.1: Schematic band edge diagram for a double quantum well. The electrons are free to move in the plane parallel to the interfaces (direction perpendicular to the page) but confined in the perpendicular direction. d is the interlayer separation, for quantum Hall bilayers is $d \approx 100\mathring{A}$

mK) at which the experiments are performed. For a treatment that includes also the spin degree of freedom see [15].

In a quantum Hall bilayer the electron can exploit the additional degree of freedom to minimize the total energy. New interesting physics arises when the interaction energy between electrons in different layers is of the same order as the interaction between electrons in the same layer. A measure of the distance between electrons in the same layer is given by the magnetic length. When the distance d between the layer is of the same order of l then the interlayer and intralayer Coulomb interactions become comparable and new broken symmetry states may arise that have peculiar properties.

Definitely the most studied quantum Hall bilayer system is the one with total filling factor $\nu = 1$. For this system the two layers both have $\nu = 1/2$. When $d \gg l$ the two layers behave essentially as two decoupled $\nu = 1/2$ quantum Hall systems

well described by the composite-fermion Fermi liquid theory [16]. In this case then we don't expect the system to have any broken symmetry and in particular we don't expect any quantum Hall effect. For $d \lesssim l$ the system has a broken symmetry ground state and we expect that in this state it will exhibit the quantum Hall effect. This is indeed what is observed in experiments, Fig. 3.2. What is remarkable in Fig. 3.2 is that when $d \lesssim l$ the quantum Hall effect survives even in the limit of zero tunneling. This tells us that the effect in a $\nu = 1$ quantum Hall bilayer is solely due the collective behavior of interacting electrons in different layers. In the absence of tunneling *spontaneous phase coherence* between electrons in different layers is necessary for the existence of the quantum Hall effect.

To understand the character of the phase coherent ground state we can perform a particle-hole transformation for the electrons in the bottom layer. In this way we can think of having a system of excitons formed by the electrons in the top layer bound to holes in the bottom layer. In this picture the broken symmetry ground state is equivalent to a an *excitonic condensate* [17]. Such a state can be described by the following wave function:

$$|\Psi[\varphi]\rangle = \prod_i \frac{1}{\sqrt{2}} \left(c^\dagger_{iT} + e^{i\varphi} c^\dagger_{iB} \right) |0\rangle. \tag{3.1}$$

where $c^\dagger_{iT}$ ($c^\dagger_{iB}$) is the creation operator for an electron in the $i-th$ orbital in the lowest Landau Level, LLL, in the top (bottom) layer. In the state (3.1) we have an electron in each LLL orbital and hence this state has $\nu = 1$ and every electron is in a superposition of a state, ψ_{iT}, localized in the top layer and one, ψ_{iB}, localized in the bottom layer. The phase between ψ_{iT} and ψ_{iT} is φ and is the same for every i, i.e. for every electron in the system: the electrons are in a phase coherent state. In this state the number of electrons in each layer is indefinite, a situation analogous to the BCS state for a superconductor for which the total number of electrons is indefinite. On the other hand in absence of tunneling the number operator for each

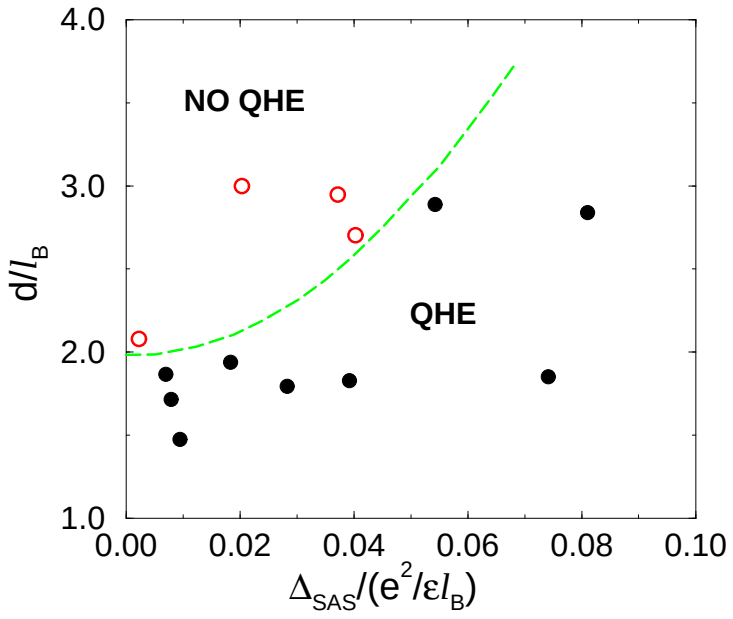

Figure 3.2: Experimental phase diagram for $\nu = 1$ quantum Hall bilayer [1].As d/l_B, l_B being the magnetic length, crosses a critical value, of the order of 1, we go from a state that exhibits Quantum Hall effect (QHE) to one that does not (NO QHE). The critical value, d_c, of d decreases with the tunneling amplitude Δ_{SAS}. What is remarkable is that d_c remains finite even in the limit of $\Delta_{SAS} \to 0$. In this condition the quantum Hall effect can only be explained in terms of a broken symmetry ground state characterized by interlayer phase coherence.

layer commutes with the Hamiltonian: in the interlayer phase coherent state (3.1) we have a spontaneously broken symmetry.

An equivalent description of the spontaneous coherent state in a quantum Hall bilayer can be done using the *pseudospin* analogy. In this description the two-component layer degree of freedom is treated as a spin degree of freedom: pseudospin up describes an electron state localized in the top layer, pseudospin down a state localized in the bottom layer. In this language we can rewrite the state (3.1) in the

form:

$$|\Psi[\varphi]\rangle = \prod_i \frac{1}{\sqrt{2}} \left(c_{i\uparrow}^\dagger + e^{i\varphi} c_{i\downarrow}^\dagger \right) |0\rangle. \tag{3.2}$$

We can define the pseudospin operators:

$$\mathbf{S}_i \equiv \frac{1}{2} \sum_{\sigma,\sigma'} c_{i\sigma}^\dagger \boldsymbol{\tau}_{\sigma\sigma'} c_{i\sigma'},$$

for each LLL orbital i, where $\boldsymbol{\tau}_{\sigma\sigma'}$ is the Pauli matrix vector and $\sigma = \uparrow; \downarrow$. The state (3.2) is characterized by the complex order parameter:

$$\langle S^+(\mathbf{r}) \rangle = \langle \Psi_\uparrow^\dagger(\mathbf{r}) \Psi_\downarrow(\mathbf{r}) \rangle = \frac{n}{2} e^{i\varphi}$$

where $\Psi_\sigma^\dagger(\mathbf{r})$ ($\Psi_\sigma(\mathbf{r})$) is the operator that creates (annihilates) an electron with pseudospin σ at position $\mathbf{r}$, $n = 1/2\pi l^2$ and $S^+ = S_x + iS_y$ is the ladder pseudospin operator. This order parameter is equivalent to the order parameter

$$m(\mathbf{r}) = \langle m_x(\mathbf{r}) + i m_y(\mathbf{r}) \rangle$$

of an XY ferromagnetic state.

Using the pseudospin analogy we map the original problem of itinerant interacting electrons to a problem of interacting pseudospins. The advantage is that normally spin problems are easier to treat and many theoretical techniques have been developed to study them. Even more important, the pseudospin mapping, by revealing the very close analogy between $\nu = 1$ quantum Hall bilayers and ferromagnetic systems, allows us to borrow ideas and techniques from one class of systems and apply them to the other. For example in the following chapter we will extensively use ideas and techniques developed for ferromagnetic systems to study quantum Hall bilayers. The analogy turns out to be very powerful especially to describe transport experiments. In Chapter 5 we will study the tunneling transport properties of $\nu = 1$

quantum Hall bilayers in which an electron is injected in the top layer at one end of the sample and extracted from the bottom layer at the other end of the sample. In the pseudospin language this is equivalent to injecting a spin up on one side and removing a spin down on the other side creating a *spin current* through the system. The interplay between the transport spin current and the order parameter gives rise to very unusual and interesting physical effects. The pseudospin mapping makes explicit the deep analogy between these experiments in $\nu = 1$ quantum Hall bilayers and experiments in the growing field of *spintronics* where the coupling between transport spins and magnetization is exploited to control the current polarization and/or the state of the ferromagnet. Using the pseudospin language we can recast some of the ideas and results valid for quantum Hall bilayers to spintronic systems. A beautiful example of this is the prediction of spin supercurrents in easy-plane ferromagnets [18]. In certain respects a quantum Hall bilayer is a perfect spintronics device. For example, by being able to selectively inject quasiparticles only on the top or bottom layer, in quantum Hall bilayers we have the analogous of being able to inject a perfectly spin polarized current in a ferromagnet, without having to deal for example with the problem of spin scattering at the interface. Also because the pseudospin degree of freedom is associated with the localization of electrons in the top or bottom layer we can expect that in principle it could be easier experimentally to study pseudospin currents that real spin currents. By using the pseudospin mapping $\nu = 1$ quantum Hall bilayers are ideal systems on which to test experimentally and theoretically novel ideas for spintronic devices.

3.2 Magnetic Wannier functions

In this section we introduce the basis of single particle wavefunctions that we will use to express the microscopic Hamiltonian. For a $\nu = 1$ quantum Hall bilayer only the LLL orbitals are occupied and we have $N = N_\phi$ i.e. one electron per each flux

quantum. If on the sample we define a square lattice with lattice constant $a = \sqrt{2\pi l^2}$ so that each cell has area $2\pi l^2$ (the area per flux quantum), a natural basis choice would be the one formed by Wannier functions centered on the lattice sites. However a strong magnetic field imposes restrictions on the localization properties of magnetic orbitals and it's known that a set of linearly independent and exponentially localized single-particle orbitals in the LLL does not exist. Nevertheless it is still possible, [19],[20] to construct a set of independent Wannier-like functions that although not exponentially localized, in the region $r \lesssim \sqrt{2\pi l^2}$ that contributes $\approx 95\%$ of the normalization integral, are very close to a Gaussian. These orbitals fall off as r^{-2} for $r > \sqrt{2\pi l^2}$.

To build the magnetic Wannier functions we start from the minimum uncertainty wavepacket localized at the origin of the lattice:

$$c_{00} = \frac{1}{\sqrt{2\pi l^2}} \exp\left(-\frac{r^2}{4l^2}\right).$$

In order to construct wavepackets, c_{mn}, localized at the other lattice sites we translate c_{00} using the magnetic translation operator:

$$T_{\mathbf{R}} \equiv e^{-\frac{1}{\hbar}\mathbf{R}\cdot\left(\mathbf{p}-\frac{e}{c}\mathbf{A}\right)}$$

that commutes with the Hamiltonian and that if acted on eigenstates, returns eigenstates. Let

$$\mathbf{R}_{mn} \equiv m\hat{\mathbf{x}} + n\hat{\mathbf{y}}; \qquad m, n \in \mathbb{N}$$

then:

$$c_{mn} = T_{\mathbf{R}_{mn}} c_{00} = \frac{(-1)^{mn}}{\sqrt{2\pi\ell^2}} \exp\left[-\frac{(\mathbf{r}-\mathbf{R}_{mn})^2}{4\ell^2} + \frac{i}{2\ell^2}\hat{z}(\mathbf{r}\times\mathbf{R}_{mn})\right]. \tag{3.3}$$

The functions c_{mn} are not orthogonal and are overcomplete by exactly one function

due to the Perelomov identity [21]:

$$\sum_{mn=-\infty}^{\infty} (-1)^{m+n} c_{mn}(\mathbf{r}) = 0.$$

This is the reason why it is not possible to find magnetic Wannier functions that are exponentially localized. This impossibility is strictly related to the fact that the Hall conductivity in the gap is not zero. As a matter of fact Thouless [22] has shown that in systems supporting a Hall current the orbitals cannot fall off with distance faster than the inverse-square law.

To orthogonalize the functions c_{mn} we can follow the standard procedure of transforming them in the Bloch representation and then go back to the site representation. The only difference being that in our case the *Bloch wave-vector* $\mathbf{k}$ will be an eigenvalue of the operator $T_{ma\hat{\mathbf{x}}}T_{na\hat{\mathbf{y}}}$ instead of the standard translation operator. Transforming c_{mn} to the momentum representation we find the Bloch functions:

$$\Psi_{\mathbf{k}}(\mathbf{r}) = \frac{1}{\sqrt{N_\phi \nu(\mathbf{k})}} \sum_{mn=-\infty}^{\infty} c_{mn}(\mathbf{r}) \exp(i\mathbf{k}\cdot\mathbf{R}_{mn})$$

where $\nu(\mathbf{k})$ is a normalization factor. We have:

$$\nu(\mathbf{k}) = \sqrt{2\pi} \sum_{mn=-\infty}^{\infty} c_{mn}(0) \cos(\mathbf{k}\cdot\mathbf{R}_{mn}). \tag{3.4}$$

The overcompleteness of the functions c_{mn} makes it impossible to find $\Psi_{\mathbf{k}}$ for $\mathbf{k}$ at the corner of the Brillouin zone using equation (3.4). By exploiting the Perelomov identity is possible to show, [20], that for $\mathbf{k} = \mathbf{k}_0$, where $\mathbf{k}_0$ is a corner of the Brillouin zone is

$$\Psi_{\mathbf{k}_0}(\mathbf{r}) = \frac{i}{a\sqrt{2N_\phi\gamma}} \sum_{mn=-\infty}^{\infty} (-1)^{m+n}(ma - ina) c_{mn}(\mathbf{r}) \tag{3.5}$$

with

$$\gamma = -\frac{1}{a}\sum_{mn=-\infty}^{\infty}(-1)^{m+n}.$$

Taking the inverse Fourier transform of $\Psi_{\mathbf{k}}$ we finally find the magnetic Wannier functions:

$$W_{mn} = \frac{1}{\sqrt{N_\phi}}\sum_{\mathbf{k}}\Psi_{\mathbf{k}}e^{-i\mathbf{k}\cdot\mathbf{R}_{mn}} \tag{3.6}$$

where the functions $\Psi_{\mathbf{k}}$ are defined for any $\mathbf{k}$ in the Brillouin zone by equations (3.4), (3.5). The functions W_{mn} by construction are orthonormal and form a complete set.

3.3 Pseudospin model

In this section we derive the pseudospin model [15] that we will use, with different approximations, in the following chapters. As a basis to represent the matrix elements of the microscopic Hamiltonian we will use the one formed by the magnetic Wannier functions introduced in the previous section. The only assumption of the model is that every Wannier orbital i is occupied by exactly one electron, i.e. we assume that there are no charge fluctuations.

We assume that the bilayer is described by the Hamiltonian

$$\begin{aligned} H = &-\frac{\Delta_t}{2}\sum_{\sigma\sigma' i} c^\dagger_{i\sigma}\tau^x_{\sigma\sigma'}c_{i\sigma'} + \\ &\frac{1}{2}\sum_{\sigma\sigma'}\sum_{i_1 i_2 i_3 i_4} c^\dagger_{i_1\sigma}c^\dagger_{i_2\sigma'}c_{i_4\sigma'}c_{i_3\sigma}\left[\langle i_1 i_2|V_+|i_3 i_4\rangle + \tau^z_{\sigma\sigma}\tau^z_{\sigma'\sigma'}\langle i_1 i_2|V_-|i_3 i_4\rangle\right]. \end{aligned} \tag{3.7}$$

where $c^\dagger_{i\sigma}$ ($c_{i\sigma}$) is the creation (annihilation) operator for an electron in the LLL orbital state i and pseudospin σ;

$$V_\pm = \frac{1}{2}(V_S \pm V_D)$$

and V_S, V_D are the 2D Coulomb interactions between electrons in the same and different layers respectively. Because we assume that each orbital is occupied by one electron ($\nu = 1$) the charge degree of freedom in (3.7) is irrelevant and we would like to rewrite the Hamiltonian only in terms of the pseudospin degree of freedom. The most convenient way to do this is through the path integral approach. Because we neglect charge fluctuations we can assume that at each discrete imaginary time the single particle Slater determinant states form a complete set. We find the imaginary time action:

$$S[\bar{z}, z] = \int_0^\beta d\tau \left[\sum_i (\langle z_i|\partial_\tau|z_i\rangle - \frac{\Delta_t}{2}\langle z_i|\tau^x|z_i\rangle) + \frac{1}{2}\sum_{ij} H_{ij}\langle z_i|\tau^z|z_i\rangle\langle z_j|\tau^z|z_j\rangle - \right.$$
$$\left. \frac{1}{2}\sum_{ij}(F_{ij}^+\langle z_i|z_j\rangle\langle z_j|z_i\rangle + F_{ij}^-\langle z_i|\tau^z|z_j\rangle\langle z_j|\tau^z|z_i\rangle) \right] \tag{3.8}$$

where $\beta = 1/K_B T$. In this equation z_i are complex fields,

$$H_{ij} = \langle ij|V_-|ij\rangle$$

is the Coulomb interaction direct two-particle matrix element and

$$F_{ij}^+ = \langle ij|V_+|ji\rangle$$
$$F_{ij}^- = \langle ij|V_-|ji\rangle$$

the Coulomb interaction exchange matrix elements.

The complex fields z_i can be associated with bosonic coherent states and then we can rewrite (3.8) in terms of bosonic operators $a_{i\sigma}^\dagger, a_{i\sigma}$. Because we assume that every orbital i is occupied exactly by one electron, for the bosonic operators

we have the constraint:

$$\sum_{\sigma} a^{\dagger}_{i\sigma} a_{i\sigma} = 1.$$

The bosonic operators $a, a^{\dagger}$ can the be thought as the Schwinger boson operators representing the pseudospin operators [23]:

$$\mathbf{S}_i = \frac{1}{2} \sum_{\sigma,\sigma'} a^{\dagger}_{i\sigma} \tau_{\sigma\sigma'} a_{i\sigma'}$$

It is readily shown that the action (3.8) is the same action that we would obtain by expressing the partition function of a system of bosons with Hamiltonian:

$$H = -\frac{1}{2}\Delta_t \sum_{i\sigma\sigma'} a^{\dagger}_{i\sigma} \tau^x_{\sigma\sigma'} a_{i\sigma'} + \frac{1}{2} \sum_{ij} \sum_{\sigma\sigma'} \Big[H_{ij} a^{\dagger}_{i\sigma} a^{\dagger}_{j\sigma'} a_{i\sigma} a_{j\sigma'} \tau^z_{\sigma\sigma} \tau^z_{\sigma'\sigma'} - F^{+}_{ij} a^{\dagger}_{i\sigma} a^{\dagger}_{j\sigma'} a_{j\sigma'} a_{i\sigma} - F^{-}_{ij} a^{\dagger}_{i\sigma} a^{\dagger}_{j\sigma'} a_{j\sigma'} a_{i\sigma} \tau^z_{\sigma\sigma} \tau^z_{\sigma'\sigma'} \Big]. \tag{3.9}$$

in a coherent state path integral representation. In terms of the spin operators $\mathbf{S}_i$ the Hamiltonian (3.9) can be rewritten in the form:

$$H = -\frac{1}{2}\Delta_t \sum_i S^x_i + \sum_{ij} \Big[(2H_{ij} - F^S_{ij}) S^z_i S^z_j - F^D_{ij} (S^x_i S^x_j + S^y_i S^y_j) \Big]. \tag{3.10}$$

where $F^S = F^+ + F^-$, $F^D = F^+ - F^-$ are the exchange interactions for electrons in the same and different layer respectively. The Hamiltonian (3.10) recasts the original problem of itinerant interacting electrons as a problem of interacting pseudospins for which we can exploit the variety of techniques developed to study spin Hamiltonians. In the absence of charge fluctuations the Hamiltonian (3.10) is exact.

3.4 Semiclassical model

Starting from the microscopic Hamiltonian (3.10) we can derive a continuum semiclassical approximation. The most convenient way to do this is by expressing the partition function Z using a path integral representation

$$Z = \int D\mathbf{m} e^{(-S[\mathbf{m}])} \tag{3.11}$$

in term of the spin coherent states $|\mathbf{m}\rangle$, [24]. The spin coherent state $|\mathbf{m}\rangle$ is defined as the eigenstate of the projection of the spin operator on the unit vector $\mathbf{m}$:

$$(\mathbf{S} \cdot \mathbf{m})|\mathbf{m}\rangle = S|\mathbf{m}\rangle$$

The action that appears in (3.11) is given by

$$S[\mathbf{m}] = -iS \sum_i \omega[\mathbf{m}_i] + \int_0^{1/T} d\tau E[\mathbf{m}(\tau)],$$

where

$$E[\mathbf{m}] \equiv \langle \mathbf{m}|H|\mathbf{m}\rangle$$

is the *classical energy functional* and

$$\omega[\mathbf{m}] = \int_0^{1/T} d\tau \mathbf{A}[\mathbf{m}] \cdot \dot{\mathbf{m}}$$

is the so called *Berry phase* and the vector potential $\mathbf{A}$ is defined by the equation:

$$\nabla_{\mathbf{m}} \times \mathbf{A} = \mathbf{m}.$$

By means of a Wick rotation we then find the *semiclassical pseudospin Lagrangian* in real time:

$$\mathcal{L} = \sum_i \mathbf{A}[\mathbf{m}_i] \cdot \dot{\mathbf{m}}_i - E[\mathbf{m}] \tag{3.12}$$

From (3.10) for the semiclassical energy functional $E[\mathbf{m}]$ we find:

$$E[\mathbf{m}] = -\frac{1}{2}\Delta_t \sum_i m^x + \frac{1}{4}\sum_{ij}\left[(2H_{ij} - F^S_{ij})m^z_i m^z_j - F^D_{ij}(m^x_i m^x_j + m^y_i m^y_j)\right]. \tag{3.13}$$

Starting from the microscopic model, assuming that there are no charge fluctuations, we have derived a semiclassical energy functional in terms of the unit vectors $\mathbf{m}_i$ that give us the direction of the pseudospin at every lattice site. In the semiclassical approximation the absence of charge fluctuations is guaranteed by the constraint $\mathbf{m}_i \cdot \mathbf{m}_i = 1$.

For wavelengths bigger than the magnetic length we can treat $\{\mathbf{m}_i\}$ as a continuous vector field, $\{\mathbf{m}_i\} \to \mathbf{m}(\mathbf{r})$, and replace the sums in (3.12), (3.13) by integrals:

$$\sum_i \to \int d^2 r n(\mathbf{r}) F(\mathbf{r}).$$

We find in this way the continuum approximation:

$$\begin{aligned}\mathcal{L} =& \hbar \int_A d^2 r n \dot{\mathbf{m}} \cdot \mathcal{A}[\mathbf{m}] - \frac{1}{2}\Delta_t \int_A d^2 r n m_x - \int_A d^2 r n m_x(\mathbf{r}) \int_A d^2 r' F_D(\mathbf{r}-\mathbf{r}') n(\mathbf{r}') m_x(\mathbf{r}') \\ &- \int_A d^2 r n m_y(\mathbf{r}) \int_A d^2 r' F_D(\mathbf{r}-\mathbf{r}') n(\mathbf{r}') m_y(\mathbf{r}') \\ &+ \int_A d^2 r n m_z(\mathbf{r}) \int_A d^2 r' [2H(\mathbf{r}-\mathbf{r}') - F_S(\mathbf{r}-\mathbf{r}')] n(\mathbf{r}') m_z(\mathbf{r}').\end{aligned} \tag{3.14}$$

Where $n(\mathbf{r})$ is the particle occupation number. To be consistent with the assumption of no charge fluctuations n must be simply equal to $1/2\pi l^2$. From the Euler-Lagrange equation:

$$\frac{d}{dt}\frac{\delta L}{\delta \dot{\mathbf{m}}} - \frac{\delta L}{\delta \mathbf{m}} = 0 \tag{3.15}$$

we find the following equation of motion for $\mathbf{m}$:

$$\frac{\partial \mathbf{m}}{\partial t} = \mathbf{m} \times \frac{\delta E}{\delta \mathbf{m}} \tag{3.16}$$

known in magnetism as the *Landau-Lifshitz equation*. The functions $H(\mathbf{r}-\mathbf{r}')$, $F_S(\mathbf{r}-\mathbf{r}')$, $F_D(\mathbf{r}-\mathbf{r}')$ are the continuum equivalent of H_{ij}, F^S_{ij}, F^D_{ij}. In reciprocal space, the Coulomb interactions, V_S, V_D, between electrons in the same and different layers are simply:

$$\begin{aligned} V_S(\mathbf{q}) &= \frac{2\pi e^2}{\epsilon q} \\ V_D(\mathbf{q}) &= \frac{2\pi e^2}{\epsilon q} e^{-qd} \end{aligned} \tag{3.17}$$

where ϵ is the $GaAs$ dielectric constant and $q = \sqrt{\mathbf{q}\cdot\mathbf{q}}$. From these expressions for V_S and V_D we find that in reciprocal space the kernels H, F_S, F_D are given by:

$$H(q) = \frac{e^2}{2\epsilon l}\frac{1-e^{-qd}}{q} e^{-\frac{1}{2}q^2l^2}; \tag{3.18}$$

$$F_S(q) = \frac{e^2}{2\epsilon}\int_0^\infty dp J_0(qpl^2)) e^{-\frac{1}{2}p^2l^2}; \tag{3.19}$$

$$F_D(q) = \frac{e^2}{2\epsilon}\int_0^\infty dp J_0(qpl^2)) e^{-\frac{1}{2}p^2l^2} e^{-pd} \tag{3.20}$$

where J_0 is the Bessel function.

For very long wavelengths we can simplify the Lagrangian (3.14) by keeping only the leading terms in a gradient expansion of $\mathbf{m}(\mathbf{r}-\mathbf{r}')$ around $\mathbf{r}$. Let's start from the semiclassical energy functional (3.13). We observe that we can write:

$$2m^z_i m^z_j = (m^z_i)^2 + (m^z_j)^2 - (m^z_i - m^z_j)^2; \tag{3.21}$$

and, using the fact that $\mathbf{m}_i \cdot \mathbf{m}_i = 1$:

$$\begin{aligned} 2(m_i^x m_j^x + m_i^y m_j^y) =& 2 - (m_i^z)^2 - (m_j^z)^2 - \\ & (m_i^x - m_j^x)^2 - (m_i^y - m_j^y)^2. \end{aligned} \tag{3.22}$$

Let's now approximate the differences $m_i^\alpha - m_j^\alpha$ ($\alpha = x, y, z$) by means of continuous derivatives:

$$m_i^\alpha - m_j^\alpha = \partial_\mu m(\mathbf{r})^\alpha \Delta r^\mu + \frac{1}{2}\partial_{\mu\nu} m(\mathbf{r})^\alpha \Delta r^\mu \Delta r^\nu + ... \tag{3.23}$$

where the partial derivatives are with respect to $\mathbf{r}$ and $\Delta r^\mu \equiv r'^\mu - r^\mu$. For pseudospin configurations that vary very slowly in space we can neglect all the terms with high derivatives in (3.23) and keep only the gradient term. In this approximation using equations (3.21), (3.22), we find for the long-wavelength limit of the semiclassical energy functional (3.13)

$$E_{lw} = \int d^2 r \left\{ -\frac{\Delta_t}{4\pi\ell^2} m_x + \beta (m_z)^2 + \frac{1}{2}\rho_s \left[(\nabla m_x)^2 + (\nabla m_y)^2 \right] \right\}, \tag{3.24}$$

where

$$\beta = \frac{1}{8\pi\ell^2 N_\Phi} \sum_j (2H_{ij} - F_{ij}^S + F_{ij}^D) \tag{3.25}$$

is the parameter describing the electrostatic cost of having an unbalanced bilayer and

$$\rho_s = \frac{1}{16\pi\ell^2 N_\Phi} \sum_j F_{ij}^D |\mathbf{r}_i - \mathbf{r}_j|^2 \tag{3.26}$$

is the pseudospin stiffness constant. Finally the Lagrangian in the long-wavelength approximation, takes the form:

$$\mathcal{L} = \hbar \int d^2 r n \dot{\mathbf{m}} \cdot \mathcal{A}[\mathbf{m}] + \frac{1}{2} \int d^2 r \left[\rho_s |\nabla \mathbf{m}_\perp|^2 + 2\beta m_z^2 - n\Delta_t m_x \right] \tag{3.27}$$

The Lagrangian (3.27) is the same Lagrangian that describes the dynamics of the magnetization in an easy-plane ferromagnet. In the long wavelength approximation a $\nu = 1$ quantum Hall bilayer then is very analogous to an easy plane ferromagnet.

3.5 Damping of collective modes in $\nu = 1$ quantum Hall bilayers

As mentioned in Chapter 2 in real quantum Hall systems there will always be disorder. One of the major sources of disorder is the donor ions used to dope the semiconductors in order to create the 2DEG. This disorder is unavoidable and, as seen in Chapter 2, also essential for the observation of the quantum Hall effect. In this section we consider the effect of the disorder on the damping of the pseudospin collective modes [9].

In a quantum Hall bilayer, to the random Coulomb potential there will be a contribution, V_T, from the ions placed above the top layer and a contribution, V_B, from the ions placed below the bottom layer. The disorder can be modeled by adding to the microscopic Hamiltonian (3.7) the term

$$V_d = \sum_{ij} \left[\langle i|V_T|j\rangle c^\dagger_{i\uparrow} c_{j\uparrow} + \langle i|V_B|j\rangle c^\dagger_{i\downarrow} c_{j\downarrow} \right]. \tag{3.28}$$

Implicit in (3.28) is the assumption that the disorder does not scatter electrons between the layers. In the pseudospin language this is equivalent to assume that the disorder commutes with the z component of $\mathbf{m}$. We also assume:

$$\begin{aligned} \overline{V_T} &= \overline{V_B} = 0 \\ \overline{V_T V_T} &= \overline{V_B V_B} \\ \overline{V_T V_B} &= \overline{V_B V_T} = 0 \end{aligned} \tag{3.29}$$

where the bar indicates disorder averaging. Equations (3.29) ensure that after averaging over disorder configurations the term (3.28) preserves the reflection symmetry of the bilayer. Finally we assume the disorder to be weak so that it can treated perturbatively.

Using the self consistent Born approximation (SCBA) we can calculate the correction due to disorder to the self energy of the mean-field quasiparticles. Once we have the disorder corrected self energy we can find the spectral function A from the retarded Green's function $G(\omega + i0^+)$:

$$A(\omega) = -2\mathrm{Im}G(\omega + i0^+).$$

The disorder broadens the quasiparticles spectral function around the mean-field quasiparticle energies. For strong enough disorder the spectral function becomes nonzero at the Fermi energy, [9].

When the disorder broadens the single-particle bands sufficiently to create a nonzero density of states at the Fermi energy the collective pseudospin waves can decay by creating particle hole excitations. Using the generalized random phase approximation (GRPA), [9], is possible to find the broadening of the collective excitations calculating the imaginary part of the pseudospin response function $\chi_{\mu\nu} \equiv \langle \hat{m}_\mu(\mathbf{q}, \tau)\hat{m}_\nu(0,0)\rangle$. In the low frequency long-wavelength limit we have, [9]:

$$\lim_{\omega\to 0; q\to 0} \frac{\mathrm{Im}\chi_\perp}{\omega} = \alpha_\varphi \approx 1; \tag{3.30}$$

$$\lim_{\omega\to 0; q\to 0} \frac{\mathrm{Im}\chi_{zz}}{\omega} = \alpha_z \approx 0. \tag{3.31}$$

We then find that in $\nu = 1$ quantum Hall bilayers, given the nature of the disorder, there is an anisotropy in the damping of the collective modes. In real systems there will always be a component of the disorder that does not commute with $\hat{m}_z$ making α_z not zero. It is however safe to assume that this part of the disorder will be much

smaller than the part considered in this section and so we can conclude that in $\nu = 1$ quantum Hall bilayer we expect $\alpha_z \ll \alpha_\varphi$.

Chapter 4

Equilibrium properties of $\nu = 1$ quantum Hall bilayers

4.1 Equations of motion

We saw in Chapter 3 that in the pseudospin language the Lagrangian for a Quantum Hall bilayer is given by (3.14) and the equation of motion for $\mathbf{m}$ by the Landau-Lifshitz equation. Starting from (3.14) we find the following equation of motion for $\mathbf{m}$:

$$\frac{\partial \mathbf{m}}{\partial t} = \mathbf{m} \times \mathbf{H}_{\text{eff}} \tag{4.1}$$

with $\mathbf{H}_{\text{eff}} \equiv \delta E / \delta \mathbf{m}$ given by:

$$\begin{aligned}
H_{\text{eff},x} &= \frac{2}{hl^2} \int_A d^2 r' F_D(\mathbf{r} - \mathbf{r}') m_x(\mathbf{r}') - \frac{\Delta_t}{2\hbar}; \\
H_{\text{eff},y} &= \frac{2}{hl^2} \int_A d^2 r' F_D(\mathbf{r} - \mathbf{r}') m_y(\mathbf{r}'); \\
H_{\text{eff},z} &= \frac{2}{hl^2} \int_A d^2 r' [2H(\mathbf{r} - \mathbf{r}') - F_S(\mathbf{r} - \mathbf{r}')] m_z(\mathbf{r}').
\end{aligned}$$

where A is the area of the sample. The pseudomagnetization therefore will precess around the field $\mathbf{H}_{\text{eff}}$.

We now want to include also the damping due to the coupling of the collective pseudospin modes to other degrees of freedom. As mentioned in Chapter 3 the presence of disorder causes a finite density of states at the Fermi energy and then, through the coupling of the quasiparticles to the pseudomagnetization, a damping of the collective modes. We can define two damping coefficients, α_φ, α_z and the dissipation (or Rayleigh) functional:

$$\mathcal{F} = \frac{\hbar}{2}\int_A d^2 r n[\alpha_\varphi(\dot{m}_x^2 + \dot{m}_y^2) + \alpha_z \dot{m}_x^2] \tag{4.2}$$

so that we can derive the dissipative equation of motion from the generalized Euler-Lagrange equations:

$$\frac{d}{dt}\frac{\delta L}{\delta \dot{\mathbf{m}}} - \frac{\delta L}{\delta \mathbf{m}} + \frac{\delta \mathcal{F}}{\delta \dot{\mathbf{m}}} = 0 \tag{4.3}$$

From this equation we find the following dynamical equations:

$$\begin{aligned}
\frac{\partial m_x}{\partial t} &= m_y H_{\text{eff},z} - m_z H_{\text{eff},y} + \alpha_\varphi m_y \dot{m}_x - \alpha_z m_z \dot{m}_y \\
\frac{\partial m_y}{\partial t} &= m_z H_{\text{eff},x} - m_x H_{\text{eff},z} - \alpha_\varphi m_x \dot{m}_z + \alpha_z m_z \dot{m}_x \\
\frac{\partial m_z}{\partial t} &= m_x H_{\text{eff},y} - m_y H_{\text{eff},x} + \alpha_z (m_x \dot{m}_y - m_y \dot{m}_x)
\end{aligned} \tag{4.4}$$

From microscopic calculations [9] for our problem we have $\alpha_\varphi \neq 0$, $\alpha_z \approx 0$. When $\alpha_z = 0$ we can have dynamical equilibrium solutions to equations (4.4). In real systems however α_z will always be not zero, for example because of the non uniformity of the tunneling amplitude Δ_t. We will then assume $\alpha_z \neq 0$ and $\alpha_z \ll \alpha_\varphi$.

In the long wavelength approximation we found in Chapter 3 that the La-

grangian can be simplified to:

$$\mathcal{L} = \hbar \int d^2 r n \dot{\mathbf{m}} \cdot \mathcal{A}[\mathbf{m}] + \frac{1}{2} \int d^2 r \left[\rho_s |\nabla \mathbf{m}_\perp|^2 + 2\beta m_z^2 - n\Delta_t m_x \right] \tag{4.5}$$

The equations of motion will have the same form given by (4.4) with $\mathbf{H}_{\text{eff}}$ given by:

$$\begin{aligned} H_{\text{eff},x} &= \frac{2\pi l^2}{\hbar} \rho_s \nabla^2 m_x - \frac{\Delta_t}{2\hbar} \\ H_{\text{eff},y} &= \frac{2\pi l^2}{\hbar} \rho_s \nabla^2 m_y \\ H_{\text{eff},z} &= \frac{4\pi l^2}{\hbar} \beta m_z \end{aligned} \tag{4.6}$$

In the limit of small oscillations of the pseudospin out of the plane, $m_z \ll 1$, we can write $\mathbf{m} = (\cos\varphi, \sin\varphi, m_z)$. In this case, assuming $\mathbf{m}$ uniform in space, the damped equations of motion reduce to:

$$\begin{aligned} \frac{\partial \varphi}{\partial t} &= -\frac{4\pi l^2 \beta}{\hbar} m_z - \alpha_\varphi \dot{m}_z \\ \frac{\partial m_z}{\partial t} &= \frac{\Delta_t}{2\hbar} \sin\varphi + \alpha_z \dot{\varphi}. \end{aligned} \tag{4.7}$$

Let us now consider the equations of motion for the magnetization in an easy-plane ferromagnet with external field along the x direction:

$$\begin{aligned} \frac{\partial \varphi}{\partial t} &= -K m_z - \alpha_\varphi \dot{m}_z \\ \frac{\partial m_z}{\partial t} &= \gamma H_x \sin\varphi + \alpha_z \dot{\varphi} \end{aligned} \tag{4.8}$$

where K is the anisotropy constant, and the equations that describe the dynamic

of a Josephson's junction:

$$\begin{aligned} \frac{\partial \varphi}{\partial t} &= \frac{2eV}{\hbar} \\ \frac{\partial V}{\partial t} &= -\frac{I_c}{2eC}\sin\varphi - \alpha_z \dot{\varphi} \end{aligned} \tag{4.9}$$

where φ here is the phase difference between the Ginzburg-Landau wavefunction in the two electrodes, V the potential across the junction and I_c the critical current. We see that equations (4.7)-(4.9) are the same when damping is not present. However if we include the damping terms the equations for the three systems are different: for a ferromagnet is usually assumed $\alpha_z \approx \alpha_\varphi$, for a Josephson junction $\alpha_z \neq 0$, $\alpha_\varphi \approx 0$ whereas we have seen in Chapter 3 that for a $\nu = 1$ quantum Hall bilayer is $\alpha_\varphi \neq 0$, $\alpha_z \approx 0$. This difference in the damping affects profoundly the dynamics. We believe that in general both α_φ, α_z in reals systems are always non zero even though their relative magnitude is in general quite different. The microscopic explanation of the observed values for α_φ, α_z in all three systems is a very interesting problem that is not fully understood. In Chapter 6 we address this problem for a ferromagnet for the case when the damping is mostly due to the coupling of the magnetization to elastic modes.

If we exclude the damping term, that in $\nu = 1$ quantum Hall bilayers is indirectly mostly due to the presence of disorder, the dynamical equations derived in this section do not take into account disorder. In order to consider the effects of disorder in quantum Hall bilayers we first have to introduce the concept of topological charge.

4.2 Topological Excitations

As seen in Chapter 2 in a quantum Hall system in any Landau Level the number of degenerate states is equal to the number of magnetic quantum fluxes piercing the

system. If we consider a filled Landau level and decrease the perpendicular magnetic field so that we reduce by one the number of magnetic fluxes, Fig. 4.1, keeping the total number of electrons, N, constant, we force one electron to jump to a higher Landau level where it will be able to move freely: by reducing the magnetic flux we have created a charge excitation. We see from this simple ideal experiment that in quantum Hall system there is a direct relation between magnetic flux and charge excitations. This relation can be justified more rigorously in the following way [6].

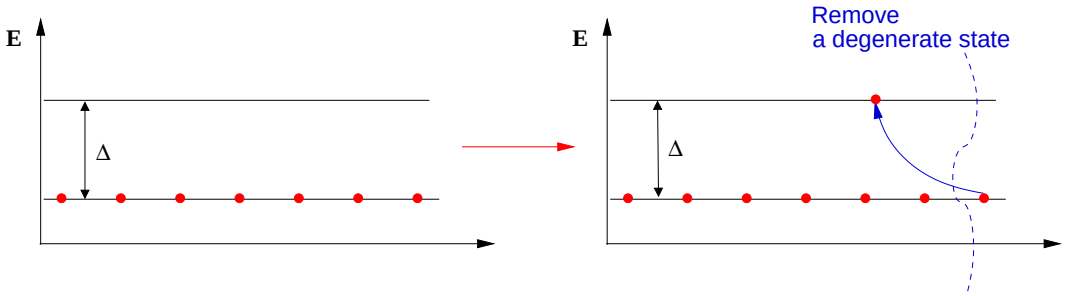

Figure 4.1: Creation of a charge excitation in a Quantum Hall system by change of the magnetic flux

Let's consider a Quantum Hall system with $N = \nu N_\phi$, $\nu = 1, 2, ...$ and let's suppose of slowly changing the magnetic flux Φ pinning the system. Because the Landau levels are perfectly filled if we change the magnetic flux on time scales bigger than $\hbar/\Delta$, where Δ is the energy spacing between Landau levels, we have no dissipation:

$$\rho_{xx} = \rho_{yy} = \sigma_{xx} = \sigma_{yy} = 0.$$

From Faraday's law we have that the change in magnetic flux will induce an electric field such that:

$$\oint_\Gamma \mathbf{E} d^2 r = -\frac{1}{c}\frac{\partial \Phi}{\partial t} \tag{4.10}$$

Through the conductivity we can now relate the electric field to a current. What is

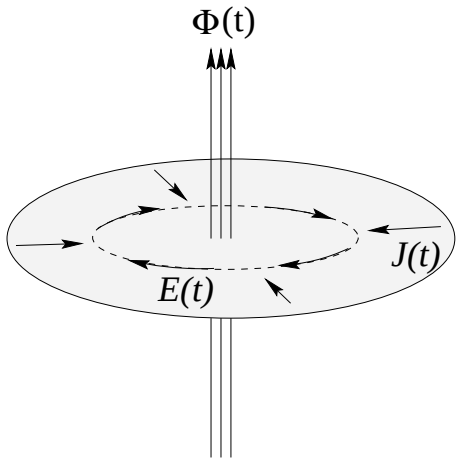

Figure 4.2: Radial current induced by a poloidal electric field in Quantum Hall system

peculiar about the quantum Hall system at filled Landau levels is that the poloidal electric field given by (4.10) will induce a radial current and not a poloidal one because the longitudinal conductivity is zero but the Hall conductivity is not: $\sigma_{xy} = \nu e^2/h$, Fig. 4.2. We then have $\mathbf{E} = \rho_{xy}\mathbf{J} \times \mathbf{z}$ that combined with (4.10) gives us:

$$\oint_{\Gamma} \mathbf{J} \cdot (\mathbf{z} \times d\mathbf{r}) = \sigma_{xy} \frac{1}{c} \frac{\partial \Phi}{\partial t} \tag{4.11}$$

But the left hand side of (4.11) is the charge entering the area surrounded by the contour Γ and we then finally find:

$$\frac{dQ}{dt} = \frac{1}{c}\sigma_{xy}\frac{\partial \Phi}{\partial t} \implies \Delta Q_{\phi} = \nu e \frac{\Delta \Phi}{\Phi_0} \tag{4.12}$$

Equation (4.12) establishes the relation between charge and magnetic flux in a quantum Hall system.

Let's now consider a pseudospin quasiparticle traveling through a $\nu = 1$ quantum Hall bilayer. The quasiparticle will have pseudospin, S, pointing up when

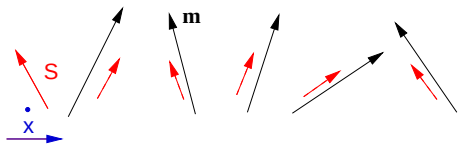

Figure 4.3: Pseudospin moving through the pseudomagnetization field.

localized in the top layer and pointing down when localized in the bottom layer. Let's assume that S aligns instantaneously at every point to the local value of the order parameter $\mathbf{m}$ as shown in Fig. 4.3. We can then write:

$$\dot{S}^\mu = S\dot{x}^\nu \frac{\partial m^\mu}{\partial x^\nu}; \qquad \mu, \nu = x, y, z$$

For the Lagrangian density we then have:

$$\begin{aligned}\mathcal{L} &= \hbar \dot{S}^\mu \mathcal{C}^\mu - \frac{e}{c}\dot{x}^\nu A_\nu + \mathcal{L}_0 \\ &= -\frac{e}{c}\dot{x}^\nu \left[-\frac{\Phi_0}{2\pi} S \frac{\partial m^\mu}{\partial x^\nu}\mathcal{C}^\mu + A_\nu \right] + \mathcal{L}_0;\end{aligned}$$

where $\mathbf{A}$ is the vector potential, $\mathcal{C}[\mathbf{m}]$ is definend through the equation $\nabla_{\mathbf{m}} \times \mathcal{C} = \mathbf{m}$ and $\mathcal{L}_0$ is the part of the Lagrangian that doesn't depend on $\dot{S}$ and $\mathbf{A}$. We see that because of the nonuniformity of the pseudospin texture, in the Lagrangian density we have an additional term akin to a vector potential,

$$c^\nu \equiv -\frac{\Phi_0}{2\pi} S \frac{\partial m^\mu}{\partial x^\nu}\mathcal{C}^\mu.$$

The field c^ν is called Berry connection and to it we can associate a fictitious magnetic

flux,

$$\begin{aligned}\Phi &= \epsilon^{\alpha\beta}\frac{\partial c^{\alpha}}{\partial x^{\beta}} \\ &= -\frac{\Phi_0}{2\pi}S\frac{1}{2}\epsilon^{\alpha\beta}\frac{\partial m^{\nu}}{\partial x^{\beta}}\frac{\partial m^{\gamma}}{\partial x^{\alpha}}\left[\frac{\partial \mathcal{A}^{\nu}}{\partial m^{\gamma}} - \frac{\partial \mathcal{A}^{\gamma}}{\partial m^{\nu}}\right]\end{aligned}$$

From the definition of $\mathcal{C}$ we have that $\nabla_{\mathbf{m}} \times \mathcal{C} = \mathbf{m}$ so that

$$\frac{\partial \mathcal{C}^{\nu}}{\partial m^{\gamma}} - \frac{\partial \mathcal{C}^{\gamma}}{\partial m^{\nu}} = \epsilon^{a\nu\gamma}m^{a}$$

We can then write:

$$\begin{aligned}\Phi_T &= -\Phi_0\left[\frac{S}{4\pi}\epsilon^{\alpha\beta}\epsilon^{a\nu\gamma}m^{a}\frac{\partial m^{\nu}}{\partial x^{\beta}}\frac{\partial m^{\gamma}}{\partial x^{\alpha}}\right] \\ &= -\Phi_0\frac{S}{4\pi}\epsilon^{ij}\mathbf{m}\cdot(\partial_i\mathbf{m}\times\partial_j\mathbf{m})\end{aligned}$$

A quasiparticle traveling through the quantum Hall bilayer will see an effective magnetic flux proportional to $\epsilon^{ij}\mathbf{m}\cdot(\partial_i\mathbf{m}\times\partial_j\mathbf{m})$. This effective magnetic flux is due to the Berry phase that the quasiparticle acquires while traveling through the pseudomagnetization field while aligning its pseudospin to the local value of $\mathbf{m}$.

We have shown before that to a magnetic flux in a Quantum Hall system corresponds a charge density through the relation (4.12). We then arrive to the important result that to the flux Φ_T corresponds the charge density:

$$\rho_T \equiv \nu e\frac{S}{4\pi}\epsilon^{ij}\mathbf{m}\cdot(\partial_i\mathbf{m}\times\partial_j\mathbf{m}). \tag{4.13}$$

In our case is $S = 1/2$ and $\nu = 1$. We have that certain excitations of the field $\mathbf{m}$ from its equilibrium uniform configuration can have charge density. This remarkable connection between charge and pseudospin excitations is peculiar to $\nu = 1$ quantum Hall bilayers [25], [26], [27], [28], [29], [30].

An important characteristic of the charge density (4.13) is that twice the total charge

$$2Q_T = 2\frac{e}{8\pi}\int d^2r\epsilon^{ij}\mathbf{m}\cdot(\partial_i\mathbf{m}\times\partial_j\mathbf{m})$$

is always an integer. As a matter of fact Q_T is a topological invariant.The fact that Q_T is a topological invariant can be shown using the following general theorem [31].

Theorem 4.2.1. *Let* $\mathbf{y} = (y_1, ...y_n)$ *be a n-dimensional* $\mathcal{C}^\infty$ *vector field defined on a d-dimensional space-time such that* $\langle\mathbf{y}|\mathbf{y}\rangle \equiv y_1^2 + ... + y_n^2 = 1$. *Then if* $n \leq d$,

$$\epsilon^{\mu_1..\mu_n..\mu_d}\epsilon_{\alpha_1...\alpha_n}y^{\alpha_1}\partial_{\mu_2}y^{\alpha_2}...\partial_{\mu_n}y^{\alpha_n} \tag{4.14}$$

is a non-dynamical conserved quantity (space-time current).

Proof. Because $\langle\mathbf{y}|\mathbf{y}\rangle = 1$ we have that $\langle\mathbf{y}|\partial_\mu\mathbf{y}\rangle = 0$. Thus if $n \leq d$, the $d\times n$ matrix $[\partial\mathbf{y}]$ must have a rank smaller than n, i.e.:

$$\epsilon^{\mu_1..\mu_n..\mu_d}\epsilon_{\alpha_1...\alpha_n}\partial_{\mu_1}y^{\alpha_1}...\partial_{\mu_n}y^{\alpha_n} = 0$$

or

$$\partial_{\mu_1}\left[\epsilon^{\mu_1..\mu_n..\mu_d}\epsilon_{\alpha_1...\alpha_n}y^{\alpha_1}\partial_{\mu_2}y^{\alpha_2}...\partial_{\mu_n}y^{\alpha_n}\right] = 0$$

q.e.d.

Notice that the fact that the quantity (4.14) is conserved does not depend on the dynamics of the field $\mathbf{y}$ but is simply due to the fact that the vector field is at every point in space and time constrained to have unit magnitude and be $\mathcal{C}^\infty$. For this reason the conserved quantities (4.14) are called topological invariants: any smooth deformation of the vector field will not change them.

For our specific case we have $n = d = 3$ and $\mu = t, x, y$, $\alpha = x, y, z$. From

the theorem 4.2.1 we can immediately find that the time-space current

$$\mathcal{J} \equiv [\rho; \mathbf{J}_T] \equiv \frac{e}{8\pi}[\mathbf{m} \cdot (\partial_x \mathbf{m} \times \partial_y \mathbf{m}); \mathbf{m} \cdot (\partial_t \mathbf{m} \times \partial_y \mathbf{m}), \mathbf{m} \cdot (\partial_x \mathbf{m} \times \partial_t \mathbf{m}), 0]$$

is conserved, i.e.:

$$\frac{\partial \rho_T}{\partial t} + \nabla \cdot \mathbf{J}_T = 0 \tag{4.15}$$

From equation (4.15) we recover that Q_T is a topological invariant and we can define the topological current $\mathbf{J}_T$

$$\mathbf{J}_T \equiv \frac{e}{8\pi}[\mathbf{m} \cdot (\partial_t \mathbf{m} \times \partial_y \mathbf{m}), \mathbf{m} \cdot (\partial_x \mathbf{m} \times \partial_t \mathbf{m}), 0]$$

The current $\mathbf{J}_T$ represents the contribution of the topological charges to the charge current in $\nu = 1$ quantum Hall bilayers.

In a $\nu = 1$ quantum Hall bilayer the topological charges are called merons. Merons are the equivalent of vortices in the XY nonlinear sigma model. A meron has a charge $e^* = \pm 1/2e$. Far away from the core of a meron the order parameter lies in the XY plane forming a vortex configuration with positive or negative vorticity. In the core of the vortex the order parameter $\mathbf{m}$ rotates either up or down out of the XY plane. In a bilayer a meron is the pseudospin configuration with minimum *gradient energy* given the constraint of vorticity. We then have four different types of merons depending on the vorticity sign and the direction of m_z in the vortex core as shown in Fig. 4.4. The charge of the meron is determined by the product of the vorticity winding number and the value of m_z at the center of the core according to the formula

$$Q = -\frac{1}{2} n_v m_z(0)$$

where n_v is the winding number and $m_z(0)$ the value of m_z at the vortex core.

Let's consider a single meron placed at the origin. Because of the high energy

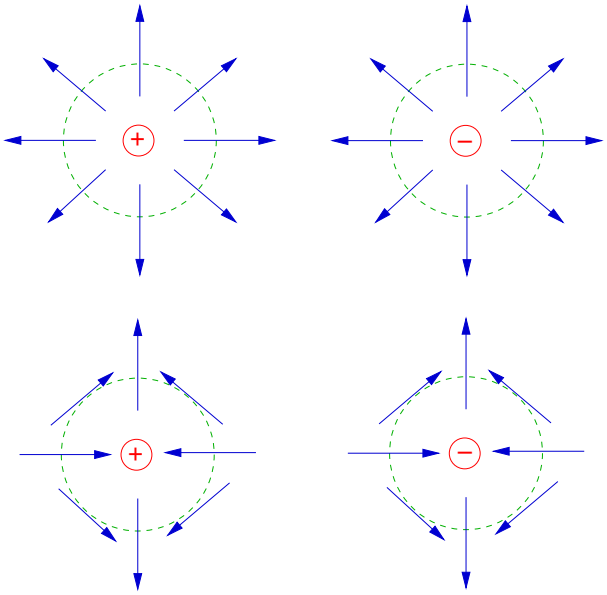

Figure 4.4: Schematic illustration of the order parameter configuration for different types of merons.

cost of creating a charge imbalance between the two layers we have that at infinite distances m_z must be zero. On the other hand the configuration of $\mathbf{m}$ at infinite distance must be continuously connected with the configuration at the center. This implies that for $r \to \infty$ $\mathbf{m}$ will have the form $(\cos\varphi; \sin\varphi, 0)$ with φ the poloidal angle in the XY plane. This configuration will have a big energy cost due to exchange as can be seen for example from (3.24). In the thermodynamic limit therefore it costs an infinite amount of energy to create a single meron. On the other hand to create a meron pair, meron-antimeron, it takes a finite energy [25]

$$E_{\mathrm{m-am}} = 2E_{\mathrm{core}} + \frac{e^2}{4R} + 2\pi \ln(R/R_{\mathrm{core}})$$

where E_{core}, R_{core} are the core energy and radius respectively of an isolated meron, and R the distance between the meron and the antimeron. What is really important for us is that for a $\nu = 1$ quantum Hall bilayer the energy, $E_{\mathrm{m-am}}$, to create a

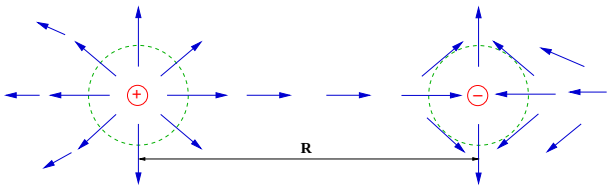

Figure 4.5: Schematic illustration of a meron-antimeron configuration

meron antimeron pair is lower, about half, the energy of a conventional quasiparticle excitation. In particular to create a meron antimeron pair with total charge zero requires less energy than to create a conventional particle-hole excitation.

4.3 Inclusion of disorder

In this section we investigate the effects of disorder on the equilibrium properties of $\nu = 1$ quantum Hall bilayers. As mentioned in Chapter 3 disorder is always present in these systems and plays an important role.

We first have to generalize the Lagrangian (3.14) to include terms due to the interaction of the order parameter with the disorder potential. The donor ions will create a random Coulomb potential in the top layer, V_T, and bottom layer V_B. We can decompose the total random potential seen by the condensate in a symmetric and antisymmetric part

$$V_S(\mathbf{r}) \equiv \frac{1}{2}(V_T(\mathbf{r}) + V_B(\mathbf{r}))$$
$$V_A(\mathbf{r}) \equiv \frac{1}{2}(V_T(\mathbf{r}) - V_B(\mathbf{r})).$$

As schematically illustrated in Fig. 4.6 the antisymmetric part of the disorder will tend locally to create a charge imbalance between the two layers, i.e., in the pseudospin language, to tilt $\mathbf{m}$ out of the plane. As a consequence in order to take

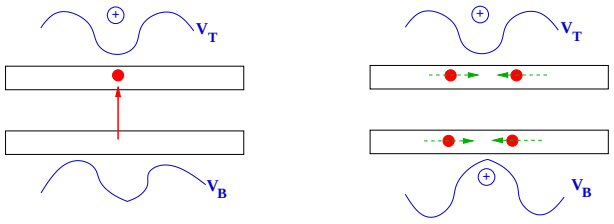

Figure 4.6: Schematic illustration of the effect of disorder on the order parameter

into account the effect of V_A we should add to the Lagrangian (3.14) the term

$$\int_A nV_A(\mathbf{r})m_z(\mathbf{r})d^2r.$$

On the other hand the symmetric part of the disorder potential will tend to change locally the charge density. If we assume the correlation length of the disorder potential to be much bigger than the magnetic length l then we can assume that the symmetric part of the disorder potential will be mostly screened by the topological charges described in section 4.2, given that is energetically cheaper to create a topological charge excitation than a conventional quasiparticle excitation. In order to take into account the effect of the symmetric part of the disorder potential we will then add to the Lagrangian (3.14) the term

$$\int_A nV_S(\mathbf{r})\rho_T(\mathbf{r})d^2r = \frac{e}{8\pi}\int_A nV_S(\mathbf{r})\mathbf{m}\cdot(\partial_x\mathbf{m}\times\partial_y\mathbf{m})d^2r.$$

This term is analogous to the one used to study dirty quantum Hall ferromagnets [32], [33].

Similarly, if we want to consider quantum Hall bilayers with filling factor $\nu = 1 \pm \epsilon$, for $\epsilon \ll 1$ we could assume the charge difference from the $\nu = 1$ state to be equal to the average topological charge: $\langle\rho_T\rangle = \epsilon$.

Finally we will have to take into account the Coulomb interaction between

the topological charges

$$\int_A d^2r \int_A d^2r' \frac{\rho_T(\mathbf{r})\rho_T(\mathbf{r}')}{|\mathbf{r}-\mathbf{r}'|}$$

The final form of the Lagrangian will then be:

$$\begin{aligned}
\mathcal{L} =& \hbar \int_A d^2r n \dot{\mathbf{m}} \cdot \mathcal{A}[\mathbf{m}] - \frac{\Delta_t}{2} \int_A d^2r n m_x - \int_A d^2r n \int_A d^2r' m_x(\mathbf{r}) F_D(\mathbf{r}-\mathbf{r}') n(\mathbf{r}') m_x(\mathbf{r}') \\
& - \int_A d^2r n \int_A d^2r' m_y(\mathbf{r}) F_D(\mathbf{r}-\mathbf{r}') n(\mathbf{r}') m_y(\mathbf{r}') \\
& + \int_A d^2r n \int_A d^2r' m_z(\mathbf{r}) [2H(\mathbf{r}-\mathbf{r}') - F_S(\mathbf{r}-\mathbf{r}')] n(\mathbf{r}') m_z(\mathbf{r}') \\
& + \int_A n V_A(\mathbf{r}) m_z(\mathbf{r}) d^2r \\
& + \frac{e}{8\pi} \int_A n V_S(\mathbf{r}) \mathbf{m} \cdot (\partial_x \mathbf{m} \times \partial_y \mathbf{m}) d^2r \\
& + \int_A d^2r \int_A d^2r' \frac{\rho_T(\mathbf{r})\rho_T(\mathbf{r}')}{|\mathbf{r}-\mathbf{r}'|}. \qquad (4.16)
\end{aligned}$$

In the remainder we will neglect the effect of the Coulomb interaction between topological charges.

4.4 Critical disorder

In this section we calculate the ground state and its properties for a $\nu = 1$ quantum Hall bilayer in presence of disorder. As shown in the previous section what is really peculiar about the system under study is the fact that particular excitations of the order parameter are characterized by non uniform charge density with the result that an external Coulomb potential affects the pseudomagnetization configuration.

In order to find the ground state we start from a random configuration for the order parameter field, $\mathbf{m}$, and then evolve the damped equations of motion (4.4) until the right hand side becomes smaller than a fixed threshold for which we can assume that an equilibrium has been reached. Once the equilibrium is reached we calculate the average properties. One of the most important average quantities is

the site-averaged pseudomagnetization $\langle \mathbf{m} \rangle$:

$$\langle \mathbf{m} \rangle \equiv \frac{1}{A} \int_A d^2 r \mathbf{m}(\mathbf{r}).$$

In particular we are interested in how the disorder affects the magnitude of the site-averaged magnetization. For this purpose we repeat the simulations for different disorder strengths. For the disorder potentials, V_A, V_S, we assume random Gaussian distributions such that:

$$\langle V_A \rangle = 0; \qquad \langle V_S \rangle = 0; \tag{4.17}$$

$$\langle V_A(\mathbf{r}) V_A(\mathbf{r}') \rangle = V_{A0} \exp\left[\frac{-(\mathbf{r}-\mathbf{r}')^2}{2\lambda_A^2}\right]; \quad \langle V_S(\mathbf{r}) V_S(\mathbf{r}') \rangle = V_{S0} \exp\left[\frac{-(\mathbf{r}-\mathbf{r}')^2}{2\lambda_S^2}\right]; \tag{4.18}$$

where the angle brackets denote average over different random configurations, V_{A0}, V_{S0}, are constants and λ_A, λ_S are the correlation lengths of the disorder. For our approach to be consistent we must assume $\lambda_A, \lambda_S \gg l$. In the remainder we will also assume $\lambda_A = \lambda_S$. To satisfy equations (4.17), (4.18) we choose [34]

$$\langle V_i(\mathbf{q}) V_i(\mathbf{q}') \rangle = \delta(\mathbf{q}-\mathbf{q}') G_i(\mathbf{q})$$

where $i = A, S$ and

$$V_i(\mathbf{q}) = \frac{1}{2\pi} \int V_i(\mathbf{r}) \mathrm{e}^{-i\mathbf{q}\cdot\mathbf{r}} d^2 r$$

$$G_i(\mathbf{q}) = \frac{V_{i0}}{2\pi} \int \exp\left[\frac{-(\mathbf{r}-\mathbf{r}')^2}{2\lambda_i^2}\right] \mathrm{e}^{-i\mathbf{q}\cdot\mathbf{r}} d^2 r = V_{i0} \lambda_i \sqrt{2\pi} \exp\left[-2(\pi\lambda_i q)^2\right].$$

Fig. 4.7 shows a typical profile for the disorder potential for a correlation length equal to 5 l.

In Fig. 4.8 the magnitude of the equilibrium site-averaged magnetization is shown as a function of the disorder strength for three different cases. The green curve shows the result when only the antisymmetric part of the disorder is present;

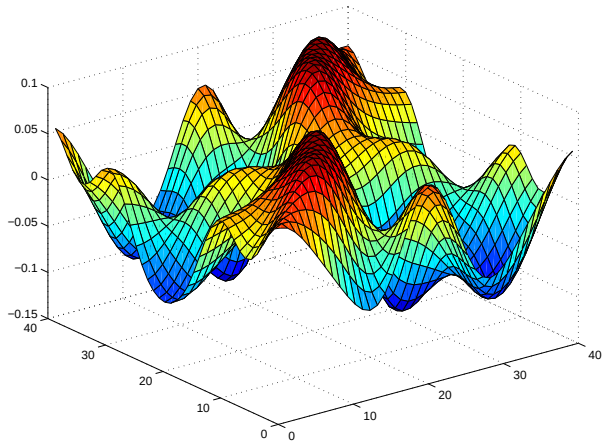

Figure 4.7: Example of disorder configuration used in the simulations. In particular in this figure the antisymmetric part of the disorder, V_A, is shown.

the blue curve the case when only the symmetric part is present and the red curve when both the symmetric and antisymmetric part of the disorder are present and of the same order of magnitude.

We immediately see that the antisymmetric part of the disorder alone has little effect in destroying the overall phase coherence of the order parameter: the pseudomagnetization slightly tilts out of the plane to follow V_A but this has little effect on the magnitude of the site-averaged pseudomagnetization.

When the symmetric part of the disorder is present we have that, past a critical value of the disorder strength, of the order of $0.25\mathrm{e}^2/\epsilon l$, the site-averaged pseudomagnetization becomes much smaller than one and the average coherence is reduced. This is the effect of the formation of topological charges that are created to screen out V_S. What is really interesting is the difference between the blue and the red curve. We see that when in addition to V_S is present also the antisymmetric part of the disorder the critical disorder is much lower. This is due to the fact that in order to create a meron pair we have to pay the activation energy for the core. This energy is in great part the anisotropy energy paid to tilt $\mathbf{m}$ out of the plane

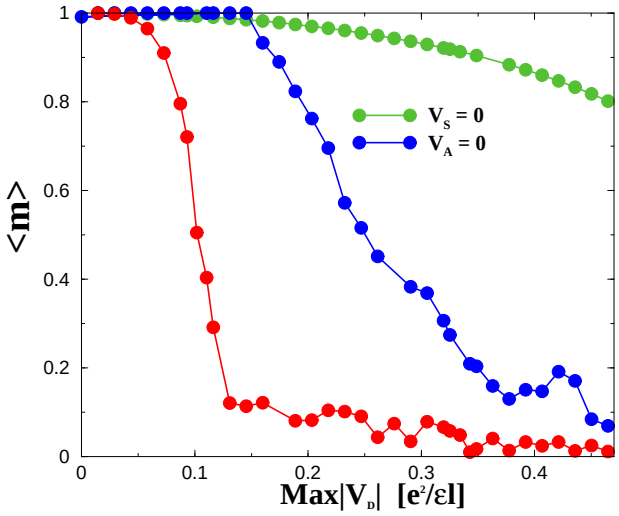

Figure 4.8: Magnitude of the site-averaged pseudomagnetization as a function of the disorder strength for three different cases. For this simulation we assumed $\Delta_t = 10^{-4}\mathrm{e}^2/\epsilon l$. Green curve: $V_A \neq 0$, $V_S = 0$. Blue curve: $V_A = 0$, $V_S \neq 0$. Red curve: $V_A \neq 0$, $V_S \neq 0$.

at the center of the meron. When V_A is different from zero there are regions of the sample where this energy is lower and then the formation of the meron is favored. When both V_S and V_A are not zero, merons will be formed in regions where the net gain between the energy gained by screening V_S and the energy paid by tilting $\mathbf{m}$ out of the plane at the center of the merons is maximized. We see that when both V_S and are V_A are present the value of the critical disorder is reduced to $\approx 0.1\mathrm{e}^2/\epsilon l$ compared to $0.25\mathrm{e}^2/\epsilon l$ when only V_S is present.

In our system the tunneling amplitude, Δ_t, plays the same role of a magnetic field along the x direction in an easy plane ferromagnet. For our system the equivalent of the magnetic susceptibility can be defined as:

$$\chi \equiv \frac{\partial \langle |\mathbf{m}| \rangle}{\partial \Delta_t}$$

We calculate χ from the change in site-averaged pseudo-magnetization, $\delta\langle|\mathrm{m}|\rangle$ as we

change the tunneling amplitude by a little amount $\delta\Delta_t$:

$$\chi \approx \frac{\delta\langle|\mathrm{m}|\rangle}{\delta\Delta_t}.$$

In Fig. 4.9 we show the results for the susceptibility χ as a function of the disorder strength calculated assuming $\Delta_t = 10^{-4}e^2/\epsilon l$ and $\delta\Delta_t = 5 \times 10^{-5}e^2/\epsilon l$ for the case when $V_S \approx V_A$. We can identify the critical disorder, V_c, as the value for

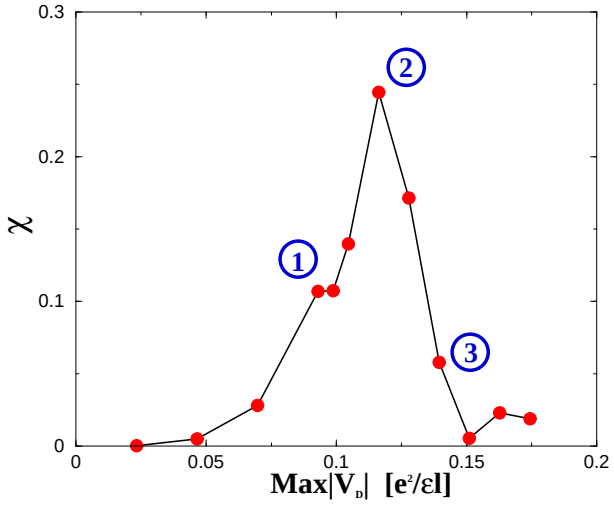

Figure 4.9: Susceptibility χ as a function of the disorder strength.

which the susceptibility χ has a maximum. From Fig. 4.9 we see that χ peaks at $V_c = 0.12\ \mathrm{e}^2/\epsilon l$.

For values of the disorder strength below V_c the the ground state is characterized by overall phase coherence: there are no vortices, or very few, the in plane component of **m** points on average in the x direction because of the biasing effect due to small but finite tunneling amplitude Δ_t, and the z component almost perfectly follows the asymmetric part of the disorder potential V_A. Fig. 4.10 shows the in plane components of **m** for a disorder strength equal to $V_D = 0.1\mathrm{e}^2/\epsilon l$, point 1 in Fig. 4.9, just below the critical disorder. We see that the texture for the in

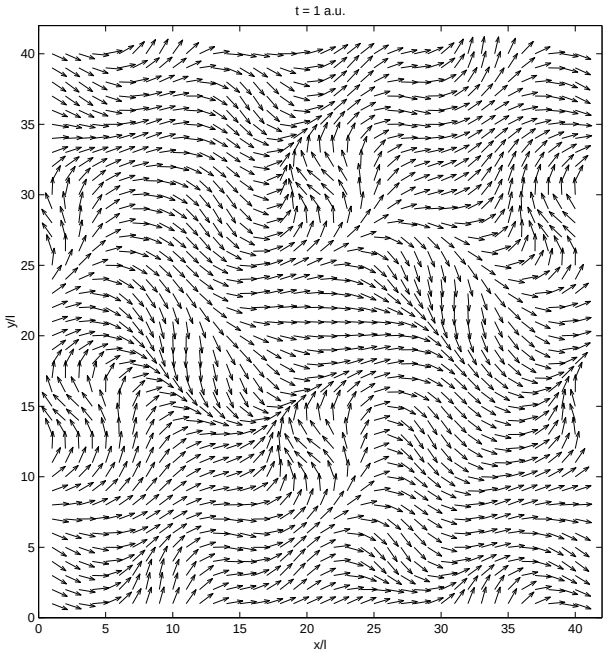

Figure 4.10: In-plane components of the pseudomagnetization **m** for a disorder strength below the critical disorder, point 1 on Fig. 4.9

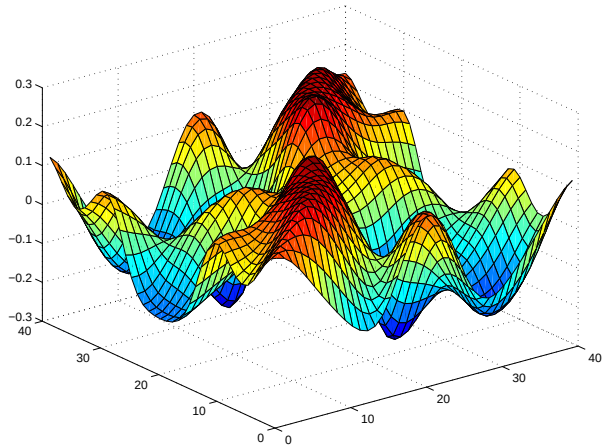

Figure 4.11: z component of the pseudomagnetization **m** for a disorder strength below the critical disorder, point 1 on Fig. 4.9. The profile of V_A used for this simulation is shown in Fig.4.7.

plane components is deformed from the situation $\mathbf{m}(\mathbf{r}) = (1; 0, 0)$ that we have for no disorder, but still we don't have any meron. Fig. 4.11 shows the z component of $\mathbf{m}$ for the same simulation for which the profile of V_A is the one shown in Fig. 4.7. We see that m_z simply follows V_A. For disorder strengths of the order of V_c or

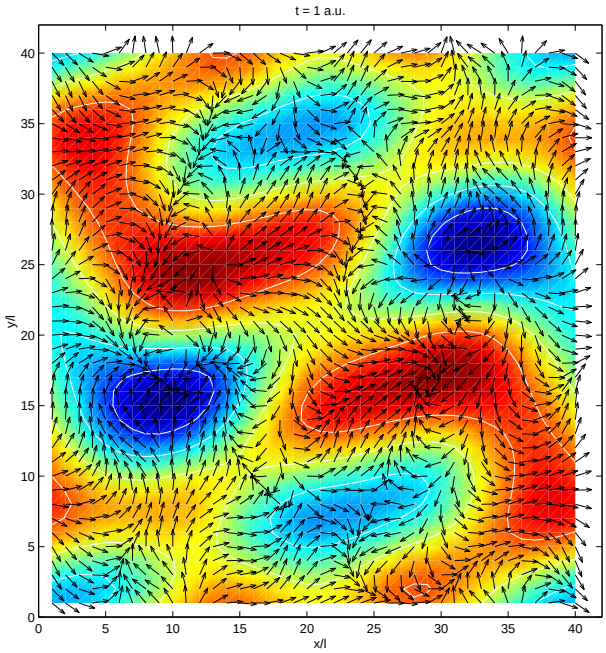

Figure 4.12: In-plane components of the pseudomagnetization $\mathbf{m}$ superimposed to the color-plot of V_S for a disorder strength equal to the critical disorder, point 2 on Fig. 4.9

bigger merons will be formed. This can be seen in Fig. 4.12 in which the in-plane components of $\mathbf{m}$ are plotted for a disorder strength equal to V_c, point 2 on Fig.4.9. The over-imposed color-plot shows the profile of the symmetric part of the potential. We can see that the merons are formed close to maxima and minima of V_S in order to screen it out. This can perhaps seen more clearly in in Fig. 4.13 where the profile of the topological charge density $\rho_T(\mathbf{r})$ is shown as a color-plot over-imposed to the level curves of V_S. We see that the maxima and minima of $\rho_T(\mathbf{r})$ are close to the

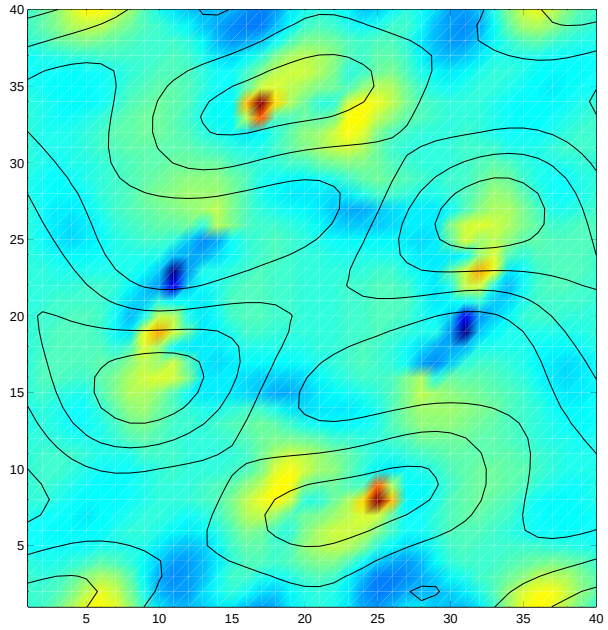

Figure 4.13: Color plot of the topological charge density $\rho_T(\mathbf{r})$ for point 2 on Fig. 4.9. The black curves are the level curves of the symmetric part of the disorder V_S.

ones of V_S but don't overlap completely. The reason is that, as mentioned above, the system has to find the best compromise between screening V_S and the energy cost of the vortex cores, cost that is minimized by placing the cores in regions where V_A is big. The z component of the magnetization still simply follows the profile of V_A as can be seen in Fig. 4.14.

Above the critical disorder V_c many vortices are present and the ground state almost completely loses any coherence. Fig. 4.15 4.16 4.17 show the in-plane magnetization,, the topological charge density ρ_T, and the z component of $\mathbf{m}$ respectively, for a disorder strength bigger than V_c, point 3 on Fig. 4.9.

If in (4.16) we replace the part that does not depend on the disorder with its equivalent long-wavelength approximation, (3.27), we find similar results but underestimate the value of the critical disorder. In Fig. 4.18 the site-averaged pseu-

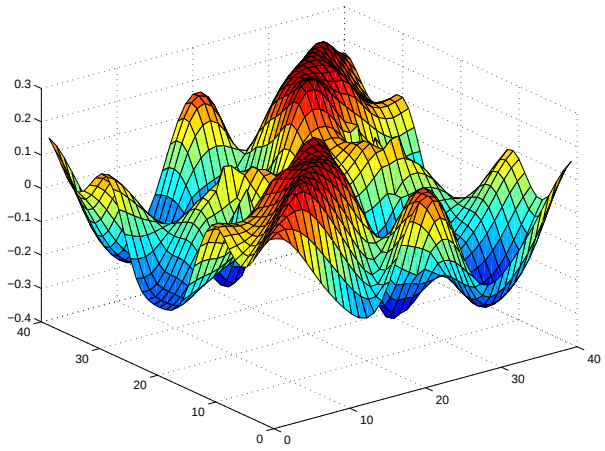

Figure 4.14: z component of the pseudomagnetization $\mathbf{m}$ for a disorder strength equal to the critical disorder, point 2 on Fig. 4.9. The profile of V_A used for this simulation is shown in Fig.4.7.

domagnetization calculated for the ground state obtained using the long wavelength approximation is plotted as a function of the disorder strength. We find that in the long-wavelength approximation the critical disorder is $V_c \approx 30\rho_s \approx 3 \times 10^{-2} e^2/\epsilon l^2$, about four times smaller than the value found using (4.16).

4.5 On the Kosterlitz-Thouless phase transition

Until now we have considered the equilibrium properties of the $\nu = 1$ quantum Hall bilayer at zero temperature. In this section we want to briefly study what is the effect of a finite temperature on the equilibrium state of our system.

Consider the semiclassical energy functional (3.24); in the limit of $\beta l^2 \gg \rho_s$ the fluctuations of m_z out of the XY plane will be very small. If we then integrate out the finite frequency fluctuations of m_z in a Gaussian approximation we recover

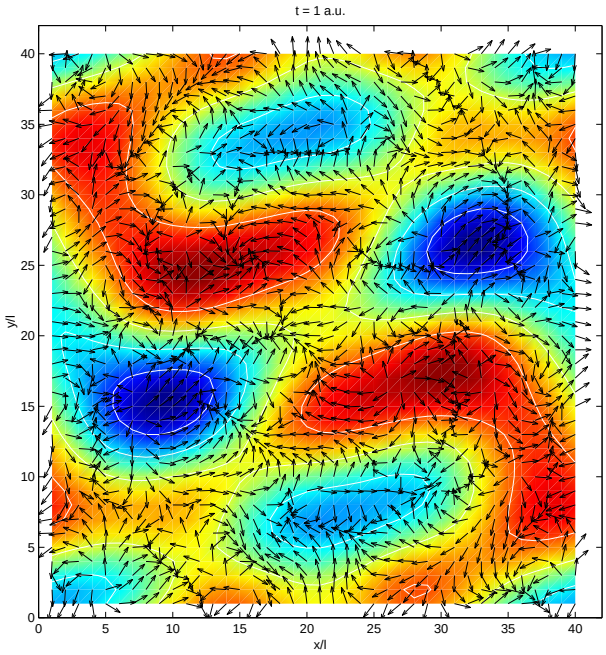

Figure 4.15: In plane components of the pseudomagnetization **m** superimposed to the color-plot of V_S for a disorder strength bigger than the critical disorder, point 3 on Fig. 4.9

an effective XY model [25] with effective action:

$$S^E_{\text{eff}} = \frac{1\rho_s}{2k_BT}\int_A d^2r|\nabla\varphi|^2.$$

which is the effective euclidean action for an XY ferromagnet. We know that the XY model undergoes a Kosterlitz-Thouless phase transition [35], [36] at a temperature T_{KT}:

$$T_{KT} = \frac{\pi}{2}\rho_s. \tag{4.19}$$

The transition separates a state characterized by superfluidity, at low temperature, from the normal state at high temperature. The supercurrent $\mathbf{J}_s$ is formally equal to $\rho_s\nabla\varphi$. In our case the pseudospin supercurrent is the difference of the number

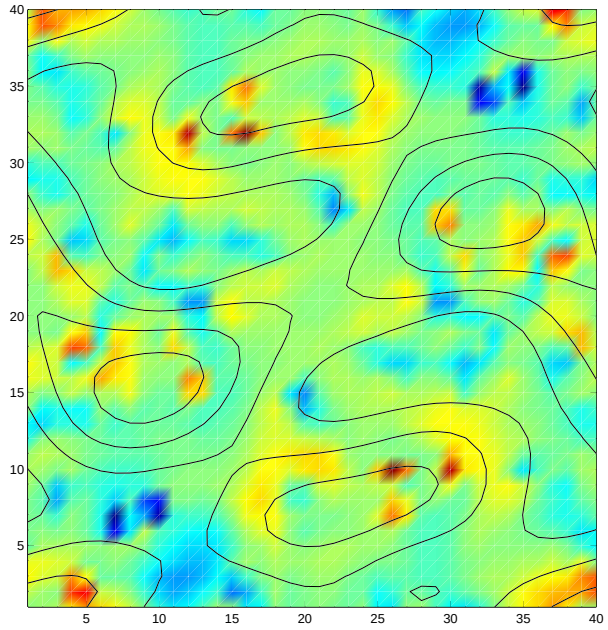

Figure 4.16: Color plot of the topological charge density $\rho_T(\mathbf{r})$ for a disorder strength above the critical disorder, point 3 on Fig. 4.9. The black curves are the level curves of the symmetric part of the disorder V_S.

current in the two layers. $\mathbf{J}_s$ is a neutral current, using the exciton analogy [17] $\mathbf{J}_s$ is the current of the excitonic condensate. Vortex-antivortex polarization renormalizations of the pseudospin stiffness ρ_s cause corrections to the expression (4.19) for T_{KT}. Thermal and quantum fluctuations also renormalize ρ_s [37]. The magnitude of the corrections to (4.19) depends on the details of the short-range physics. For the 2D nearest-neighbor-coupling XY model on a square lattice we have:

$$T_{KT} \approx 0.9\rho_s. \tag{4.20}$$

In our case the value of T_{KT} will be further reduced by fluctuations of the pseudospin order parameter out of the XY plane. However numerical studies [25, 38] show that these corrections are important only for very weak anisotropy: $\beta\ell^2 < 0.1\rho_s$. Such

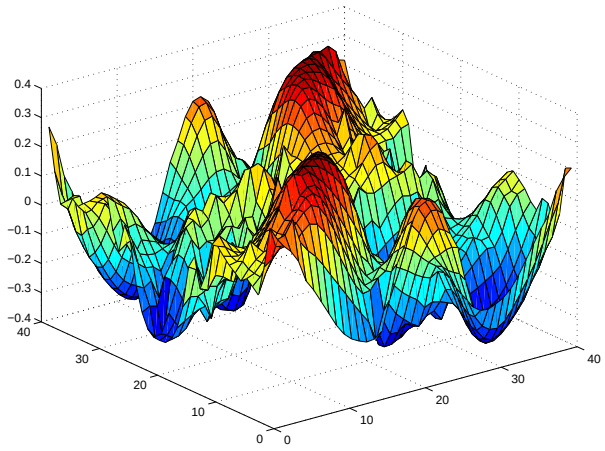

Figure 4.17: z component of the pseudomagnetization $\mathbf{m}$ for a disorder strength above the critical disorder, point 3 on Fig. 4.9. The profile of V_A used for this simulation is shown in Fig.4.7.

weak anisotropies occur in $\nu = 1$ quantum Hall bilayers only for $d < 0.3\ell$ [25], a regime which is not experimentally accessible.

In analogy to what happens in XY models we should then expect to be able to observe a Kosterlitz-Thouless phase transition in $\nu = 1$ quantum Hall bilayers connected with the unbinding of meron-antimeron pairs. However in experiments no sign of a Kosterlitz-Thouless phase transition has been observed so far. The most likely reason for lack of experimental observation of a Kosterlitz-Thouless phase transition in $\nu = 1$ quantum Hall bilayers is disorder. In presence of strong disorder the phase coherence is lost and therefore the vortex pairs appear to be separated by the disorder. For enough strong disorder then the system doesn't undergo a Kosterlitz-Thouless phase transition at any finite temperature.

One possible way to find T_{KT} would be to look for the temperature for which the supercurrent goes to zero. This however is a quite challenging task given that we want to study the case of strong disorder. We then follow a different approach [39]. We first calculate the order parameter configuration assuming periodic boundary

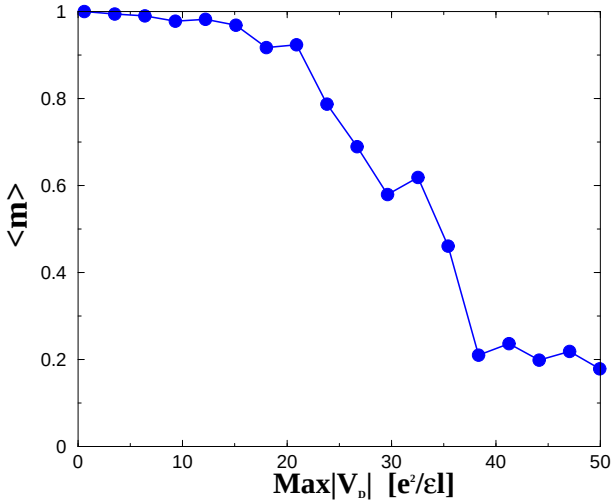

Figure 4.18: Site-averaged pseudomagnetization as a function of the disorder strength for the ground state calculated using the long-wavelength approximation for the energy functional, Eq. (3.24).

conditions. Starting from this equilibrium configuration we take the values of $\mathbf{m}$ at one edge of the system and rotate them by an angle θ. We then find the new equilibrium keeping the values of $\mathbf{m}$ at the edge where we rotated them by θ, and at the opposite edge, fixed. We define the helicity modulus η [39] as:

$$\eta(T) \equiv \frac{F(\theta) - F(0)}{2\theta^2}. \tag{4.21}$$

where $F(\theta)$ is the free energy of the *twisted* configuration and $F(0)$ the free energy of the equilibrium obtained using periodic boundary conditions. At the Kosterlitz-Thouless phase transition, in the thermodynamic limit, the helicity modulus has a finite jump, Fig. 4.19. We can then use use the dependence of η on the temperature to locate T_{KT}. However this is also not an easy task, given that in order to calculate the free energy we have to calculate the entropy. Starting from the definition (4.21)

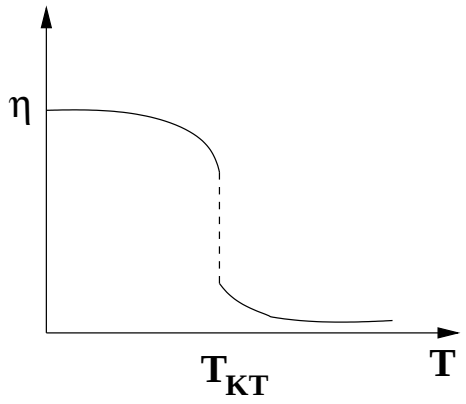

Figure 4.19: Helicity modulus (η) as a function of temperature for the XY model. At the Kosterlitz-Thouless temperature T_{KT} η has a finite jump in the thermodynamic limit.

it's easy to show that:

$$\frac{d(\beta\eta)}{d\beta} = \frac{E(\theta) - E(0)}{2\theta^2}$$

where $E(\theta)$ is the energy of the *twisted* configuration and $E(0)$ the internal energy of the equilibrium with periodic boundary conditions. At the transition temperature T_{KT} the derivative $d(\beta\eta)/d\beta$ has a peak, Fig. 4.20. We will then locate the temperature T_{KT} by the position of the peak of $d(\beta\eta)/d\beta$.

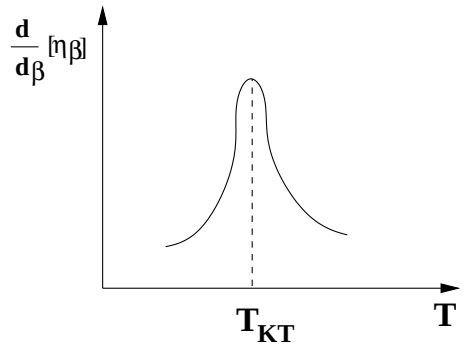

Figure 4.20: Typical profile of $d(\beta\eta)/d\beta$ as a function of temperature for an XY ferromagnet. $d(\beta\eta)/d\beta$ has a peak at $T = T_{KT}$.

We start from the energy functional valid in the long wavelength limit (3.24) and then we find the ground state via Monte Carlo simulations. For the interactions we use the first neighbor approximation. For the Monte Carlo simulations we use the Metropolis algorithm with simulated annealing starting from a temperature much bigger than $\beta l^2/k_B$ and slowly reducing it to the desired value. We first find the ground sate for periodic boundary condition in x and y and then find the ground sate for anti-periodic boundary conditions along x, i.e. we set $\theta = \pi$. We then calculate the difference between the average energies $\langle E(\pi)\rangle$ and $\langle E(0)\rangle$ so obtaining $d(\beta\eta)/d\beta$. The results are shown in Fig. 4.21 for different values of the disorder strength assuming $V_{S0} \approx V_{A0}$. We see that as the disorder strength increases

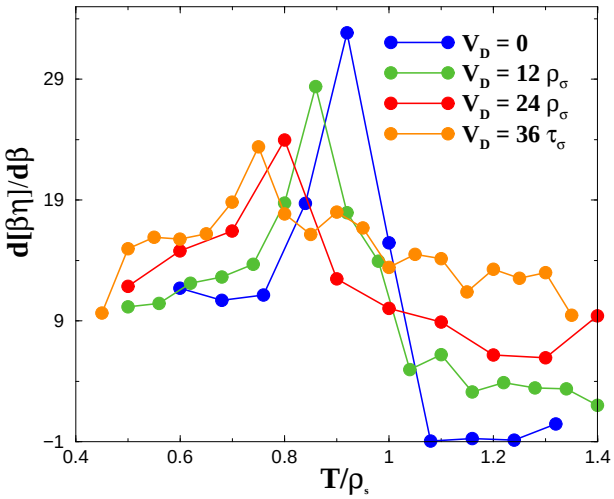

Figure 4.21: $d(\beta\eta)/d\beta$ as a function of temperature for a $\nu = 1$ quantum Hall bilayer with disorder.

the peak denoting the Kosterlitz-Thouless phase transition becomes smaller and shifts to lower temperatures. We find that for disorder strengths bigger than the critical disorder V_c the peak disappears indicating that there will not be a Kosterlitz-Thouless phase transition.

Chapter 5

Transport properties of $\nu = 1$ quantum Hall bilayers

5.1 Introduction

In recent years remarkable anomalous transport properties have been discovered in quantum Hall bilayers in particular in quantum Hall bilayers with total filling factor $\nu = 1$ [2],[40], [41], [42]. We will focus on the tunneling geometry in which a current

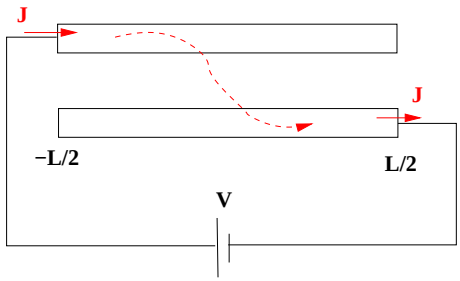

Figure 5.1: Schematic representation of the tunneling configuration studied in [2].

is injected in the top layer and extracted from the bottom one as schematically shown in Fig. 5.1. In Fig. 5.2 the measured differential tunneling conductance is shown

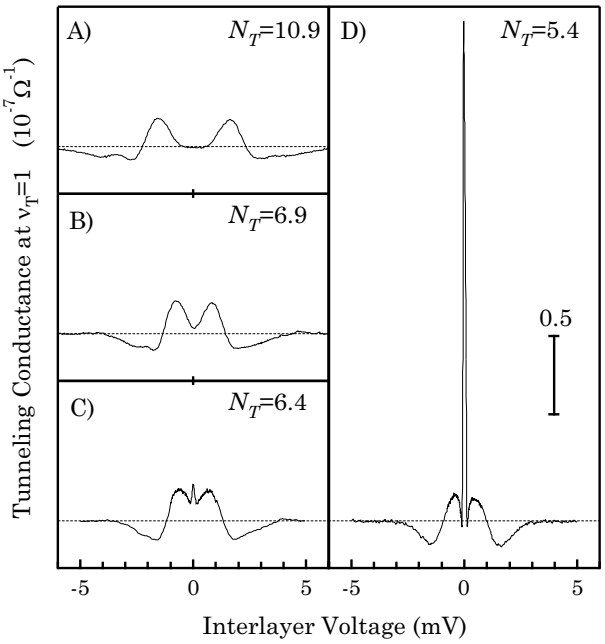

Figure 5.2: Differential tunneling conductance measurements by Spielman et al. [2] for a $\nu = 1$ quantum Hall bilayer for different values of the total density N_T in units of 10^{10} cm^{-2}

as a function of the interlayer voltage for different values of the total density N_T in units of 10^{10} cm^{-2}. For each trace the total Landau level filling factor ν was kept equal to 1 by tuning the perpendicular magnetic field. In this condition to decrease N_T is equivalent to increase the magnetic length l. The remarkable result shown in Fig. 5.2 is that when $d \lesssim l$ a huge peak in the tunneling conductance is observed. We know that when $d \lesssim l$ a $\nu = 1$ quantum Hall bilayer has a broken symmetry ground state characterized by interlayer phase coherence. This state is the analogous of the ground state in a XY magnet. We can then associate the appearance of the peak for $d \lesssim l$ in the tunneling conductance to a collective behavior. In Fig. 5.3 the tunneling current as a function of the interlayer voltage for the case of high tunneling conductance is shown. The presence of a peak in the low bias conductance when the system is supposed to be in the broken symmetry ground state is reminiscent of

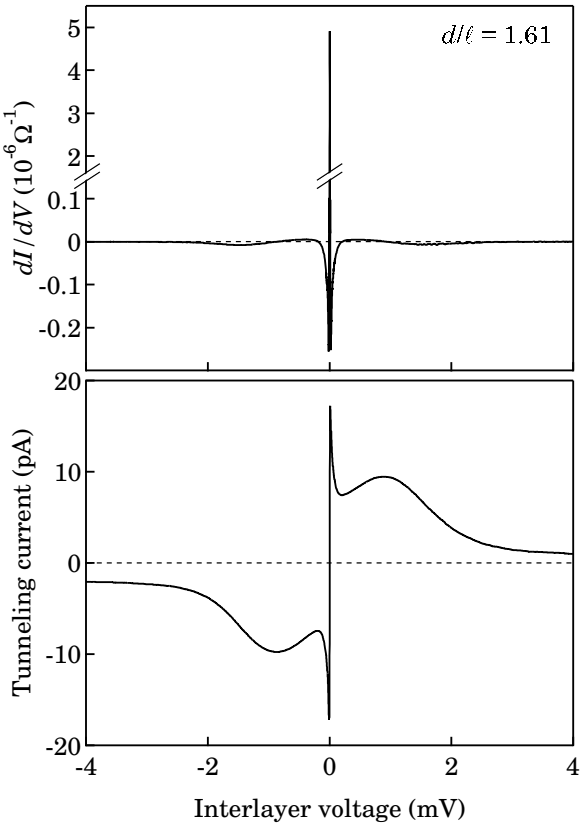

Figure 5.3: Tunneling current and differential tunneling conductance measurements by Spielman et al. [2] for a $\nu = 1$ quantum Hall bilayers for $d \lesssim l$.

the d.c. Josephson effect [43], [44]. Notice however that in all the experiments even when $d \ll l$ the low bias interlayer tunneling conductance is never infinite, i.e. we never have a finite current for exactly zero interlayer voltage bias [9] as we have in the d.c. Josephson effect.

Another remarkable discovery of the experiments performed by the group of Dr. Eisenstein is the behavior of the interlayer tunneling conductance when an in plane magnetic field is applied. Experimentally a parallel component of the magnetic field is generated by simply tilting the sample relative to the orientation of $\mathbf{B}$. In Fig. 5.4 the measured interlayer tunneling conductance is shown for different values

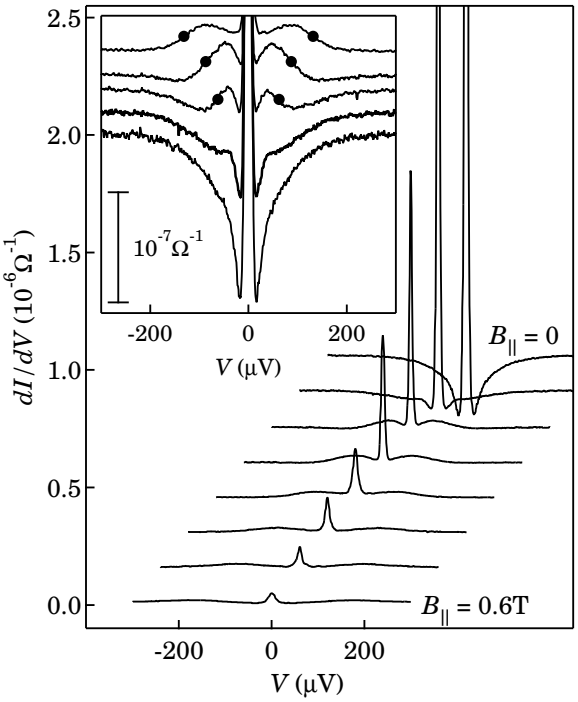

Figure 5.4: Differential tunneling conductance measurements by Spielman et al. [2] for a $\nu = 1$ quantum Hall bilayers for different values of the in plane magnetic field $B_{\|}$

of an applied in plane magnetic field $B_{\|}$ for a $\nu = 1$ quantum Hall bilayer with $d \lesssim l$. We see that a small in plane magnetic field causes a big reduction of the low bias peak of the tunneling conductance.

To summarize from our perspective the main results of the interlayer tunneling experiments are:

- Huge increase of the low bias interlayer conductance when d becomes of the order or smaller than l;
- The interlayer tunneling conductance remains finite even when $d \ll l$ and for the lowest temperature so far reached in the experiments;

- When an in-plane magnetic field is applied both the tunneling current and the tunneling conductance are highly suppressed.

Motivated by these results we developed a model to describe the transport properties of $\nu = 1$ quantum Hall bilayers. In this chapter we present the model and compare its predictions to the experimental results.

5.2 Dynamical equations for condensate coupled to quasiparticle currents

Let's start from the Lagrangian (3.27) valid in the long-wavelength regime. We want to describe low energy collective excitations. The biggest energy scale in (3.27) is βl^2. We can then assume that for the low energy excitations is $m_z \ll 1$. In this case we can write $\mathbf{m} = (\cos\varphi; \sin\varphi; m_z)$ and the Lagrangian (3.27) reduces to:

$$\mathcal{L} = \int_A n\dot{\mathbf{m}} \cdot \mathcal{A}[\mathbf{m}] d^2r + \frac{1}{2}\rho_s \int_A |\nabla\varphi|^2 d^2r + \beta \int_A m_z^2 d^2r - \frac{\Delta_t}{2} \int n\cos\varphi d^2r \quad (5.1)$$

We now want to generalize this Lagrangian to include also the effect of an in-plane component of the magnetic field. Let's assume for definiteness $\mathbf{B}_\parallel = \nabla \times \mathbf{A}$ with $\mathbf{A} = B_\parallel(0, 0, x)$. In this gauge $\mathbf{A}$ points in the direction perpendicular to the plane and as a consequence an electron will acquire an Aharanov-Bohm phase only when it tunnels between layers. Therefore only the tunneling will be affected by the presence of an in-plane field. The tunneling functional in (5.1) is

$$E_t = -\frac{\Delta_t}{2} \int n\cos\varphi \; d^2r.$$

This is the semiclassical approximation to the tunneling Hamiltonian:

$$H_t = -\frac{\Delta_t}{2} \int d^2r \left[\Psi_T^\dagger(\mathbf{r})\Psi_B(\mathbf{r}) + \Psi_B^\dagger(\mathbf{r})\Psi_T(\mathbf{r})\right].$$

As it is shown in Fig. 5.5 when an electron tunnels between layers the tunneling matrix element will acquire the phase $e^{iQ_\parallel x}$ with

$$Q_\parallel \equiv \frac{2\pi B_\parallel d}{\phi_0} = \frac{B_\parallel d}{B_\perp l^2}.$$

Going back to the semiclassical approximation we have that the tunneling part of

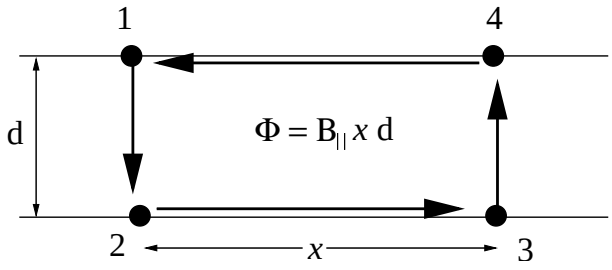

Figure 5.5: Process in which an electron tunnels from the top layer to the bottom layer and back to the top layer keeping its phase coherence. A possible interpretation of this process is that after the electron tunnels from the top to the bottom layer, $1 \rightarrow 2$, the resulting particle-hole travels coherently for the distance x, $2 \rightarrow 3$, and then is annihilated by an opposite tunneling event $3 \rightarrow 4$.

the Lagrangian (5.1) in presence of in-plane magnetic field becomes:

$$E_T = \frac{\Delta_t}{2} \int n \cos(\varphi - Q_\parallel x) d^2 r. \tag{5.2}$$

For the remainder of this section it is convenient to define the phase

$$\tilde{\varphi}(\mathbf{r}) \equiv \varphi(\mathbf{r}) - Q_\parallel x.$$

From (5.1), with the form of the tunneling term given by (5.2) to allow

$B_\parallel \neq 0$ we find the following Euler-Lagrange equations:

$$\frac{\partial \tilde{\varphi}}{\partial t} = -\frac{4\pi l^2 \beta}{\hbar} m_z \tag{5.3}$$

$$\frac{\partial m_z}{\partial t} = \frac{\Delta_t}{2\hbar} \sin \tilde{\varphi} - \frac{2\pi l^2 \rho_s}{\hbar} \nabla^2 \tilde{\varphi} \tag{5.4}$$

The right hand side of (5.3) describes precession of the the collective pseudospin order parameter field around the z direction. The two terms on the right hand side of (5.4) can be identified as representing the collective interlayer tunneling and the two-dimensional supercurrent contributions to $\partial m_z/\partial t$. Notice that in equations (5.3), (5.4) the in-plane field doesn't appear explicitly because it just adds a constant and a total derivative term to the energy functional. However $B_\parallel$ influences the energy indirectly through the tunneling term favoring solutions with winding. To include damping terms we can follow the same recipe used in Chapter 4 to derive equations (4.4). In this way we find the following equations of motion:

$$\frac{\partial \tilde{\varphi}}{\partial t} = -\frac{4\pi l^2 \beta}{\hbar} m_z - \alpha_\varphi \dot{m}_z \tag{5.5}$$

$$\frac{\partial m_z}{\partial t} = \frac{\Delta_t}{2\hbar} \sin \tilde{\varphi} - \frac{2\pi l^2 \rho_s}{\hbar} \nabla^2 \tilde{\varphi} + \alpha_z \dot{\tilde{\varphi}} \tag{5.6}$$

Finally we include a term to take into account the presence of interlayer quasiparticle currents $\mathbf{j}_{qp}$. We assume the current $\mathbf{j}_{qp}$ to be proportional to the gradient of the chemical potential difference $\Delta\mu$ between the two layers. On the other hand we have $e\Delta\mu = 4\pi l^2 \beta m_z$ and so we can write:

$$\mathbf{j}_{qp} = \sigma_z \frac{4\pi l^2 \beta}{e} \nabla m_z$$

where σ_z is the quasiparticle conductivity. An estimate of σ_z can been obtained [45] in the same way as done for the damping coefficients α_φ, α_z. The only difference is that to estimate σ_z we have to keep also terms quadratic in the wavevector when

calculating the response function. We have $\sigma_z \approx e^2/h$, [45]. With the inclusion of the contribution due to the quasiparticle currents to $\partial m_z/\partial t$ we find the equations:

$$\frac{\partial \tilde{\varphi}}{\partial t} = -\frac{4\pi l^2 \beta}{\hbar} m_z - \frac{\alpha_\varphi}{\hbar}\left[\frac{\Delta_t}{2}\sin\tilde{\varphi} - 2\pi l^2 \rho_s \nabla^2 \tilde{\varphi}\right] \tag{5.7}$$

$$\frac{\partial m_z}{\partial t} = \frac{1}{\hbar}\left[\frac{\Delta_t}{2}\sin\tilde{\varphi} - 2\pi l^2 \rho_s \nabla^2 \tilde{\varphi}\right] - \frac{4\pi l^2 \beta \alpha_z}{\hbar} m_z + \frac{8\pi^2 l^4 \beta \sigma_z}{e^2 M_0}\nabla^2 m_z \tag{5.8}$$

where M_0 is the site-averaged magnitude of the order parameter.

5.3 Results

We now want to use equations (5.7), (5.8) to derive the $I-V$ curve for the bilayer in the tunneling configuration. The condensed matter theory community has struggled for more than five years to try to explain these experiments. In some pictures, [44], [43] at low bias the system is seen as a d.c. Josephson junction in which quantum or thermal fluctuations in presence of disorder cause the resistivity to be non zero. The model encoded by equations (5.7) and (5.8) is able to capture some of the aspects of the tunneling experiment in $\nu = 1$ quantum Hall bilayers. In particular using this model we are able to describe the transition from stationary solutions to time dependent solutions for the order parameter at a critical value, V_{max}, of the interlayer voltage. This model however overestimates the value of the low bias tunneling conductance. To explain quantitatively the low bias $I-V$ curve we have to consider in detail the edge character of the quasiparticle currents in $\nu = 1$ quantum Hall bilayers as we do in section 5.4.

To fully define our model we need to set the boundary conditions. In the remainder of this section we restrict ourselves to the one dimensional case assuming $\tilde{\varphi}$, m_z to depend only on x and time. Because of the symmetry of the configuration, Fig. 5.1, we can set

$$\mu_z|_{-L/2} = \frac{eV}{2}; \qquad \mu_z|_{L/2} = \frac{eV}{2};$$

and then for m_z we have the boundary conditions:

$$m_z|_{-L/2} = \frac{eV}{2\beta}; \qquad m_z|_{L/2} = \frac{eV}{2\beta}. \tag{5.9}$$

We obtain the boundary conditions for φ requiring that no supercurrent flows in or out of the sample:

$$\left.\frac{\partial\varphi}{\partial x}\right|_{-L/2} = 0 \Longrightarrow \left.\frac{\partial\tilde{\varphi}}{\partial x}\right|_{-L/2} = -Q_{\parallel}; \qquad \left.\frac{\partial\varphi}{\partial x}\right|_{L/2} = 0 \Longrightarrow \left.\frac{\partial\tilde{\varphi}}{\partial x}\right|_{L/2} = -Q_{\parallel}; \tag{5.10}$$

To find the $I-V$ curve we solve equations (5.7), (5.8) with different values of the applied bias potential V. We then calculate the current density as the time average of $\mathbf{j}_{qp}$:

$$j = \frac{4\pi l^2\beta\sigma_z}{e}\lim_{T\to\infty}\frac{1}{T}\int_0^T \left.\frac{\partial m_z}{\partial x}\right|_{\pm L/2} dt \tag{5.11}$$

In this section we assume $\alpha_z = 0$ so that the damping of m_z can only occur when the microscopic pseudospin-polarized quasiparticle currents have finite divergence.

Let's first look for stationary solutions. Setting the time derivatives to zero in equations (5.7), (5.8), we find:

$$\frac{d^2\Omega_z}{dx^2} - \frac{1}{L_z^2}\Omega_z = 0 \tag{5.12}$$

$$\frac{d^2\tilde{\varphi}}{dx^2} - \frac{1}{\lambda_j^2}\sin\tilde{\varphi} = \frac{2\beta}{\alpha_\varphi\rho_s}\Omega_z \tag{5.13}$$

where:

$$L_z \equiv l\sqrt{\frac{2\pi\hbar\sigma_z\alpha_\varphi}{e^2M_0\left(1+\alpha_z\alpha_\varphi\right)}};$$

$$\lambda_j \equiv l\sqrt{\frac{4\pi\rho_s}{\Delta_t}}.$$

λ_j is the equivalent in our case of the Josephson length in an extended Josephson's

junction. Using the boundary conditions (5.9) we can easily solve (5.12) to find:

$$\Omega_z = \frac{eV}{8\pi l^2 \beta \cosh\left(\frac{L}{2L_z}\right)} \cosh\left(\frac{x}{L_z}\right) \tag{5.14}$$

If we now insert this solution in equation (5.7) we find:

$$\frac{d^2\tilde{\varphi}}{dx^2} - \frac{1}{\lambda_j^2}\sin\tilde{\varphi} = \frac{eV}{4\pi\alpha_\varphi \rho_s l^2 \cosh\left(\frac{L}{2L_z}\right)} \cosh\left(\frac{x}{L_z}\right) \tag{5.15}$$

Equation (5.15), with the boundary conditions (5.10), admits solutions only up to a maximum value, $V_{\max}$, of the applied bias potential. We find $V_{\max} \approx 10^{-4} e^2/\epsilon l = 10^{-6} eV$. For $V < V_{\max}$ using the solution (5.14), from the expression for the current density (5.11) we find the following linear relation:

$$j = \frac{\sigma_z}{2L_z} \tanh\left(\frac{L}{2L_z}\right) V. \tag{5.16}$$

In the limit of very low bias we then find the tunneling conductance

$$\sigma_{\text{tunnel}} = \sigma_z \frac{L_c}{2L_z} \tanh\left(\frac{L}{2L_z}\right)$$

where L_c is the length of the contact of the bilayer to the external current sources. Assuming $l = 10\text{nm}$, $\rho_s = 10^{-3} e^2/\epsilon l$, $\beta = 10^{-2} e^2/\epsilon l^3$, [25], $\Delta_t = 10^{-6} e^2/\epsilon l$, $\alpha_\varphi = 1$, $\sigma_z = 1$ we have

$$L_z \approx l \ll L.$$

We then find, in the limit $V < V_{\max}$

$$\sigma_{\text{tunnel}} = \sigma_z \frac{L_c}{2L_z}.$$

In experiments the length L_c of the contact is much bigger than $L_z \approx l$. In this

situation we find a value for the conductance σ_{tunnel} and the maximum tunneling current orders of magnitude bigger than the one observed experimentally. Also all the other theories so far proposed are affected by the same problem. The explanation of this discrepancy is the focus of the following sections in this chapter.

For values of V bigger than $V_{\max}$ we must solve the time dependent equations (5.7), (5.8). As shown in Fig. 5.6, Fig. 5.7 as we increase V past $V_{\max}$ the current density starts oscillating in time more and more so that the time average (5.11) becomes smaller and smaller. The result is a non-monotonic $I - V$ curve as shown in Fig. 5.8.

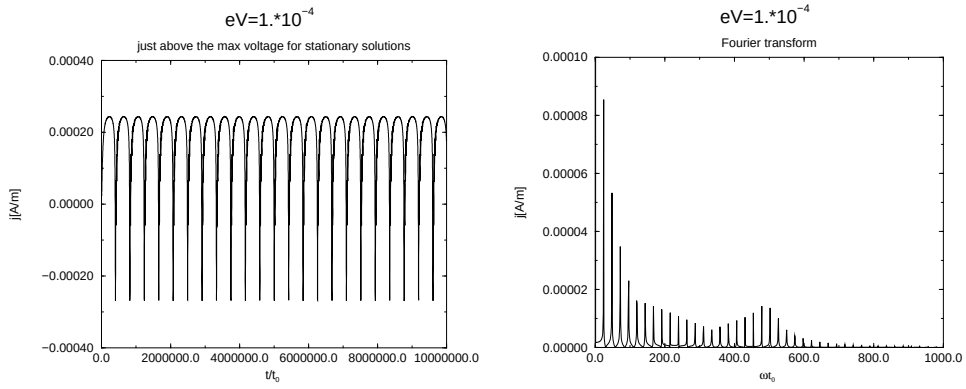

(a) (b)

Figure 5.6: (a)Current density versus time for V slightly above $V_{\max}$. (b)Power spectrum of $j(t)$.

The effect of an in-plane magnetic field is to make $Q_{\|} \neq 0$. The current voltage characteristics for $Q_{\|} \neq 2 \times 10^{-2}$ and $Q_{\|} \neq 3 \times 10^{-2}$ are shown in Fig. 5.9. We see how a small in plane field greatly suppress the maximum current and therefore the tunneling conductivity (notice the difference in scale for the current between Fig. 5.8 and Fig. 5.9).

We see how the $I - V$ characteristics that we obtain reproduce qualitatively

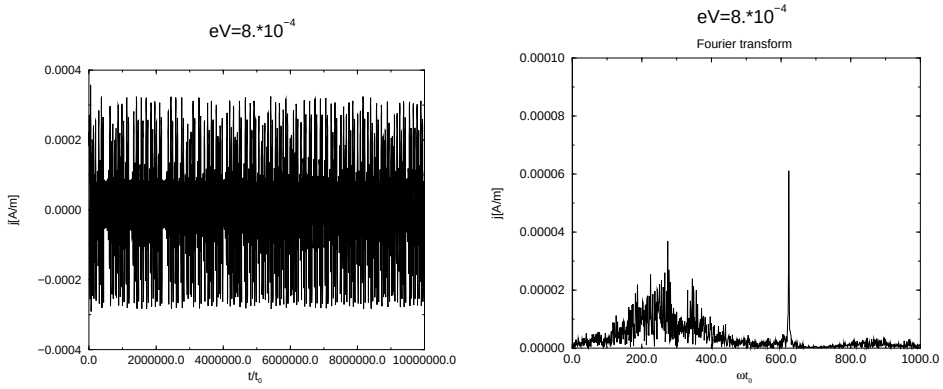

(a) (b)

Figure 5.7: (a)Current density $j(t)$ versus time for V much bigger than $V_{\max}$. (b)Power spectrum of $j(t)$.

the $I - V$ characteristics obtained experimentally, lower panel of Fig. 5.3. In particular in agreement with experiments we find:

- Non zero tunneling resistivity for $V \to 0$;
- Non monotonic current voltage characteristics;
- Big suppression of both the tunneling current and tunneling conductivity in presence of an in-plane magnetic field;
- Value of the voltage for which we have the maximum current of the right order of magnitude.

The results presented in this section describe a situation in which a quasiparticle current injected at one end in the top layer causes a non zero divergence of the supercurrent $\rho_s \nabla \varphi$ that is counterbalanced in the bulk of the bilayer by coherent tunneling. At the other end of the sample the divergence of the supercurrent returns to zero being converted back to a quasiparticle current that is then extracted from

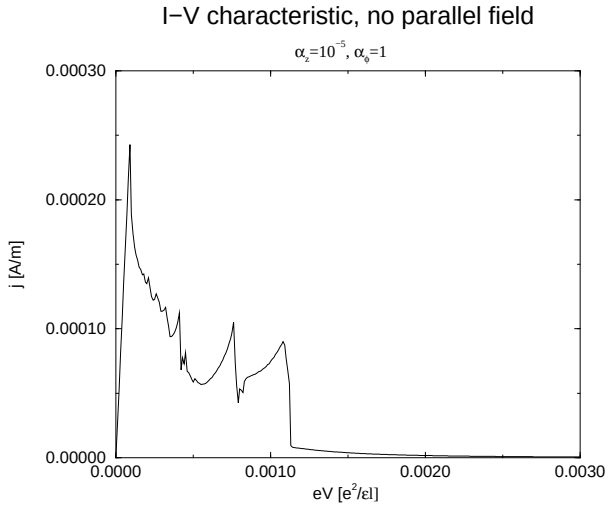

Figure 5.8: Current voltage characteristic for the case when no in plane field is present.

the bottom layer. In our model the finite tunneling resistivity is due to the edge resistance encountered by the quasiparticles. Because the charge current in and out of the system has to be necessarily carried by quasiparticles the tunneling resistance is always non zero even when $d < l$ and the bilayer is in the broken symmetry ground state. The maximum voltage $V_{\max}$ is set by the maximum V for which we have stationary solutions and the corresponding maximum current density is equal to $\sigma_z V_{\max}/2L_z$. The non-monotonic character of the $I - V$ curves is connected to the fact that for $V > V_{\max}$ we have non-stationary solutions and as a consequence the time averaged current is always smaller than for $V = V_{max}$. The big suppression of the tunneling current in presence of an in-plane magnetic field can be understood considering that because of the boundary conditions (5.10) $Q_{\|} \neq 0$ decreases the maximum quasiparticle current for which we have a stationary solution. However the results presented in this section also show the limits of the model described in section 5.2: we find a tunneling current density and conductivity that are both much bigger than the ones observed in experiments. In the following sections we address

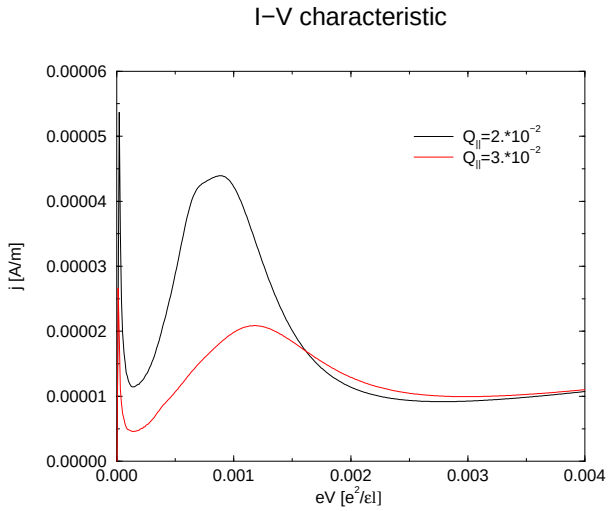

Figure 5.9: Current voltage characteristic for in plane field different from zero.

this discrepancy.

5.4 Edge state interlayer transport

Since a quantum Hall effect occurs in parallel transport when the interlayer transport conductivity is very high ($d \lesssim l$) — which we believe means that we have interlayer phase coherence — then we know that the system is incompressible. We have seen in Chapter (2) that in an incompressible system only at the edge there are empty states crossing the Fermi energy and as a consequence any current will be also localized at the edges. In the previous section we assumed that the whole condensate was taking part in the dynamics driven by the quasiparticle currents. In reality the quasiparticles can only live at the edges of the incompressible regions and then only these edges will be driven by the coupling to quasiparticles currents. In this section we refine our theory to take into account that in a $\nu = 1$ quantum Hall bilayer only the edges of the incompressible regions can give a contribution to charge transport properties.

In the ordered state, the quasiparticles in the bulk of the quantum Hall bilayer experience an interlayer tunneling amplitude that includes a self-energy contribution which can be represented by an in-plane pseudospin effective *magnetic field*:

$$\begin{aligned} \Delta_x(X) &= \Delta_t + \frac{1}{L}\sum_X n_{X'} F_D(X - X')\cos(\varphi_{X'}) \\ \Delta_y(X) &= \frac{1}{L}\sum_{X'} n_{X'} F_D(X - X')\sin(\varphi_{X'}) \end{aligned} \tag{5.17}$$

where $X = \ell^2 k$ labels a guiding center state which is delocalized along the edge of the system, F_D, defined in Chapter 3, is the interlayer exchange integral between guiding centers X and X' and $n_{X'}$ is the guiding center occupation number. The field $\mathbf{\Delta} \equiv (\Delta_x, \Delta_y, 0)$ is the analogous of the magnetic field that real spins would experience in an easy plane ferromagnet. In the absence of a transport current, the quasiparticle pseudospin will align with the effective magnetic field for each guiding center:

$$\frac{\cos(\varphi_X)}{\sin(\varphi_X)} = \frac{\Delta_x(X)}{\Delta_y(X)}. \tag{5.18}$$

It is easy to verify that in this case the only solution to Eq.(5.18) is $\sin(\varphi_X) \equiv 0$; the small single-particle tunneling amplitude selects the phase difference between the two layers and the effective tunneling amplitude is enormously enhanced by interactions.

When the system carries a current, the quasiparticle Schröedinger equation must be solved with scattering boundary conditions, incident from the high chemical potential contact. Under these circumstances, the pseudospin orientation need not match that of the effective magnetic field experienced by the quasiparticles. For a given orbital the pseudospin polarization will vary along the edge and depend on the random potential along the edge of the system. Alternately on a $\nu = 1$ chiral edge, the Schröedinger equation can be mapped to that of a zero-dimensional spin

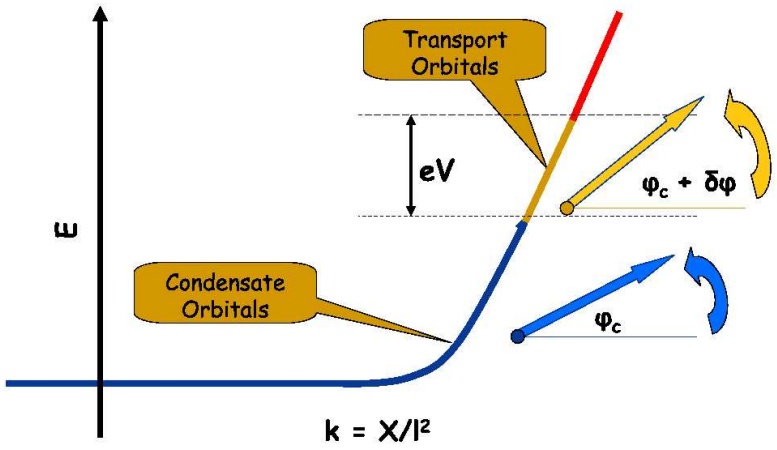

Figure 5.10: Schematic illustration of pseudospin transfer torques in quantum Hall bilayers. Each orbital makes a contribution to the pseudospin exchange field that is in the direction of its pseudospin orientation. Unlike equilibrium orbitals, transport orbitals do not align with their pseudospin fields, giving rise to a pseudospin transfer torque. Large interlayer conductance occurs when the pseudospin transfer torque can be canceled by a pseudospin torque due to the bare interlayer tunneling term in the Hamiltonian.

in a time-dependent field, since the transport electrons move in one direction along the edge at the edge magnetoplasmon velocity $v_{emp} \sim 2 \times 10^6 \mathrm{m\,s^{-1}}$. $f_{emp} = v_{emp}/P$ where P is the sample perimeter is the fundamental edge magnetoplasmon frequency. Averaging along the edge, the rate of spin precession from up (top layer) to down (bottom layer) is proportional to the mean torque that acts on the planar spin. The necessity of this torque implies that the in-plane pseudospin orientation can not be equal to the quasiparticle effective magnetic field.

For the interlayer current density j_{tr} of the transport electrons we have:

$$j_{tr} = g\frac{1}{t_{transit}} = g\frac{v_{emp}}{L}. \tag{5.19}$$

where$g$ is the probability that an electron injected in the top layer will make its way to the bottom layer, and $t_{transit} = L/v_{emp}$ is the time required for an edge electron to travel along the sample, L being the distance between the contacts. On the other hand we have:

$$\begin{aligned} j_{tr} &= \frac{\partial \mathbf{S}_{tr}}{\partial t} \\ &= \frac{1}{\hbar}\mathbf{S}_{tr} \times \left.\frac{\delta E}{\delta \mathbf{m}}\right|_{X_e} \end{aligned} \tag{5.20}$$

where $\mathbf{S}_{tr}$ is the pseudospin of the transport quasiparticles and X_e is the guiding center at the edge. Assuming $m_z \ll 1$ and neglecting the contribution due to the bare tunneling to $\delta E/\delta \mathbf{m}$ from (5.20) we find:

$$j_{tr} = \frac{\Delta^E_{QP}}{\hbar}\sin(\varphi_{tr} - \varphi_c). \tag{5.21}$$

In Eq. (5.21) $\varphi_c \equiv \tan^{-1}(\Delta_y/\Delta_x)$ is the orientation of the pseudospin effective field at the edge, Δ^E_{QP} is the magnitude of the exchange effective magnetic field at the edge of the system:

$$\Delta^E_{QP} \equiv \frac{1}{L}\sum_{X'<X} F_D(X - X').$$

Since $g < 1$, $\Delta^E_{QP} \sim 10^{-4}$eV [46], [47] and $L \sim 10^{-2}$cm in typical samples, from equations (5.19), (5.21) it follows that $\delta\varphi \equiv \varphi_{tr} - \varphi_c$ is small and that $\sin(\delta\varphi) \approx \delta\varphi$.

In the presence of current induced pseudospin-torques the pseudospin effective magnetic field seen by the quasiparticles in the bilayer at the edge X_e of the

incompressible region becomes:

$$\Delta_x(X_e) = \Delta_t + \frac{1}{L}\sum_{X<X_e} F_D(X-X')\cos\varphi_{X'} + \frac{N_{tr}}{L}F_D(0)\cos[\varphi_c+\delta\varphi] \qquad (5.22)$$

$$\Delta_y(X_e) = \frac{1}{L}\sum_{X<X_e} F_D(X-X')\sin\varphi_{X'} + \frac{N_{tr}}{L}F_D(0)\sin[\varphi_c+\delta\varphi] \qquad (5.23)$$

where $N_{tr} = LeV/(hv_{emp})$ is the number of edge states in the narrow transport window with energy width eV and V is the applied interlayer bias voltage. The bias voltage is assumed to be small enough that the guiding center width of the transport window is much smaller than the range ℓ [46], [47] of the $F_D(X-X')$ exchange integral. Neglecting the variation of φ from its maximally deflected value at the edge to its value deep in the bulk ($\varphi = 0$) since this occurs on a length scale ($\ell\sqrt{\Delta^E_{QP}/\Delta_t}$) we can rewrite equations (5.22), (5.23) in the form

$$\begin{aligned}\Delta_x(X_e) &= \Delta_t + \Delta^E_{QP}\cos(\varphi_c) + \frac{F_D(0)N_{tr}}{L}\cos(\varphi_c+\delta\varphi)\\ \Delta_y(X_e) &= \Delta^E_{QP}\sin(\varphi_c) + \frac{F_D(0)N_{tr}}{L}\sin(\varphi_c+\delta\varphi).\end{aligned} \qquad (5.24)$$

The terms proportional to Δ^E_{QP} in Eq.(5.24) are edge self-energies in the absence of transport currents and the terms proportional to $F_D(0)$ are the pseudospin torque contributions.

We propose that the tunneling anomaly in quantum Hall bilayers occurs when it is possible to achieve a self-consistent solution of the mean-field equations in the presence of current induced pseudospin-torques i.e. when the pseudospin of the quasiparticles inside the bilayer aligns with the effective pseudospin field $\mathbf{\Delta}$:

$$\mathbf{S}(X_e) \parallel \mathbf{\Delta}. \qquad (5.25)$$

In the limit $m_z \ll 1$ we have $\mathbf{S}(X) = (\cos\varphi_X, \sin\varphi_X, 0)$ and then from the condition

(5.25) and equations (5.24) we find:

$$\Delta_t \sin(\varphi_c) = \frac{F_D(0) N_{tr}}{L} \delta\varphi \tag{5.26}$$

and hence that the maximum value of the bias voltage for which a time-independent solution of the mean-field equations exists is

$$V_{\max} = \frac{\Delta_t v_{emp} h}{e F_D(0) \delta\varphi} = \frac{2\pi \Delta_t \Delta_{QP}^E L}{e g F_D(0)}. \tag{5.27}$$

Since [46], [47] $F_D(0) \sim e^2/(\epsilon) \sim 10^{-2}\text{eV}\ell$, it follows that the width of the low-bias tunneling anomaly at the lowest temperatures when the quantum Hall effect is most strongly developed should be $\sim 10^{-6}$eV. This results is similar to the one found in the previous section and is consistent with experiments. For $V > V_{\max}$ we have time dependent solutions and then, as we saw in the previous section, the time averaged current will be smaller than the current corresponding to $V = V_{\max}$.

When a time independent solution of the mean-field equations is possible, the conductance is given simply by the Landauer-Buttiker [48], [49],[50],[51] scattering theory picture of transport:

$$\sigma_{\text{tunnel}} = g \frac{e^2}{h}.$$

In this picture then assuming that an electron injected in the top layer has a maximum 50% chance of being found in either layer at later times we have that the maximum interlayer conductance is:

$$\sigma_{\text{tunnel}} = \frac{e^2}{2h}.$$

With this value of the conductance we find

$$I_{\max} = \frac{e^2}{2h} V_{\max} = \frac{\Delta_{QP}^E \Delta_t L}{\hbar F_D(0)}$$

Both these values are very close to the values measured in the tunneling experiments performed on the highest quality samples and at the lowest temperatures.

We can conclude that the theory presented in this section is able to quantitatively describe the low-bias anomaly of the tunneling conductance for $\nu = 1$ quantum Hall bilayers. It also gives the right order of magnitude for maximum tunneling current and $V_{\max}$. It greatly improves the model presented in section 5.2 by taking into account that only the edges of the incompressible regions participate in the dynamics and then in the transport of charges between the layers when quasiparticle currents are injected in the system.

5.5 Inclusion of disorder

In the absence of disorder g should approach 0.5 when the pseudospin precession length $L_{pr} \equiv v_{emp}\,\hbar/\Delta_{QP}^{E}$ is less than L, *i.e.* when Δ_{QP}^{E} is larger than $\sim 10^{-5}eV$, a condition that we expect to be satisfied quickly once the ordered state is entered. Instead g is almost always substantially smaller than 1 in experiment. We ascribe this behavior to disorder, which is assisted in suppressing interlayer tunneling by the large edge magnetoplasmon velocity. Even in bilayer samples for which large purely single-particle interlayer tunneling occurs, the interlayer conductance in the quantum Hall regime ends up being much smaller [52, 53] than naively expected. Electrons traveling rapidly (at velocity v_{emp}) along the edge see differences in the random disorder potential in the two layers as a rapidly varying $\hat{z}$ direction pseudospin field. The typical rate at which the pseudospin random field varies is $v_{emp}V_{dis}/L_{dis}$ where V_{dis} and L_{dis} are the typical size and correlation length of the potential difference between the layers. In the bulk of the two-dimensional electron system these random pseudospin field fluctuations can be screened out [54, 55, 25] by tilting the pseudospin slightly out of the easy plane as we saw in chapter 4. Levels cross and electrons following the adiabatic path will cross between layers when

the disorder potential changes sign as illustrated in Fig.(5.11). We can estimate g as the product of the number of attempts —L/L_{dis} — and the probability P of crossing between layers in a given attempt [56, 57]:

$$P = 1 - \exp\left(-\left|\frac{2(\Delta_{QP}^{E})^2}{\hbar v_{emp} V_{dis}/L_{dis}}\right|\right).$$

so that we find:

$$\begin{aligned} g &= \frac{L}{L_{dis}}\left[1 - \exp\left(\frac{-2(\Delta_{QP}^{E})^2 L_{dis}}{\hbar v_{emp} V_{dis}}\right)\right] \\ &\sim \frac{2(\Delta_{QP}^{E})^2 L}{\hbar v_{emp} V_{dis}}. \end{aligned} \tag{5.28}$$

The small argument expansion for the Landau-Zener tunneling formula is justified by experiment which tells us that the tunneling probability per attempt is always small. Combining Eq.(5.28) and Eq.(5.27) we find that

$$V_{max} = \frac{\Delta_t}{\Delta_{QP}^{E}} \frac{h V_{dis} v_{emp}}{e F_D(0)}. \tag{5.29}$$

In our theory, the temperature dependence of the transport anomaly follows from thermal fluctuations in the condensate phase which reduce the order parameter and Δ_{QP}^{E} [37, 9]. The increase [2, 40] of V_{max} by a factor of approximately 40 between 20 mK and 0.3 K is consistent with the size of suppression that is expected, although the detailed behavior is certainly disorder-dependent and sample specific. The decrease [2, 40] in zero-bias conductance by a factor of 2000 over the same temperature is then consistent with the predictions of Eq.(5.28). Our theory also accounts qualitatively for in-plane field dependence of the anomaly which is marked [2, 40] by a strong decrease in conductance and with little change in voltage width. This behavior is predicted by our theory since Δ_{QP}^{E} and Δ_t have similar field dependence, both dropping [46, 9, 58] by a factor ~ 1 when $B_{\|}/B_{\perp} \sim d/\ell$.

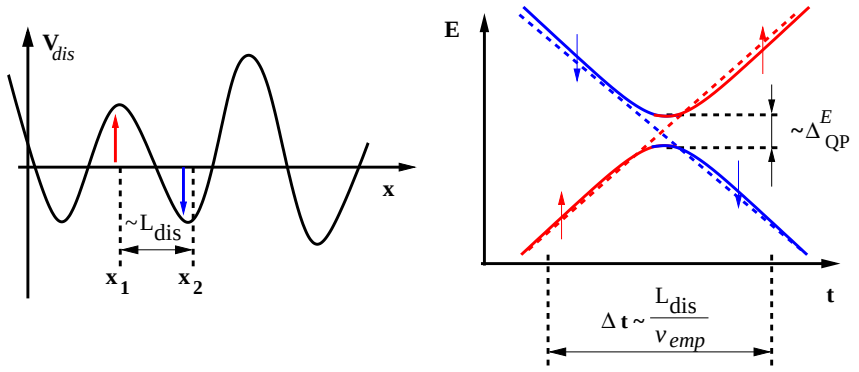

Figure 5.11: Schematic illustration of the suppression of the interlayer tunneling by disorder. Differences in the random potential in the two layer gives rise to substantial pseudospin fields in the $\hat{z}$ direction V_{dis} which cannot be screened at the edge of the system. Along much of the edge, V_{dis} is larger than the in-plane coherence induced exchange field Δ^E_{QP}. When the disorder potential difference changes sign, quasiparticles will cross between layers if they follow the adiabatic path. Because of the high velocity of edge particles, quasiparticles are likely to Landau-Zener tunnel to the higher energy state and remain in the same layer.

Finally we explore the possibility that the thermal fluctuations of the pseudospin order parameter can themselves add a source of dissipation because of thermally induced phase slips. For this purpose we assume the external interlayer current to be present across the all phase coherent region of area A. With this assumption we are able to estimate only grossly the ratio K_BT/nA at which the thermally induced phase slips are relevant for the low bias conductance. As a matter of fact this assumption is an oversimplification because as we have seen in the previous section the quasiparticle current is only present at the edges of the incompressible regions. By doing an analysis assuming the interlayer current to be present only at the edges of the sample we would find a much higher value of the ratio K_BT/nA for the thermally induced phase slips to give an important contribution to the interlayer resistance.

Let's consider a single region with phase coherence. Assuming the pseudospin

order parameter to be uniform inside this region we can reduce the dynamical equation for **m** inside this region to simple ordinary differential equations. Starting from equations (5.5), (5.6), valid in the limit $m_z \ll 1$, for a uniform **m** we find:

$$\begin{aligned} \frac{\partial \varphi}{\partial t} &= -\frac{4\pi l^2 \beta}{\hbar} m_z - \alpha_\varphi \dot{m}_z \\ \frac{\partial m_z}{\partial t} &= \frac{\Delta_t}{2\hbar} \sin\varphi \end{aligned} \tag{5.30}$$

where we have assumed $\alpha_z = 0$. If we include an external interlayer current J and thermal fluctuations equations (5.30) become:

$$\begin{aligned} \frac{\partial \varphi}{\partial t} &= -\frac{4\pi l^2 \beta}{\hbar} m_z - \alpha_\varphi \dot{m}_z + y_\varphi \\ \frac{\partial m_z}{\partial t} &= \frac{\Delta_t}{2\hbar} \sin\varphi - J \end{aligned} \tag{5.31}$$

where y_φ is a random term that describes thermal fluctuations. From the fluctuation dissipation theorem we know that y_φ must have the following Gaussian Statistical properties:

$$\begin{aligned} \langle y_\varphi \rangle &= 0; \\ \langle y_\varphi(t) y_\varphi(t') \rangle &= \frac{2K_B T}{nA} \alpha_\varphi \delta(t - t'). \end{aligned}$$

By setting the value of J and then calculating the potential

$$V = \frac{4\pi\beta l^2}{e} \lim_{t\to\infty} \frac{1}{t} \int_0^t m_z(t')dt' \tag{5.32}$$

we can find the $I - V$ characteristics. Equations (5.31) can be combined in a single equation for φ:

$$\frac{\partial^2 \varphi}{\partial t^2} = -\frac{4\pi l^2 \beta \Delta_t}{2\hbar^2} \sin\varphi + \frac{4\pi l^2 \beta}{\hbar} J - \alpha_\varphi \left(\frac{\Delta_t}{2\hbar} \sin\varphi - J \right) + y_\varphi. \tag{5.33}$$

Equation (5.33) is a Langevin equation. Apart from the damping term proportional to α_φ and the random force y_φ, equation (5.33) is the same equation describing the dynamics of a particle in a dashboard potential

$$U = -\frac{4\pi l^2 \beta \Delta_t}{2\hbar^2} \cos\varphi - \frac{4\pi l^2 \beta}{\hbar} J\varphi,$$

subject to the random force y_φ. Because of the tilting of the potential U due to J, if the random force y_φ is big enough φ on average will keep growing jumping to lower minima of U. The exact magnitude of the random force for this to happen depends on J, for small values of J we can see from equation (5.33) that is of the order of $2\pi l^2 \beta \Delta_t / \hbar^2$. This phase slipping process gives rise to a non zero average for the time derivative of φ. But, as we can see from (5.31) a non zero average of $\partial\varphi/\partial t$ implies a non zero average of m_z and then, through (5.32) a non zero voltage. In analogy to what happens in a small Josephson junction [59], [60] the thermally induced phase slips cause an increase of the interlayer potential. We find that for a temperature of 50 mK the thermally induced phase slips could give an important contribution to the interlayer voltage if the linear size of the phase coherent region is of the order or smaller than the Josephson length λ_j.

5.6 Conclusions

Our theory sees interlayer tunneling phenomena as partially analogous to both tunneling across a Josephson junction and spin-transfer phenomena in ferromagnetic metals [61, 62, 63, 64, 65]. The key difference between these two examples of current-biased order parameter manipulation is that the bias is applied by the superconducting condensate in the former case and by dissipative quasiparticles in the latter. Tunneling in quantum Hall bilayers is an example of (pseudospin) transfer, with the additional feature that the transport quasiparticles are localized at the edge of the

system when order is strong and the quantum Hall effect firmly established.

The *dc* Josephson effect occurs because the quasiparticles are in equilibrium with the condensate when $I_c \sin(\varphi) = I_{bias}$; the current bias influences microscopic self-energy of the quasiparticles so that the phase change across the junction is no longer zero when the quasiparticles density matrix is at equilibrium. Current then flows across the junction without dissipation.

In $\nu = 1$ quantum Hall bilayer tunneling experiments the situation is very similar to the one of spin-transfer phenomena in ferromagnetic metals. The spin-transfer torque term in the equation of motion for the magnetization in presence of nonequilbrium transport spins, like the bias term in the Josephson junction case, arises[66] microscopically from a change in the self-energy experienced by the quasiparticles. In the presence of the transport current the magnetic nanoparticle quasiparticles are in equilibrium not when the in-plane magnetization is aligned with the external field, but when its orientation in the easy-plane direction is displaced from the field direction by an angle proportional to the current. The key difference between a current-biased Josephson junction and a current-biased nanomagnet, is that the bias field experienced by the quasiparticles is applied in one case by the condensate, and in the other case by transport quasiparticles that are held out of equilibrium by a bias voltage. The current in spin-transport devices and tunneling experiment in $\nu = 1$ quantum Hall bilayers is always dissipative.

Chapter 6

Dynamics of magnetization coupled to a thermal bath of elastic modes

6.1 Introduction

In the previous chapter we have studied the dynamics of the order parameter that characterizes the broken symmetry ground state of $\nu = 1$ quantum Hall bilayers taking into account its coupling to quasiparticle currents. Using the pseudospin mapping we saw the deep analogy between the order parameter in a $\nu = 1$ quantum Hall bilayer and the magnetization, $\mathbf{M}$, in an easy plane ferromagnet. We saw however, in section 4.1, that if we include damping the equation of motion for the order parameter of a quantum Hall bilayer and the magnetization in a ferromagnet are different: in the quantum Hall bilayer the damping is anisotropic whereas the phenomenological damping usually adopted to describe the damped dynamics of the magnetization is isotropic. We also saw how both cases differ from the case of a damped Josephson junction. It is natural to wonder about the microscopic reason

of these differences.

At the end of chapter 3 we saw that the damping of the collective modes in a quantum Hall bilayer is ultimately due to the presence of disorder that to a good approximation commutes with the z component of the pseudospin. This is the microscopic reason of the anisotropy of the damping in quantum Hall bilayers: $\alpha_\varphi \neq 0$, $\alpha_z \approx 0$. The problem of the damping of the magnetization is a long standing one [67],[68], [69], [70] whose details are still not completely understood. The problem arises from the fact that different mechanisms for the damping of the magnetization are possible and in some cases a detailed description can be achieved only by taking all of them into account. In this chapter we consider the case when the coupling of the magnetization $\mathbf{M}$ to elastic modes is the main source of damping for $\mathbf{M}$. One of the main results of this chapter is that we show, starting from the physical coupling of the magnetization to the elastic modes, that in general also for the order parameter in a ferromagnet the damping can be non isotropic. This fact can be of notable importance when we try to control the magnetization, either using spin currents as in spintronic devices or by more conventional means.

Through the fluctuation-dissipation theorem we have that in thermal equilibrium there is a very simple connection between damping and thermal fluctuations. A knowledge of the details of the damping properties will then also allow us to characterize in detail the thermal fluctuations. The standard approach toward modeling magnetization fluctuations is to start from the Landau-Lifshitz-Gilbert-Brown equation [71]

$$\frac{\partial \mathbf{\Omega}}{\partial t} = \frac{\gamma}{M_s}\mathbf{\Omega} \times \left[\frac{\delta E}{\delta \mathbf{\Omega}} + \mathbf{h}\right] + \alpha \mathbf{\Omega} \times \frac{\partial \mathbf{\Omega}}{\partial t}, \tag{6.1}$$

where γ is the gyromagnetic ratio, $\mathbf{\Omega} = \mathbf{M}/M_s$ is the magnetization direction, $\mathbf{M}$ is the magnetization, M_S the magnitude of the saturation magnetization, E the free energy and $\mathbf{h}$ a random magnetic field. This equation assumes that the characteristic time scale of the magnetization dynamics is longer than the typical time scale

of the environment that is responsible for the dissipative term proportional to α. In practice the use of this equation is partially inconsistent, resulting in some practical limitations to its application [72, 73]. The source of the problem is that the dissipation is local in time. Because of the fluctuations dissipation theorem, this implicitly requires the random field to have white noise properties i.e. to have zero autocorrelation time. Since the contribution of the random field to the magnetization dynamics $\gamma\mathbf{\Omega} \times \mathbf{h}$ depends on $\mathbf{\Omega}$, equation (6.1) exhibits white multiplicative noise [74]. It follows that in order to integrate equation(6.1) reliably we need to track the evolution of $\mathbf{\Omega}$ on very short time scales for which the white noise approximation for $\mathbf{h}$ is likely to be unphysical.

The problem of the dynamics of the magnetization when coupled to elastic modes has been studied before, see for example the book by Sparks [69] and references therein. In most of the previous works a damping coefficient was calculated by means of the Fermi golden rule and for the case of an infinite ferromagnet. As we show in the next section the Fermi golden rule has some limitations. Also with the increasing advances of nanotechnology smaller and smaller magnetic devices are being realized for which the bulk approximation is of limited applicability. In this chapter based on a Caldeira-Leggett [10] approach, we present a theory that overcomes some of the limitations of the Fermi golden rule and that is applicable to magnetic systems of any size (and shape) for which a semiclassical approach is valid.

6.2 Limits of applicability of the Fermi golden rule

In this section we present the limits of the Fermi golden rule to describe damped dynamics. We consider a simple system formed by a central harmonic oscillator coupled to a bath of harmonic oscillators. We first derive the equation of motion of the central oscillator integrating out the reservoir harmonic oscillators in the Caldeira-

Legget approach. We then use the Fermi golden rule to do find the expression for the relaxation rate for the central oscillator. At the end, by comparing the results obtained with the two approaches we find the limits of applicability of the Fermi golden rule to describe dissipation.

Let (q, p) be the canonical coordinates of a central harmonic oscillator coupled to a reservoir of harmonic oscillator with coordinates (q_α, p_α). The total Hamiltonian will be:

$$H = H_s(q, p) + H_R(q_\alpha, p_\alpha) + H_I(q, q_\alpha)$$

where

$$H_s = \frac{p^2}{2m} + \frac{\omega^2 m}{2} q^2$$

is the Hamiltonian for the isolated central oscillator

$$H_R = \sum_\alpha \left(\frac{p_\alpha^2}{2m_\alpha} + \frac{\omega_\alpha^2 m_\alpha}{2} q_\alpha^2 \right)$$

is the Hamiltonian for the isolated reservoir and

$$H_I = -\sum_\alpha c_\alpha q_\alpha q$$

is the interaction Hamiltonian that couples the central oscillator to the reservoir degrees of freedom.

For the reservoir degrees of freedom we then find the following dynamical: equations:

$$\dot{q_\alpha} = \frac{p_\alpha}{m_\alpha}$$
$$\dot{p_\alpha} = -\omega_\alpha^2 m_\alpha q_\alpha + c_\alpha q$$

Integrating these equations:

$$q_\alpha = q_\alpha(0)\cos(\omega_\alpha t) + \frac{p_\alpha(0)}{m_\alpha\omega_\alpha}\sin(\omega_\alpha t) + \frac{c_\alpha}{m_\alpha\omega_\alpha}\int_0^t dt' \sin[\omega_\alpha(t-t')]q(t') \qquad (6.2)$$

For the the central, (q,p), oscillator we have:

$$\begin{aligned}\dot{q} &= \frac{p}{m} \\ \dot{p} &= -\omega^2 m q + \sum_\alpha c_\alpha q_\alpha\end{aligned}$$

From which we find:

$$\ddot{q} = -\omega^2 q + \frac{1}{m}\sum_\alpha c_\alpha q_\alpha \qquad (6.3)$$

If we now use equation (6.2) from (6.3) we find:

$$\begin{aligned}\ddot{q} = -\omega^2 q &+ \frac{1}{m}\sum_\alpha c_\alpha\left[q_\alpha(0)\cos(\omega_\alpha t) + \frac{p_\alpha(0)}{m_\alpha\omega_\alpha}\sin(\omega_\alpha t)\right] \\ &+ \frac{1}{m}\sum_\alpha \frac{c_\alpha^2}{m_\alpha\omega_\alpha}\int_0^t dt' \sin[\omega_\alpha(t-t')]q(t')\end{aligned} \qquad (6.4)$$

Integrating by part the last term we find:

$$\begin{aligned}\ddot{q} = -\omega^2 q &+ \frac{1}{m}\sum_\alpha c_\alpha\left[q_\alpha(0)\cos(\omega_\alpha t) + \frac{p_\alpha(0)}{m_\alpha\omega_\alpha}\sin(\omega_\alpha t)\right] \\ &- \frac{1}{m}\sum_\alpha \frac{c_\alpha^2}{m_\alpha\omega_\alpha^2}\int_0^t dt' \cos[\omega_\alpha(t-t')]\dot{q}(t') \\ &+ \frac{1}{m}\sum_\alpha \frac{c_\alpha^2}{m_\alpha\omega_\alpha^2}[q(t) - \cos(\omega_\alpha t)q(0)]\end{aligned} \qquad (6.5)$$

The last term is the sum of a frequency renormalizing term and of a term that depends on the initial condition. Because we don't want the coupling to the reservoir to cause renormalization of the central oscillator frequency we should neglect the renormalizing term. Also, without loss of generality, we can neglect the term that

depends on the initial state. We then finally find:

$$\ddot{q} = -\omega^2 q + \frac{1}{m}\sum_\alpha c_\alpha \left[q_\alpha(0)\cos(\omega_\alpha t) + \frac{p_\alpha(0)}{m_\alpha \omega_\alpha}\sin(\omega_\alpha t)\right] - \frac{1}{m}\sum_\alpha \frac{c_\alpha^2}{m_\alpha \omega_\alpha^2}\int_0^t dt' \cos[\omega_\alpha(t-t')]\dot{q}(t') \tag{6.6}$$

Let

$$\gamma(t-t') = \Theta(t-t')\frac{1}{m}\sum_\alpha \frac{c_\alpha^2}{m_\alpha\omega_\alpha^2}\cos[\omega_\alpha(t-t')]$$

and

$$y = \frac{1}{m}\sum_\alpha c_\alpha \left[q_\alpha(0)\cos(\omega_\alpha t) + \frac{p_\alpha(0)}{m_\alpha\omega_\alpha}\sin(\omega_\alpha t)\right]$$

Now if we take the average with respect to the initial states, $q_\alpha(0), p_\alpha(0)$, using the reservoir classical equilibrium density we find:

$$\langle y(t)t(t')\rangle = \frac{2K_BT}{m}\gamma(t-t')$$

and in Fourier space:

$$\langle y^2(\omega)\rangle = \frac{2K_BT}{m}\gamma(\omega) \tag{6.7}$$

This is the classical form of the Fluctuation Dissipation Theorem. In terms of γ and y the dynamical equations for q will be:

$$q = -\omega^2 q - \int_0^t dt'\gamma(t-t')q(t') + y \tag{6.8}$$

For this model is quite simple to do a quantum mechanical treatment in terms of path integrals and effectively integrate out the reservoir degrees of freedom, [10], [75]. Even in the quantum mechanical treatment the average expectation value for q satisfies equation (6.8). In the semiclassical limit in which only the Gaussian fluctuations are taken into account the only difference from the classical treatment

and the quantum mechanical one appears in the modification of equation (6.7) that becomes:

$$\langle y^2(\omega)\rangle = \frac{\hbar\omega}{m}\gamma(\omega)\coth\left(\frac{\hbar\omega}{K_BT}\right) \tag{6.9}$$

It's easy to see that (6.9) reduces to (6.7) in the limit $\hbar \to 0$

The point that we want to make here is that the damping kernel γ doesn't depend on the temperature and also doesn't depend on the frequency difference $|\omega_\alpha - \omega|$. In particular we find that if the main harmonic oscillator is not in the ground state it will be damped to lower energy states even at 0 temperature and independent of the difference $|\omega_\alpha - \omega|$, as long as it's coupled to the reservoir degrees of freedom. The only thing that depends on the temperature is the amplitude of the thermal fluctuations.

Let's now briefly review, for the same system, the Fermi golden rule approach. Using the standard canonical transformation:

$$a \equiv \sqrt{\frac{m\omega}{2\hbar}}\left(q + \frac{ip}{m\omega}\right); \qquad a^\dagger \equiv \sqrt{\frac{m\omega}{2\hbar}}\left(q - \frac{ip}{m\omega}\right);$$

we can rewrite the Hamiltonian in the form:

$$H = \hbar\omega\left(a^\dagger a + \frac{1}{2}\right) + \sum_\alpha \hbar\omega_\alpha\left(a_\alpha^\dagger a_\alpha + \frac{1}{2}\right) + H_I$$

with

$$H_I = \frac{\hbar}{2}(m\omega)^{-1/2}\sum_\alpha (m_\alpha\omega_\alpha)^{-1/2}c_\alpha\left[a_\alpha a + a_\alpha a^\dagger + a_\alpha^\dagger a + a_\alpha^\dagger a^\dagger\right]$$

Let's now use the Fermi golden rule to estimate the transition probability per unit

time, w^-, from the state $|n; n_\alpha\rangle$ to the state $|n-1; n_\alpha+1\rangle$. We have:

$$w^- = \frac{2\pi}{\hbar}\sum_\alpha |\langle n-1; n_\alpha+1|H_I|n; n_\alpha\rangle|^2 \delta(\hbar\omega - \hbar\omega_\alpha) \tag{6.10}$$

$$= \frac{\pi\hbar}{2}\sum_\alpha \frac{c_\alpha^2}{m m_\alpha \omega\omega_\alpha} n(n_\alpha+1)\delta(\hbar\omega - \hbar\omega_\alpha) \tag{6.11}$$

Similarly for the transition probability per unit time, w^+, from the state $|n; n_\alpha\rangle$ to the state $|n+1; n_\alpha-1\rangle$ we find:

$$w^+ = \frac{\pi\hbar}{2}\sum_\alpha \frac{c_\alpha^2}{m m_\alpha \omega\omega_\alpha}(n+1)n_\alpha\delta(\hbar\omega - \hbar\omega_\alpha)$$

Therefore the net change of the central oscillator occupation number will be given by:

$$\frac{dn}{dt} = w^+ - w^- = -\sum_\alpha \frac{\pi\hbar c_\alpha^2}{2m m_\alpha\omega_\alpha\omega}(n-n_\alpha)\delta(\hbar\omega - \hbar\omega_\alpha) \tag{6.12}$$

In order to estimate the relaxation rate Γ we then assume:

$$\frac{dn}{dt} = -\Gamma(n-\overline{n}) \tag{6.13}$$

where $\overline{n}$ is the thermal equilibrium distribution function. In order to proceed further we now assume $n_\alpha = \overline{n_\alpha}$. Because of the energy delta function in (6.12) we can then assume $\overline{n_\alpha} = \overline{n}$. Comparing (6.12) with (6.13) we then find:

$$\Gamma = \sum_\alpha \frac{\pi\hbar c_\alpha^2}{2m m_\alpha\omega_\alpha\omega}\delta(\hbar\omega - \hbar\omega_\alpha) \tag{6.14}$$

We can compare this result to the expression for $\gamma(t-t')$, found previously, in the limit $t \to t'$, $\omega \to \omega_\alpha$.

We then see that according to (6.14) the relaxation rate depends on the difference $|\omega - \omega_\alpha|$. As a consequence, for example, if we have discrete modes and

for any α is $\omega_\alpha \neq \omega$ equation (6.14) tells us that there won't be any damping of the central oscillator excited state. But this is obviously wrong because for example the state $|n > 0; 0\rangle$ is obviously not an eigenstate of the total Hamiltonian and as a consequence it cannot be a stationary state. The contradiction is resolved if we recall that in the derivation of the Fermi golden rule it is assumed that the transition probability (w^-, w^+ in our notation) is time independent. But this is true only if the energy difference between the initial state and the final state is infinitesimally small. Therefore if we have discrete energy levels we cannot use the Fermi golden rule. Also note that in deriving (6.14) we had to assume the reservoir to be in thermal equilibrium ($n_\alpha = \overline{n_\alpha}$). In the derivation of γ given at the beginning we didn't have to make this assumption and we used the fact that the reservoir was in thermal equilibrium only to find the correlation of the random force. The fact that in order to find Γ we had to assume $n_\alpha = \overline{n_\alpha}$ implies that we can only use the Fermi golden rule when the relaxation times are bigger than the thermalization time of the reservoir, $\hbar/K_B T$. This fact in particular makes the Fermi golden rule inapplicable in the zero temperature limit. Summarizing the limits of applicability of the Fermi golden rule are:

- We must have a continuous distribution of initial and final states;
- The relaxation time must be bigger than the thermalization time $\hbar/K_B T$;
- We must be in a situation in which we can use the Born approximation;
- We can only use it in the limit of applicability of the Markow approximation.

The last point tells us that we can us the Fermi golden rule only for situation for which we can assume the damping kernel $\gamma(t, t')$ to be a Dirac's delta : $\gamma(t, t') \propto \delta(t - t')$. The use of the Fermi golden rule doesn't allow us to find a damping kernel nonlocal in time and then doesn't allow a correct description of colored noise.

The fact that the damping kernel doesn't depend on the temperature can be understood considering that in our toy model the coupling between the central harmonic oscillator and the reservoir degrees of freedom is always present, at any temperature. Using the method shown in the first part of these notes we can assume the expression of γ to be valid all the way to 0 temperature. If the reservoir in the initial state is at 0 T and the central oscillator is in an excited state, because of the coupling, the motion of the central oscillator will excite the reservoir degrees of freedom with the final result of: damping of the central oscillator motion, increase of the temperature of the reservoir.

6.3 Equation of motion of the magnetization when coupled to a thermal bath of elastic modes

Calling q_n the degrees of freedom of the reservoir, we consider the following form for the total Lagrangian:

$$\mathcal{L} = \mathcal{L}_S[\mathbf{\Omega}(\mathbf{x}), \dot{\mathbf{\Omega}}(\mathbf{x})] + \mathcal{L}_R[q_n, \dot{q}_n] + \mathcal{L}_I[\mathbf{\Omega}(\mathbf{x}), q_n] - \Delta\mathcal{L}[\mathbf{\Omega}(\mathbf{x})], \tag{6.15}$$

where $\mathcal{L}_S[\mathbf{\Omega}(\mathbf{x}), \dot{\mathbf{\Omega}}(\mathbf{x})]$ is the Lagrangian that describes the dynamics of the magnetization when not coupled to external degrees of freedom, $\mathcal{L}_R[q_n, \dot{q}_n]$ is the Lagrangian for the the reservoir and $\mathcal{L}_I[\mathbf{\Omega}(\mathbf{x}), q_n]$ is the interaction Lagrangian that couples the magnetization to the reservoir degrees of freedom. The term $\Delta\mathcal{L}[\mathbf{\Omega}(\mathbf{x})]$ is a counter term that depends on $\mathbf{\Omega}$ and the parameters of the reservoir but not on the dynamic variables of the reservoir [10, 75]. This term is introduced to compensate a renormalization of the energy of the system caused by its coupling to the reservoir [10].

The Landau-Liftshitz equations for the decoupled system magnetization fol-

low from the magnetic Lagrangian,

$$\mathcal{L}_S = \int_{V_M} \left[\frac{M_s}{\gamma} \mathbf{A}[\mathbf{\Omega}] \cdot \dot{\mathbf{\Omega}} - E_s[\mathbf{\Omega}] \right] d\mathbf{x}, \tag{6.16}$$

where $\mathbf{A}$ is a vector field defined by the equation: $\nabla_{\mathbf{\Omega}} \times \mathbf{A}[\mathbf{\Omega}] = \mathbf{\Omega}$, $E_S[\mathbf{\Omega}]$ is the magnetic free energy functional, V_M the volume of the ferromagnet and γ the gyromagnetic ratio. We model the reservoir as a set of classical degrees of freedom:

$$\mathcal{L}_R = \frac{1}{2} \sum_n m_n \dot{q}_n^2 - E_R(q_n). \tag{6.17}$$

The Euler-Lagrange equations for the total Lagrangian (6.15) yield the following coupled dynamical equations:

$$m_n \ddot{q}_n = \frac{\partial}{\partial q_n} [\mathcal{L}_R(q_n, \dot{q}_n) + \mathcal{L}_I[\mathbf{\Omega}, q_n]] \tag{6.18}$$

$$\frac{\partial \mathbf{\Omega}}{\partial t} = \mathbf{\Omega} \times \frac{\gamma}{M_s} \frac{\delta}{\delta \mathbf{\Omega}} [E_S[\mathbf{\Omega}, \dot{\mathbf{\Omega}}] - \mathcal{L}_I[\mathbf{\Omega}, q_n] + \Delta\mathcal{L}[\mathbf{\Omega}]]. \tag{6.19}$$

When $\mathcal{L}_I$ is linear in the coordinates of the bath, we can formally integrate (6.18) to get $q^{(n)}(t)$ as a function only of the initial conditions and $\mathbf{\Omega}$ and then insert the result in (6.19) to eliminate the reservoir coordinates from the dynamical equations for $\mathbf{\Omega}$, integrating out the reservoir degrees of freedom. An example of the application of this procedure for a quantum mechanical model of the interaction between magnetization and reservoir degrees of freedom can be found in Ref. [76].

If we consider only long wavelength vibrations we can treat the lattice as a continuous medium and use results from elasticity theory. The free energy, E_R, of the elastic medium can then be expressed in terms of the strain tensor $u_{i,j}$,

$$u_{ij} \equiv \frac{1}{2} \left(\frac{\partial u_i}{\partial x_j} + \frac{\partial u_j}{\partial x_i} \right)$$

where $\mathbf{u}$ is the displacement vector field.

We will be interested in applying our results to polycrystalline elastic media which can be treated as isotropic to a good approximation. (It's quite straightforward, albeit quite tedious, to extend our results to the case of non-isotropic media with specific lattice symmetries). For isotropic elastic media it follows from general symmetry considerations that, to lowest order, we can express the magnetoelastic energy in the form, [77]

$$E_I = B_1 \sum_{i,j=1}^{3} \int_{V_M} \Omega_i \Omega_j u_{ij} d\mathbf{x} \tag{6.20}$$

where B_1 is the magnetoelastic coupling constant. For the case of soft ferromagnet thin films, the main contribution to the magnetoelastic energy will be given by the magnetostatic energy dependence on strain. This contribution to E_I is normally referred as the the form effect [78]. The constant B_1 can be extracted from magnetostriction data. For an isotropic elastic medium with isotropic magnetostriction, λ, we have [77] that

$$B_1 = \frac{3}{2}\lambda \frac{E}{2-\sigma}, \tag{6.21}$$

where E is the Young's modulus and σ the Poisson's ratio.

The Lagrangian for the reservoir $\mathcal{L}_R$ is,

$$\mathcal{L}_R = \frac{1}{2}\int_V \rho\, \dot{\mathbf{u}}^2 d\mathbf{x} - E_R, \tag{6.22}$$

where ρ is the mass density, V the total volume of the elastic medium (magnetic film plus substrate) and E_R is given by [79]:

$$E_R = \int_V \left[\frac{E}{2(1+\sigma)} \sum_{i,j=1}^{3} u_{ij}^2 + \frac{\sigma E}{2(1+\sigma)(1-2\sigma)} \sum_{i=1}^{3} u_{ii}^2. \right] d\mathbf{x} \tag{6.23}$$

The equation of motion for the displacement will then be,

$$\rho\frac{\partial^2\mathbf{u}}{\partial t^2} = -\frac{\delta}{\delta\mathbf{u}(\mathbf{x})}(E_R[\mathbf{u}] + E_I[\mathbf{\Omega},\mathbf{u}]). \tag{6.24}$$

It will prove useful to expand $\mathbf{u}$ in terms of the elastic normal modes $\mathbf{f}^{(n)}$:

$$\mathbf{u} = \sum_n q^{(n)}(t)\mathbf{f}^{(n)}(\mathbf{x}) \tag{6.25}$$

where the functions $\mathbf{f}^{(n)}$ satisfy the boundary conditions appropriate for $\mathbf{u}$ and satisfy:

$$\frac{\delta E_R[\mathbf{f}^{(n)}]}{\delta\mathbf{f}^{(n)}(\mathbf{x})} = \omega_n^2\rho\mathbf{f}^{(n)}(\mathbf{x}); \quad n \in N \tag{6.26}$$

$$\frac{1}{M}\int_V \rho\mathbf{f}^{(n)}(\mathbf{x})\cdot\mathbf{f}^{(m)}(\mathbf{x})d\mathbf{x} = \delta_{nm} \tag{6.27}$$

where M is the total mass, $M \equiv \int_V \rho d\mathbf{x}$.

In terms of the degrees of freedom, $q^{(n)}$, we have:

$$\mathcal{L}_I = -E_I = -B_1\sum_n q^{(n)}\sum_{i,j}\int_{V_M}\Omega_i\Omega_j f_{ij}^{(n)}d\mathbf{x} \tag{6.28}$$

with

$$f_{ij}^{(n)} \equiv \frac{1}{2}\left(\frac{\partial f_i^{(n)}}{\partial x_j} + \frac{\partial f_j^{(n)}}{\partial x_i}\right).$$

We then see that the interaction Lagrangian is linear in the coordinates $q^{(n)}$, with coupling constants:

$$c^{(n)}[\mathbf{\Omega}] \equiv \sum_{i,j}\int_{V_M}\Omega_i\Omega_j f_{ij}^{(n)}d\mathbf{x} \tag{6.29}$$

This property will allow us to integrate out the reservoir degrees of freedom to obtain an equation for the dynamics of the magnetization in term of $\mathbf{\Omega}$ alone.

Let's first discuss the dynamics of the reservoir degrees of freedom $q^{(n)}$. Using

equations (6.24)-(6.27) we find the dynamical equations:

$$\ddot{q}^{(n)} = -\omega_n^2 q^{(n)} - \frac{B_1}{M} c^{(n)}[\mathbf{\Omega}] \tag{6.30}$$

Integrating (6.30) we find

$$\begin{aligned} q^{(n)}(t) =& q^{(n)}|_0 \cos(\omega_n t) + \frac{\dot{q}^{(n)}|_0}{\omega_n} \sin(\omega_n t) \\ & - \frac{B_1}{M\omega_n} \int_0^t \sin(\omega_n (t-t')) c^{(n)}[\mathbf{\Omega}(t')] dt', \end{aligned} \tag{6.31}$$

where $q^{(n)}|_0$ and $\dot{q}^{(n)}|_0$ are the initial values of $q^{(n)}$ and $\dot{q}^{(n)}$ respectively. The coupling of the magnetization to the reservoir will cause damping and frequency renormalization. In order to be able to separate the two effects is useful to integrate the last term on the right hand side of (6.31) by parts obtaining:

$$\begin{aligned} q^{(n)}(t) =& q^{(n)}|_0 \cos(\omega_n t) + \frac{\dot{q}^{(n)}|_0}{\omega_n} \sin(\omega_n t) \\ & - \frac{B_1}{M\omega_n^2} c^{(n)}[\mathbf{\Omega}(t)] + \frac{B_1}{M\omega_n^2} c^{(n)}[\mathbf{\Omega}(0)] \cos(\omega_n t) \\ & + \frac{B_1}{M\omega_n^2} \int_0^t dt' \left[\cos(\omega_n (t-t')) \int_{V_M} \left. \frac{\delta c^{(n)}}{\delta \mathbf{\Omega}} \right|_{\mathbf{x}',t'} \cdot \left. \frac{\partial \mathbf{\Omega}}{\partial t'} \right|_{\mathbf{x}'} d\mathbf{x}' \right]. \end{aligned} \tag{6.32}$$

Using the expression of the interaction Lagrangian given by (6.28) and the definition of the coupling constants $c^{(n)}$ we have:

$$\frac{\delta \mathcal{L}_I}{\delta \mathbf{\Omega}} = -B_1 \sum_n q^{(n)} \frac{\delta c^{(n)}}{\delta \mathbf{\Omega}}. \tag{6.33}$$

Combining equations (6.19), (6.32) and (6.33) for the dynamics of the magnetization

we find:

$$\begin{aligned}\frac{\partial \mathbf{\Omega}}{\partial t} =& \mathbf{\Omega} \times \frac{\gamma}{M_s}\frac{\delta E_S}{\delta \mathbf{\Omega}} + \mathbf{\Omega} \times \frac{\gamma}{M_s}\frac{\delta \Delta\mathcal{L}(\mathbf{\Omega})}{\delta \mathbf{\Omega}} \\ &+ \mathbf{\Omega} \times \frac{\gamma}{M_s}\sum_n \left[B_1 \left.\frac{\delta c^{(n)}}{\delta \mathbf{\Omega}}\right|_{\mathbf{x},t} \left(q^{(n)}|_0 \cos(\omega_n t) + \frac{\dot{q}^{(n)}|_0}{\omega_n}\sin(\omega_n t)\right)\right. \\ &- \frac{B_1^2}{M\omega_n^2} c^{(n)}[\mathbf{\Omega}(t)] \left.\frac{\delta c^{(n)}}{\delta \mathbf{\Omega}}\right|_{\mathbf{x},t} + \frac{B_1^2}{M\omega_n^2} c^{(n)}[\mathbf{\Omega}(0)]\cos(\omega_n t) \left.\frac{\delta c^{(n)}}{\delta \mathbf{\Omega}}\right|_{\mathbf{x},t} \\ &+ \left.\frac{B_1^2}{M\omega_n^2}\int_0^t dt' \int_{V_M} d\mathbf{x}' \cos(\omega_n(t-t')) \left.\frac{\delta c^{(n)}}{\delta \mathbf{\Omega}}\right|_{\mathbf{x}',t'} \cdot \left.\frac{\partial \mathbf{\Omega}}{\partial t'}\right|_{\mathbf{x}'} \left.\frac{\delta c^{(n)}}{\delta \mathbf{\Omega}}\right|_{\mathbf{x},t}\right]. \end{aligned} \tag{6.34}$$

The counter term $\Delta\mathcal{L}$ of the total Lagrangian is defined to cancel the frequency renormalizing term:

$$\mathbf{\Omega} \times \frac{\gamma}{M_s}\sum_{i,n} \frac{B_1^2}{M\omega_n^2} c^{(n)}[\mathbf{\Omega}(t)] \left.\frac{\delta c^{(n)}}{\delta \mathbf{\Omega}}\right|_{\mathbf{x},t} \tag{6.35}$$

It follows from Eq. (6.29) that

$$\frac{\delta c^{(n)}}{\delta \Omega_l} = \sum_i \Omega_i \left[\frac{\partial f_l^{(n)}}{\partial x_i} + \frac{\partial f_i^{(n)}}{\partial x_l}\right] \tag{6.36}$$

To simplify and extract the physical content from these cumbersome equations, we identify the memory friction kernel tensor γ_{jm}:

$$\gamma_{jm}(t,t',\mathbf{x},\mathbf{x}') \equiv \Theta(t-t')\sum_n \frac{\gamma}{M_s}\frac{B_1^2}{M\omega_n^2}\cos(\omega_n(t-t')) \left.\frac{\delta c^{(n)}}{\delta \Omega_m}\right|_{\mathbf{x}',t'} \left.\frac{\delta c^{(n)}}{\delta \Omega_j}\right|_{\mathbf{x},t} \tag{6.37}$$

where $\Theta(t-t')$ is the Heaviside function. We also recognize the random field $\mathbf{h}$:

$$\mathbf{h}(\mathbf{x},t) \equiv \frac{B_1}{M_s}\sum_n \left[q^{(n)}|_0 \cos(\omega_n t) + \frac{\dot{q}^{(n)}|_0}{\omega_n}\sin(\omega_n t)\right] \frac{\delta c^{(n)}}{\delta \mathbf{\Omega}}. \tag{6.38}$$

Assuming that the distribution of initial positions of the environment degrees of freedom follows the canonical classical equilibrium density for the unperturbed reservoir we find that

$$\langle \mathbf{h}(\mathbf{x},t)\rangle = 0, \tag{6.39}$$

$$\langle h_j(\mathbf{x},t)h_m(\mathbf{x}',t')\rangle = \frac{2K_BT}{\gamma M_s}\gamma_{jm}(t,t',\mathbf{x},\mathbf{x}'). \tag{6.40}$$

In terms of γ_{jm} and $\mathbf{h}$ the dynamical equation for $\mathbf{\Omega}$ takes the form:

$$\begin{aligned}\frac{\partial \Omega_l}{\partial t} =& \epsilon_{ijl}\Omega_i\frac{\gamma}{M_s}\frac{\delta E_S}{\delta \Omega_j} + \gamma\epsilon_{ijl}\Omega_i h_j \\ &+ \epsilon_{ijl}\Omega_i\int_0^t dt'\int_{V_M} d\mathbf{x}'\sum_m \gamma_{jm}(t,t',\mathbf{x},\mathbf{x}')\left.\frac{\partial \Omega_m}{\partial t'}\right|_{\mathbf{x}'} \\ &+ \epsilon_{ijl}\Omega_i\frac{\gamma}{M_s}\sum_{i,n}\frac{B_1^2}{M\omega_n^2}c^{(n)}[\mathbf{\Omega}(0)]\cos(\omega_n t)\frac{\delta c^{(n)}}{\delta \Omega_j}\end{aligned}$$

The final term is an artifact of the assumption that in the initial state the reservoir was decoupled from the system [75, 80]. Dropping this term, the dynamical equations for magnetization coupled to a thermal bath of elastic modes is:

$$\frac{\partial \Omega_l}{\partial t} = \epsilon_{ijl}\Omega_i\frac{\gamma}{M_s}\frac{\delta E_S}{\delta \Omega_j} + \gamma\epsilon_{ijl}\Omega_i h_j + \epsilon_{ijl}\Omega_i\int_0^t dt'\int_{V_M} d\mathbf{x}'\sum_m \gamma_{jm}(t,t',\mathbf{x},\mathbf{x}')\left.\frac{\partial \Omega_m}{\partial t'}\right|_{\mathbf{x}'} \tag{6.41}$$

with γ_{jm} defined by (6.37) and $\mathbf{h}$ a random field with statistical properties given by (6.39) and (6.40). Equation (6.41) is quite general. In particular notice that to obtain (6.41) we didn't perform any expansion in $\mathbf{\Omega}$. As a consequence, as long as we keep the exact form for $E_S(\mathbf{\Omega})$, equations (6.41) includes also the effects of spin wave interactions. In principle we could also include in E_S a term to take into account the scattering of spin waves due to disorder. Equation (6.41) does not, however, take into account the coupling between the magnetization and particle-hole excitations.

As we discuss in Section 6.6, this coupling appears to be of critical importance in many metallic ferromagnets.

Equation (6.41) is very different from the standard stochastic Landau-Lifshitz-Gilbert (s-LLG) equation, Eq. (6.1). Because the magnetoelastic energy, E_I, (6.20), is nonlinear in the magnetization, in (6.41) both the damping kernel and the random field depend on the magnetization and therefore are state dependent. This is in contrast with the s-LLG equation for which both the damping kernel, $\alpha\delta(t-t')$, and the random field are independent of $\mathbf{\Omega}$.

Another difference between Eq. (6.41) and the s-LLG equation is that the damping kernel, γ_{jm}, is in general a tensor. The tensor character of the damping has been suggested previously on phenomenological grounds [73]. Starting from the physical coupling (6.20), in our approach the tensor character of γ_{jm} appears naturally as a consequence of: *(a)* the nonlinearity in $\mathbf{\Omega}$ of the magnetoelastic coupling (6.20), *(b)* the anisotropy of the elastic modes due to the boundary conditions and/or anisotropy of the elastic properties. For small oscillations of $\mathbf{\Omega}$ around its equilibrium (up to quadratic order), the kernel γ_{jm} can be assumed to be independent of $\mathbf{\Omega}$. Even in this linearized case, the damping kernel that appears in (6.41) will still have a tensor form due to the anisotropy of the elastic modes.

As mentioned above, the standard s-LLG damping kernel is simply $\alpha\delta(t-t')$, *i.e.* the damping is frequency-independent. As a consequence, from the Fluctuation Dissipation Theorem, we have that the spectrum of the random field that appears in (6.1) is also frequency-independent. This differs from equation (6.41) for which the damping kernel, and therefore the spectrum of the random field, is frequency-dependent.

Given the geometry and the material properties of the system we can find the elastic modes, $\mathbf{f}^{(n)}$, and then integrate equation (6.41) using a micromagnetic approach. The integration of equation (6.41) could give insight in particular on the

damping of the uniform magnetization mode for different geometries and show the range of validity of the classic picture [69] of a two stage damping process in which the motion of the coherent magnetization induces non uniform magnetic modes on short time scales that then decay to lattice vibrations.

We now study the dynamics of the uniform magnetic mode in the case when we can neglect its interaction with spin waves and the only coupling to external degrees of freedom is magnetoelastic. Projecting Eq. (6.41) on the uniform mode we find that

$$\begin{aligned}\frac{d\Omega_l}{dt} =&\epsilon_{ijl}\Omega_i\frac{\gamma}{V_M M_s}\int_{V_M}\frac{\delta E_S}{\delta\Omega_j}d\mathbf{x} + \epsilon_{ijl}\Omega_i\frac{\gamma}{V_M}\int_{V_M} h_j d\mathbf{x} \\ &+ \epsilon_{ijl}\Omega_i\frac{1}{V_M}\int_0^t dt'\int_{V_M}d\mathbf{x}\int_{V_M}d\mathbf{x}'\sum_m \gamma_{jm}(t,t',\mathbf{x},\mathbf{x}')\frac{d\Omega_m}{dt'}\end{aligned} \tag{6.42}$$

Let's define the space averaged error field

$$\bar{\mathbf{h}}(t) \equiv \frac{1}{V_M}\int_{V_M}\mathbf{h}(\mathbf{x},t)d\mathbf{x},$$

the damping kernel

$$\bar{\gamma}_{jm}(t,t') \equiv \frac{1}{V_M}\int_{V_M}d\mathbf{x}\int_{V_M}d\mathbf{x}'\gamma_{jm}(t,t',\mathbf{x},\mathbf{x}'),$$

and the coefficients

$$c_l^{(n)} \equiv \int_{V_M}\frac{\delta c^{(n)}}{\delta\Omega_l}d\mathbf{x}.$$

Using the fact that $\mathbf{\Omega}$ is uniform we obtain

$$c_l^{(n)} = \sum_i \Omega_i\int_{V_M}\left[\frac{\partial f_l^{(n)}}{\partial x_i} + \frac{\partial f_i^{(n)}}{\partial x_l}\right]d\mathbf{x}. \tag{6.43}$$

In terms of the coefficients $c_l^{(n)}$ we can then write:

$$\bar{h}_l = \frac{B_1}{M_s V_M} \sum_n c_l^{(n)} \left(q^{(n)}|_0 \cos(\omega_n t) + \frac{\dot{q}^{(n)}|_0}{\omega_n} \sin(\omega_n t) \right)$$

and

$$\bar{\gamma}_{jm} = \Theta(t-t') \frac{\gamma B_1^2}{M_s M V_M} \sum_n \frac{1}{\omega_n^2} c_j^{(n)}(t) c_m^{(n)}(t') \cos(\omega_n (t-t')). \tag{6.44}$$

The uniform magnetization dynamics can then be expressed in terms of the spatially averaged random field $\bar{\mathbf{h}}$ and memory friction kernel $\bar{\gamma}_{jl}$:

$$\frac{d\Omega_l}{dt} = \epsilon_{ijl}\Omega_i \frac{1}{V_M}\frac{\gamma}{M_s} \int_{V_M} \frac{\delta E_S}{\delta \Omega_j} d\mathbf{x} + \gamma \epsilon_{ijl}\Omega_i \bar{h}_j + \epsilon_{ijl}\Omega_i \int_0^t dt' \sum_m \bar{\gamma}_{jm}(t,t') \frac{d\Omega_m}{dt'} \tag{6.45}$$

with

$$\langle \bar{\mathbf{h}} \rangle = 0 \tag{6.46}$$

and

$$\langle \bar{h}_j(t) \bar{h}_m(t') \rangle = \frac{2K_B T}{\gamma V_M M_s} \bar{\gamma}_{jm}(t,t'). \tag{6.47}$$

6.4 Thin Film Uniform Magnetization: damping kernel and random fields

We now apply equation (6.45) to study the dynamics of the uniform magnetization in a thin ferromagnetic film placed on top of a non magnetic substrate and covered by a non-magnetic capping layer, as illustrated in Fig. 6.1. We assume that all media are polycrystalline and treat them as isotropic. We will assume the lateral size, L_s, Fig. 6.1, to be much bigger than the film thickness h. Notice that if we

take L_s bigger than the domain wall width our assumption that the non uniform magnetic modes are quenched wouldn't be valid anymore. We will consider only oscillations of the magnetization around an equilibrium position parallel to the x_3 axis so that we can calculate the damping kernel tensor γ_{jm} assuming the elastic modes to depend only on x_3. Otherwise, to find the correct damping kernel, we would have to take into account the fact that the lateral size, L_s, is finite and solve the full 3D elasticity problem for the elastic modes. To find the dynamics of the

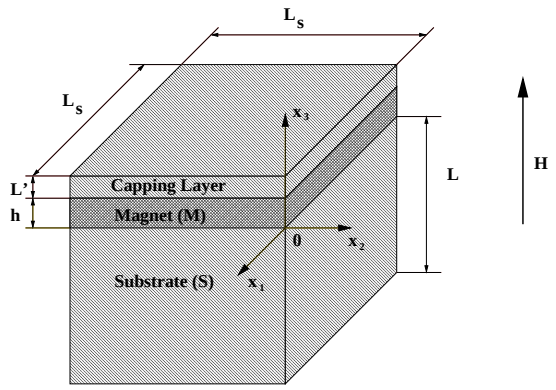

Figure 6.1: Geometry considered for the case of a thin ferromagnetic film on a non-magnetic substrate.

magnetization using equation (6.45) we need to evaluate the memory friction kernel γ_{jm}. The first step in this calculation is the determination of the elastic normal modes $\mathbf{f}^{(n)}$ which satisfy the following equation:

$$\omega_n^2 \rho \mathbf{f}^{(n)} = -\frac{E}{2(1+\sigma)} \nabla^2 \mathbf{f}^{(n)} - \frac{E}{2(1+\sigma)(1-2\sigma)} \nabla(\nabla \cdot \mathbf{f}^{(n)}). \tag{6.48}$$

We allow the film, the substrate, and the capping layer to have different elastic properties and solve equation (6.48) separately in the different subsystems using the appropriate elastic constants. We assume for the sake of definiteness that the substrate and capping layer material is identical. We then match solutions by imposing

the continuity of displacement and stresses at the interfaces $x_3 = 0$, and $x_3 = h$. As boundary conditions we assume the top surface of the capping layer to be free and no displacement at the bottom of the substrate.

Because in our case the elastic modes only depend on x_3, Eq. (6.43) simplifies to

$$c_l^{(n)} = L_s^2 \sum_i \Delta f_i^{(n)} [\delta_{il}\Omega_3 + \Omega_i \delta_{3l}]$$

with

$$\Delta f_i^{(n)} \equiv f_i^{(n)}(h) - f_i^{(n)}(0)$$

The spatially averaged damping coefficients have a simple expression in terms of the $\Delta f_i^{(n)}$:

$$\begin{aligned}\bar{\gamma}_{jl} =& \Theta(t-t') \frac{L_s^2 B_1^2}{Mh} \sum_n \frac{[\Delta f_i^{(n)}]^2}{\omega_n^2} \cos(\omega_n (t-t')) \\ & \times [\delta_{ij}\Omega_3(t) + \Omega_i(t)\delta_{3j}][\delta_{il}\Omega_3(t') + \Omega_i(t')\delta_{3l}]. \end{aligned} \tag{6.49}$$

Eq. 6.49 follows from the completeness relation of the polarization vectors. Once we know the coefficients $\Delta f_i^{(n)}$, Eqs. (6.49), (6.46), and (6.47) completely specify the dynamical equation (6.45) for the magnetization.

As an example we consider the case of a polycrystalline ferromagnetic thin film, like YIG, placed on a substrate of a polycrystalline paramagnet like Tantalum, *Ta*. As typical values we take [81] the ones listed in Table 6.1. For the magnetostriction we assume $\lambda = 2 \times 10^{-6}$. Using equation (6.21), we find that $B_1 = 4 \times 10^6 \text{ergs/cm}^3$. Given the elastic modes implied by these parameter values, we can calculate the coefficients $\Delta f_i^{(n)}$. Once we know the coefficients $\Delta f_i^{(n)}$ we have all the elements to completely specify equation (6.45).

To integrate (6.45) we generate a stochastic field $\bar{\mathbf{h}}$ with the correct statistical

Table 6.1: Elastic properties. c_t, c_l are the transverse and longitudinal speed of sound respectively.

	Magnetic Film	Substrate/Capping Layer
E	200 Gpa	180 Gpa
σ	0.33	0.33
ρ	5.0 g/cm^3	16.6 g/cm^3
c_t	4.0 km/s	2.0 km/s
c_l	5.0 km/s	4.1 km/s

properties by using its Fourier representation. To obtain

$$\langle y(t)y(t')\rangle = G(t-t') \tag{6.50}$$

we choose [34]

$$\langle y(\omega)y(\omega')\rangle = \delta(\omega-\omega')G(\omega) \tag{6.51}$$

where

$$y(\omega) = \frac{1}{2\pi}\int_{-\infty}^{\infty} y(t)\mathrm{e}^{-i\omega t}dt$$

and

$$G(\omega) = \frac{1}{2\pi}\int_{-\infty}^{\infty} G(\tau)\mathrm{e}^{-i\omega\tau}d\tau.$$

In our case we have from Eq. (6.44), that the memory friction kernel $\bar{\gamma}_{jl}$ depends separately on t and t'. As a consequence, through (6.47), we have that the average $\langle\bar{\mathbf{h}}(t)\bar{\mathbf{h}}(t')\rangle$ doesn't depend only on the time difference $\tau = t-t'$. The random field $\bar{\mathbf{h}}(t)$ therefore doesn't define an ergodic process and in particular we cannot use equation (6.51). For this reason it is convenient to define the auxiliary random variables:

$$x_i \equiv \sum_n \Delta f_i^{(n)}\left[q^{(n)}|_0\cos(\omega_n t) + \frac{\dot{q}^{(n)}|_0}{\omega_n}\sin(\omega_n t)\right]$$

and the auxiliary kernels:

$$g_i(t-t') \equiv \Theta(t-t') \sum_n \frac{[\Delta f_i^{(n)}]^2}{\omega_n^2} \cos(\omega_n(t-t'))$$

so that we have:

$$\langle x_i(t) x_j(t') \rangle = \frac{2K_B T}{M} g_i(t-t') \delta_{ij}.$$

The random variables $x_i(t)$ therefore describe an ergodic process and we can use equation (6.51) to generate them. In terms of x_i and g_i we have:

$$\bar{h}_l = \frac{B_1}{M_s h} \sum_i x_i [\delta_{il} \Omega_3(t') + \Omega_i(t') \delta_{3l}]$$

$$\bar{\gamma}_{jm} = \frac{\gamma L_s^2 B_1^2}{M_s M h} \sum_i g_i [\delta_{ij} \Omega_3(t) + \Omega_i(t) \delta_{3j}] \times [\delta_{im} \Omega_3(t') + \Omega_i(t') \delta_{3m}] \tag{6.52}$$

To generate the random field and calculate $\bar{\gamma}_{jl}$ we then have to calculate the quantities $g_i(\tau)$ and their Fourier transforms $g_i(\omega)$. Figures 6.2(a)-6.3(b) show some typical profiles for $g_i(\tau)$ and $g_i(\omega)$ using for the mechanical properties the values of table 6.1. We find that in general $g_i(\tau)$ doesn't depend on the thickness of the capping layer L'.

In the limit in which we can linearize the magnetoelastic interaction with respect to $\mathbf{\Omega}$, we have:

$$\bar{\gamma}_{jm}(\tau) = \frac{\gamma B_1^2 L_s^2}{M_s M h} g_j(\tau) \delta_{jm} \tag{6.53}$$

The damping kernel is diagonal with components equal, apart from an overall constant, to $g_j(\tau)$, in contrast to the s-LLG equation for which we have $\bar{\gamma}_{jl}(\tau) = \alpha \delta(\tau) \delta_{jl}$. The power spectrum of the random field component, h_j, is then proportional to $g_j(\omega)$, in contrast to the s-LLG equation for which the power spectrum of each component h_j is simply a constant. Notice that even in this limit $\bar{\gamma}_{jm}$ pre-

serves its tensor form due to the anisotropy of the elastic modes. In our specific case we have $g_1 = g_2 \neq g_3$ due to the difference between the transverse and longitudinal speeds of sound.

From figures 6.2(a), 6.2(b), we see that $g_i(\tau)$ goes to zero for times longer than $\tau_D \approx 5 \times 10^{-2}\tau_0 = 5h/c_{t,M}$. For a film 20 nm thick we then find $\tau_D \approx 10$ps . When the relevant frequencies of $\mathbf{\Omega}$ are much lower than $1/\tau_D$, we can replace the damping kernel given by (6.53) with the simple kernel

$$\gamma_{jm} = \gamma_{j\text{eff}}\delta(\tau)\delta_{jm}$$

with $\gamma_{j\text{eff}}$ given by:

$$\begin{aligned}\gamma_{jeff} &= \frac{\gamma B_1^2 L_s^2}{M_s M h}\int_0^\infty g_j(\tau)d\tau \\ &= \frac{\gamma B_1^2}{M_s \rho c^2}\int_0^\infty \hat{g}_j(\tau)d\tau \end{aligned} \tag{6.54}$$

where

$$\hat{g}_j(\tau) \equiv \frac{c^2}{h(L+h+L')}g_j(\tau).$$

In this limit we recover a damping kernel of the same form as the one that appears in the s-LLG equation. Here $\gamma_{j\text{eff}}$ is the equivalent to α in (6.1). Integrating $\hat{g}_j(\tau)$, shown in Fig. 6.2(a), 6.2(b), between 0 and ∞ we find

$$\int_0^\infty \hat{g}_j(\tau)d\tau \approx \frac{h}{c}$$

and then finally

$$\gamma_{j\text{eff}} \approx \frac{\gamma B_1^2}{M_s \rho c^2}\frac{h}{c}. \tag{6.55}$$

We then see that the effective damping kernel is proportional to the ratio h/c. This ratio is a measure of the time that it takes to an elastic mode to travel through

the ferromagnetic layer. We then find the intuitive result that the damping of the magnetization is proportional to the time that the elastic modes spend in the ferromagnet. This result can be understood also by the following simple estimate. Let's start from the definition of $\bar{\gamma}_{jm}$ (equation (6.44)). Assuming that at equilibrium is $\mathbf{\Omega} = (0, 0, 1)$ and keeping only the leading terms in $\mathbf{\Omega}$ in the expression for $c_l^{(n)}$ we have:

$$c_l^{(n)} = L_s^2 \Delta f_l^{(n)}$$

Let's now expand the collective index n in its components $\mathbf{k}, s$ where s is the polarization index of the elastic modes. Then, using the completeness of the polarization vectors and the fact that the polarization directions are parallel to the axis x_1, x_2, x_3 we have:

$$\begin{aligned}
\bar{\gamma}_{jm} =& \Theta(t-t') \frac{\gamma B_1^2}{M_s M V_M} \sum_n \frac{1}{\omega_n^2} c_j^{(n)}(t) c_m^{(n)}(t') \cos(\omega_n (t-t')) \\
=& \Theta(t-t') \frac{\gamma B_1^2}{M_s M V_M} L_s^4 \sum_{\mathbf{k},s} \frac{1}{\omega_{\mathbf{k},s}^2} \Delta f_j^{\mathbf{k},s} \Delta f_m^{\mathbf{k},s} \cos(\omega_{\mathbf{k},s} (t-t')) \\
=& \Theta(t-t') \frac{\gamma B_1^2}{M_s M V_M} L_s^4 \sum_{\mathbf{k}} \frac{1}{\omega_{\mathbf{k},j}^2} \Delta f_j^{\mathbf{k}} \Delta f_m^{\mathbf{k}} \delta_{jm} \cos(\omega_{\mathbf{k},j} (t-t'))
\end{aligned}$$

Now note that:

$$M = \rho L_s^2 L (1 + \hat{h} + \hat{L}'); \qquad V_M = L_s^2 h;$$

where $\hat{h} \equiv h/L$,$\hat{L}' \equiv L'/L$. Then we can write:

$$\bar{\gamma}_{jm} = \Theta(t-t') \frac{\gamma B_1^2}{M_s \rho L (1 + \hat{h} + \hat{L}') h} \sum_{\mathbf{k}} \frac{[\Delta f_j^{\mathbf{k}}]^2}{\omega_{\mathbf{k},j}^2} \delta_{jm} \cos(\omega_{\mathbf{k},j} (t-t')).$$

For small enough h/L we can assume $\Delta f_j^{(k)} \approx kh$ with a cutoff for k_D such that $k_D h = 1$.We can then define the cutoff frequency $\omega_D \equiv c k_D = c/h$. With this

approximation we have:

$$\begin{aligned}\sum_{\mathbf{k}} \frac{[\Delta f_j^{\mathbf{k}}]^2}{\omega_{\mathbf{k},j}^2} \cos(\omega_{\mathbf{k},j}(t-t')) =& \sum_{\mathbf{k}} \frac{1}{\omega_{\mathbf{k},j}^2 + \omega_D^2} \cos(\omega_{\mathbf{k},j}(t-t')) \\ =& \frac{1}{\omega_D^2} \int_0^\infty \delta(\omega - \omega_{\mathbf{k},j}) \frac{\omega_D^2}{\omega^2 + \omega_D^2} \cos(\omega(t-t'))d\omega \\ \approx& \frac{1}{\omega_D^2} \frac{1}{\omega_0} \int_0^\infty \frac{\omega_D^2}{\omega^2 + \omega_D^2} \cos(\omega(t-t'))d\omega \\ =& \frac{1}{\omega_D^2} \frac{1}{\omega_0} \omega_D \mathrm{e}^{-\omega_D(t-t')}\end{aligned}$$

where $\omega_0 \equiv c/L$. In this approximation we can then write:

$$\bar{\gamma}_{jm}(\tau) \approx \Theta(t-t') \frac{\gamma B_1^2}{M_s \rho L(1+\hat{h}+\hat{L}')h} \frac{1}{\omega_D^2} \frac{1}{\omega_0} \omega_D \mathrm{e}^{-\omega_D \tau}.$$

Integrating this expression between $\tau = 0$ and $\tau = \infty$ we find

$$\begin{aligned}\bar{\gamma}_{\text{eff}} =& \frac{\gamma B_1^2}{M_s \rho L(1+\hat{h}+\hat{L}')h} \frac{1}{\omega_D^2} \frac{1}{\omega_0} \\ =& \frac{\gamma B_1^2}{M_s \rho L(1+\hat{h}+\hat{L}')h} \frac{h^2}{c^2} \frac{L}{c} \\ =& \frac{\gamma B_1^2}{M_s \rho (1+\hat{h}+\hat{L}')c^2} \frac{h}{c}\end{aligned} \tag{6.56}$$

analogously to what we found before, (6.55).

Assuming the values given in Table 6.2 we find $\gamma_{1\text{eff}} = \gamma_{2\text{eff}} \approx 2 \times 10^{-4}$.

Table 6.2: Values of physical quantities

Quantity	Value
γ	$1.76 \times 10^7 \text{s}^{-1}\text{G}^{-1}$
B_1	$4 \times 10^6 \text{ergs/cm}^3$;
M_s	150G
L	1μm
h	20nm

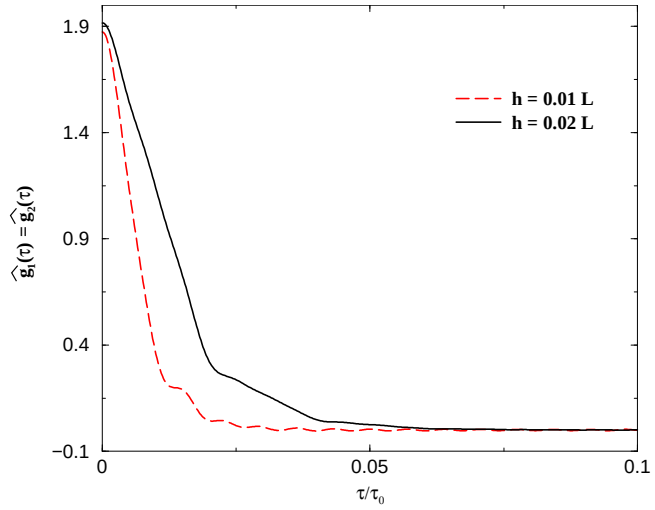

(a)

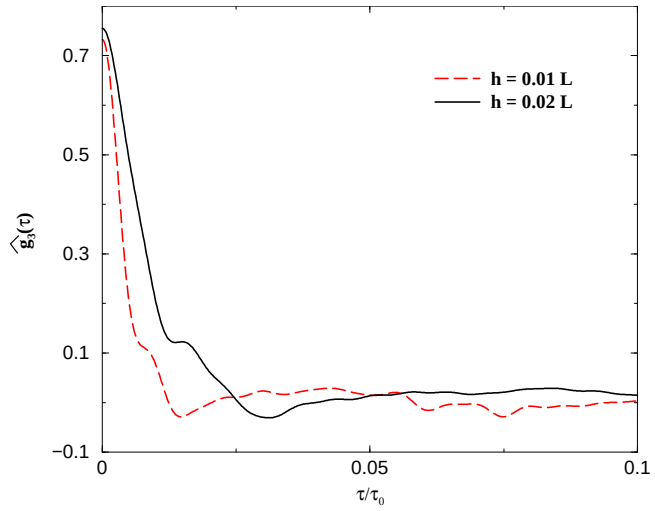

(b)

Figure 6.2: Profiles of $\hat{g}_1 \equiv g_1(\tau)c^2/[h(L+h+L')]$, (a), and $\hat{g}_3 \equiv g_3(\tau)c^2/[h(L+h+L')]$, (b), for the case of a thin magnetic film on a Tantalum substrate; $\tau_0 \equiv L/c_{t,M}$. For the standard s-LLG equation $g_i(\tau)$ would simply be a Dirac's delta centered at $\tau = 0$.

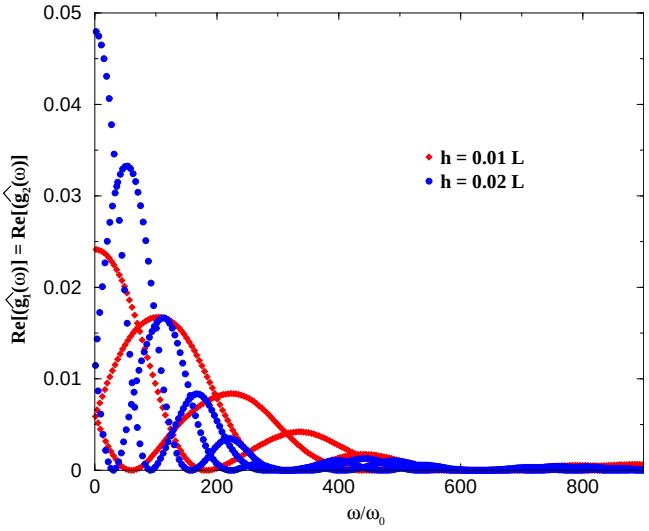

(a)

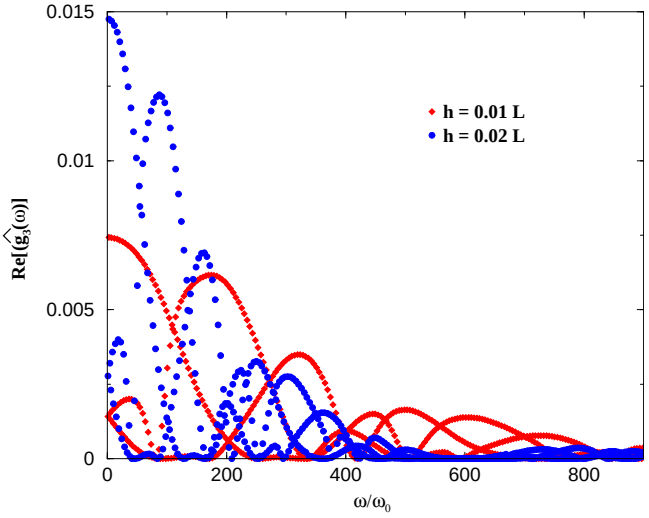

(b)

Figure 6.3: Profiles of $\mathrm{Re}[\hat{g}_1(\omega)] \equiv \mathrm{Re}[g_1(\omega)]c^2/[h(L+h+L')]$, (a), and $\mathrm{Re}[\hat{g}_3(\omega)] \equiv \mathrm{Re}[g_3(\omega)]c^2/[h(L+h+L')]$, (b), for the case of a thin film ferromagnetic film on a Tantalum substrate; $\omega_0 \equiv c_{t,M}/L$. For the standard s-LLG equation $g_i(\omega)$ would simply be a constant.

6.5 Thin Film Uniform Magnetization: stochastic dynamics

After generating the random field $\bar{\mathbf{h}}$ in the way described above we can proceed to integrate equation (6.45). We assume $\delta E_S/\delta\mathbf{\Omega} = -V_M M_s \mathbf{H}_{\text{eff}}$ with $\mathbf{H}_{\text{eff}} = (0, 0, H_{\text{eff}})$ and H_{eff} simply a constant. Let's define the dimensionless quantities:

$$\hat{t} \equiv \gamma H_{\text{eff}} t; \quad \hat{\mathbf{H}}_{\text{eff}} \equiv \frac{\mathbf{H}_{\text{eff}}}{H_{\text{eff}}}; \quad \hat{\mathbf{h}} \equiv \frac{\mathbf{h}}{H_{\text{eff}}}; \quad \hat{\gamma}_{jm} \equiv \frac{\bar{\gamma}_{jm}}{\gamma H_{\text{eff}}}; \quad \hat{T} \equiv \frac{2K_B T}{H_{\text{eff}} M_s V_M};$$

then in dimensionless form equation (6.45) takes the form,

$$\frac{d\Omega_l}{d\hat{t}} = -\epsilon_{ijl}\Omega_i \hat{H}_{\text{eff}j} + \epsilon_{ijl}\Omega_i \hat{h}_j + \epsilon_{ijl}\Omega_i \int_0^{\hat{t}} d\hat{t}' \sum_m \hat{\gamma}_{jm}(\hat{t}, \hat{t}') \frac{d\Omega_m}{d\hat{t}'} \tag{6.57}$$

with

$$\langle \hat{h}_j(\hat{t}) \rangle = 0; \quad \langle \hat{h}_j(\hat{t}) \hat{h}_m(\hat{t}') \rangle = \hat{T} \hat{\gamma}_{jm}(\hat{t}, \hat{t}') \tag{6.58}$$

Similarly, for $\delta E_S/\delta\mathbf{\Omega} = -V_M M_s \mathbf{H}_{\text{eff}}$, the standard s-LLG equation, (6.1), for the uniform mode, takes the dimensionless form:

$$\frac{d\mathbf{\Omega}}{d\hat{t}} = -\mathbf{\Omega} \times \hat{\mathbf{H}}_{\text{eff}} + \mathbf{\Omega} \times \hat{\mathbf{h}} + \alpha \mathbf{\Omega} \times \frac{d\mathbf{\Omega}}{d\hat{t}} \tag{6.59}$$

with

$$\langle \hat{h}_j(\hat{t}) \rangle = 0; \quad \langle \hat{h}_j(\hat{t}) \hat{h}_m(\hat{t}') \rangle = \alpha \hat{T} \delta(\hat{t} - \hat{t}'). \tag{6.60}$$

Using for $\bar{\gamma}_{jm}$ the expression (6.52) and for $g_i(\tau)$, $g_i(\omega)$ the results shown in figures 6.2(a)-6.3(b) and assuming $\hat{T} = 10^{-2}$ and the values given in Table 6.2 we integrate equation (6.57). We used the stochastic Heun scheme that ensures convergence to the Stratonovich solution even in the limit of zero autocorrelation time for the random field [74]. The results of the integration are shown in figures 6.4(a),6.4(b),6.5(a). As initial condition we took $\mathbf{\Omega} = (0.6, 0, 0.8)$, $d\mathbf{\Omega}/d\hat{t} = 0$.

We then integrated equation (6.59) setting $\alpha = \gamma_{1\text{eff}}$ with $\gamma_{1\text{eff}}$ calculated using (6.54). The results of the integration are shown in figures 6.4(a),6.4(b),6.5(b).

From figures 6.4(a)-6.5(b) we see that on average equation (6.57) and (6.59) give very similar results. This is expected because for the initial conditions chosen we are in the limit of small oscillations around the equilibrium position and therefore the dependence of $\hat{\gamma}_{jm}$ on $\mathbf{\Omega}$ is negligible. The main differences, for the case considered, between the results obtained using (6.57) and (6.59) are in the random fluctuations of $\mathbf{\Omega}$. This is a consequence of the different correlation in time of the random field $\mathbf{h}$ used in (6.57) and (6.59). For example we notice that equation (6.57) seems to give a less noisy dynamics than (6.59) even though for both simulation $|\hat{h}|^2$ is of the same order of magnitude. If we zoom on a short time interval, fig. 6.4(b), as a matter of fact, we see that on very short time scales the amplitude of the random fluctuations for the two simulations is very similar. However for (6.59) fluctuations with the same sign are much more likely than for (6.57). This is due to the different spectral density of the random field. For (6.59) we simply have $|\bar{h}_j(\omega)|^2 = \alpha\bar{T}$, whereas for (6.57) $|\bar{h}_j(\omega)|^2$ is equal to $g_j(\omega)$ (considering that for our simulation, to a good approximation, we can neglect the dependence of the random field on $\mathbf{\Omega}$). In particular for (6.57) $|\bar{h}_j(\omega)|^2$ has a low frequency cutoff at $\omega = \omega_0 \equiv c_{t,M}/L$ where $c_{t,M}$ is the transverse speed of sound in the ferromagnet. This implies that for (6.57) we have a much lower probability than for (6.59) to have consecutive fluctuations of the random field with the same sign with the result that the dynamics appears less noisy.

6.6 Conclusions

In this chapter we derived the equation for the dynamics of the magnetization taking into account its coupling to the lattice vibrations. The equation that we obtain, (6.41), is quite general. Equation (6.41) will have the same form also if we include

spin-spin and spin-disorder interactions. To take into account these phenomena it is necessary only to add the appropriate terms to the energy functional $E_S[\mathbf{\Omega}]$.

From the general equation we derived the equation, (6.45), for the dynamics of the uniform magnetic mode in a thin magnetic film when nonuniform magnetic modes can be assumed frozen out. We find that in general the random field that appears in the dynamical equation for the magnetization has a correlation time, τ_D, of the order of the ratio between the film thickness, h, and the sound velocity c. When the timescale for the dynamics of the magnetization is much longer that τ_D, we recover the stochastic LLG equation. In this limit we calculated the value of the effective Gilbert damping constant, α. For typical ferromagnetic insulators, like YIG, we find $\alpha \approx 10^{-4}$, in good agreement with the values measured in experiments [69, 82]. We can then conclude that for magnetic insulators magnetoelastic coupling is the main source of magnetization damping.

For ferromagnetic metals, like permalloy, we also find $\alpha \approx 10^{-4}$. This value is about two orders of magnitude smaller than the value observed experimentally [83]. The reason is that in ferromagnetic metals the electronic degrees of freedom are the main source of dissipation for the magnetization [68, 70].Starting from a model of localized d spins exchange-coupled to s-band electron, the interaction Lagrangian will be:

$$\mathcal{L}_I = J_{sd} \int d\mathbf{x} \mathbf{\Omega}(\mathbf{x}) \cdot \mathbf{s}(\mathbf{x})$$

where J_{sd} is the exchange coupling constant and $\mathbf{s}$ is the conduction electrons spin density:

$$\mathbf{s}(\mathbf{x}) = \frac{1}{2} \sum_{a,b} \Psi_a^\dagger(\mathbf{x}) \boldsymbol{\tau}_{ab} \Psi_b(\mathbf{x})$$

where Ψ are the s-band carrier field operators and $\boldsymbol{\tau}_{ab}$ the representation of the spin operator in terms of Pauli matrices. By integrating out the s-band degrees of freedom, in the linear response approximation Sinova et al. [84], for the damping of

the uniform magnetic mode find:

$$\alpha = \lim_{\omega \to 0} \frac{g\mu_B J_{sd}^2}{2M_s \hbar\omega} \int \frac{d^3k}{(2\pi)^3} \sum_{a,b} |\langle \psi_a(\mathbf{k}) | \tau^+ | \psi_b(\mathbf{k}) \rangle|^2 \times \int \frac{d\epsilon}{2\pi} A_{a,\mathbf{k}}(\epsilon) A_{b,\mathbf{k}}(\epsilon + \hbar\omega)[f(\epsilon) - f(\epsilon + \hbar\omega)] \tag{6.61}$$

where $A_{a,\mathbf{k}}(\epsilon)$ and $A_{b,\mathbf{k}}(\epsilon)$ are the spectral functions for s-band quasiparticles and $f(\epsilon)$ is the Fermi-Dirac distribution. Equation (6.61) gives zero damping unless there is a finite-measure Fermi surface area with spin degeneracy or there is a broadening of the spectral function due to disorder [85]. Characterizing the quasiparticle broadening by a simple number $\Gamma \equiv \hbar/\tau_s$, where τ_s is the quasiparticle lifetime, we can assume:

$$A_{a,\mathbf{k}}(\epsilon) = \frac{\Gamma}{(\epsilon - \epsilon_{a,\mathbf{k}})^2 + \Gamma^2/4}. \tag{6.62}$$

Inserting this expression for the spectral functions in (6.61) we find α as a function of the phenomenological scattering rate Γ. Notice that (6.61) includes the contribution both of intra-band, and inter-band [86, 87, 88] quasiparticles scattering events. The intra-band contribution is due to spin-flip scattering within a spin-split band and is nonzero only when intrinsic spin-orbit coupling is present. From equation (6.61), using the expression for $A_{a,\mathbf{k}}(\epsilon)$ given in (6.62), we see that in the limit of weak disorder, small Γ, the intra-band contribution to α is proportional to $1/\Gamma$, in agreement with experimental results for clean ferromagnetic metals with strong spin-orbit coupling [89, 90, 91, 92] and previous theoretical work [87, 93, 94, 95, 96, 88]. Similarly from (6.61) we see that the inter-band contribution to α is proportional to Γ. This result agrees with the experimental results for ferromagnetic metals with strong disorder [97] and previous theoretical work [86, 87, 88]. Notice that equation (6.61) implicitly also includes the contribution due to the so called spin-pumping effect [62, 98, 99, 100, 101] in which spins are transferred from the ferromagnetic film to adjacent normal metal layers as a consequence of the precession of the mag-

netization. In order to calculate this effect in first approximation we simply have to substitute in (6.61) the conduction band quasiparticle states, ψ, calculated taking into account the heterogeneity of the sample. Assuming for the scattering rate, $1/\tau_s$, typical values estimated by transport experiments, from equation (6.61) we find values of α in good agreement with experiments.

In summary we have studied in detail the effect of the magnetoelastic coupling to the dynamics of the magnetization. Starting from a realistic form for the magnetoelastic coupling we have found the expression for the damping kernel, γ_{jm}. We find that in general γ_{jm} is a nondiagonal tensor non-local in time and space. The knowledge of the exact expression of γ_{jm} allows us to correctly take into account the autocorrelation of the noise term overcoming the zero correlation approximation of the stochastic Landau-Lifshitz-Gilbert equation. We find that for thin films for which the single domain approximation is valid, both the damping and the fluctuations correlation time are proportional to the film thickness. Our results apply to systems for which the direct coupling of the magnetization to the lattice vibrations is the main source of the magnetization relaxation. We have shown that this is the case for ferromagnetic insulators whereas for ferromagnetic metals the magnetization relaxation is mainly due to the s-d exchange coupling.

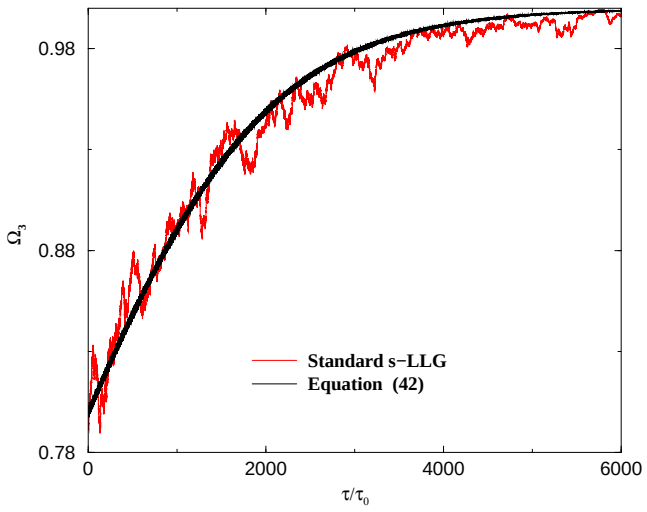

(a)

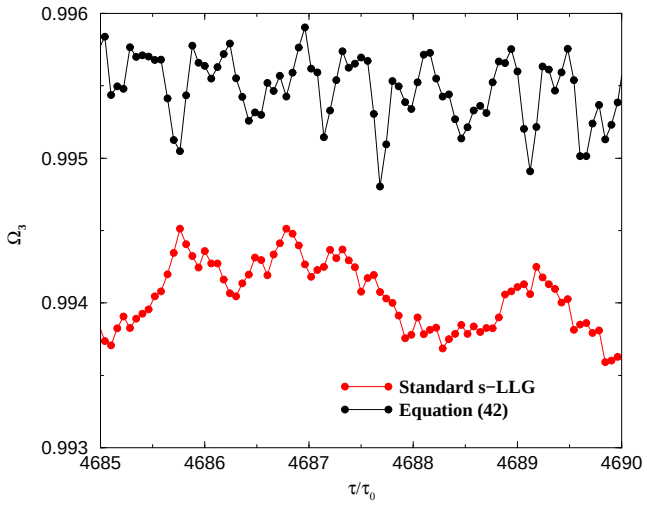

(b)

Figure 6.4: Ω_3 as a function of time obtained integrating the standard s-LLG equation, (6.59), and equation (6.57)

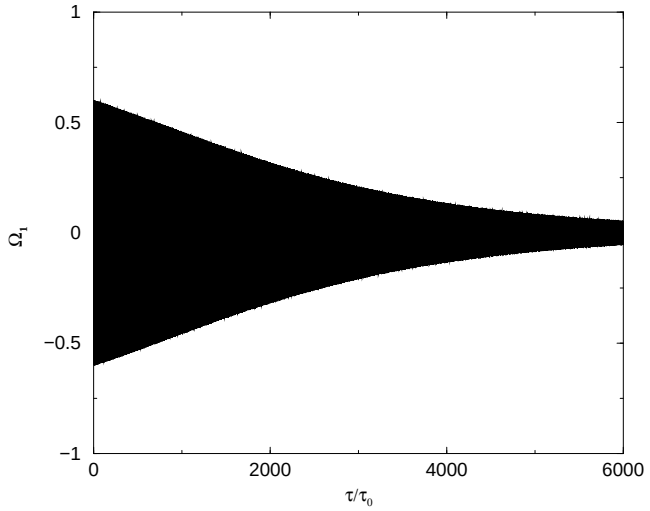

(a)

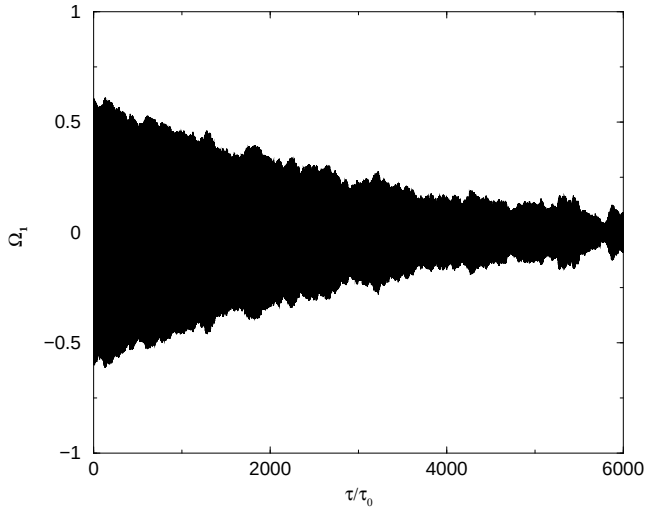

(b)

Figure 6.5: Ω_1 as a function of time obtained integrating equation (6.57), (a), and integrating the standard s-LLG equation, (6.59), (b).

Chapter 7

Nonlinear dynamics of tearing modes

7.1 Introduction

In this chapter we will study the dynamics of a particular class of collective modes in magnetically confined plasmas [102], [103]. A plasma is a ionized gas with almost zero resistivity. The charge separation between the electrons and the ions gives rise to electric fields and charged particle flows give rise to currents and magnetic fields. Through these fields the different parts of a plasma interact on long range scales, resulting in a very complex dynamics. In presence of a magnetic field a free charged particle precesses around the magnetic field line at the cyclotron frequency with a radius equal to the Larmor radius. In first approximation in a magnetically confined plasma electrons and ions are free to move along the field lines but in the perpendicular direction their motion is limited to the Larmor precession that, for $\mathbf{B}$ big enough, is much smaller than the plasma size. In order to confine a plasma then the magnetic field lines should lie on a close surface S: $\mathbf{B}$ should always be tangent to S and never vanish. According to a famous Poincaré's theorem this can only

happen if S is a torus. In a magnetically confined plasma then the magnetic field lines lie on nested toroidal surfaces. The topology of this surfaces cannot change unless we allow for a finite resistivity of the plasma. In this case we can have the remarkable phenomenon of *magnetic reconnection*.

Tearing modes are collective modes that are naturally unstable in magnetically confined plasmas. They are driven by radial gradients in the plasma current density [104] and plasma pressure [105]. In a tearing mode magnetic reconnection takes place around particular magnetic surfaces that as a consequence tear and reconnect forming helical chains of *magnetic islands* inside the plasma, Fig. 7.1. Such

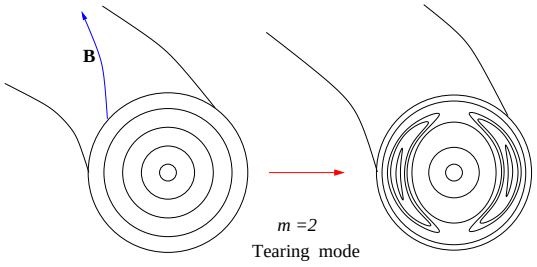

Figure 7.1: On the left we show the magnetic surfaces before the instability. On the right we have the flux surfaces after a tearing mode instability. In the poloidal cross section magnetic islands are present. In this picture the width of the magnetic islands is greatly exaggerated.

islands degrade the plasma confinement because both heat and particles are able to travel radially from one side of an island chain to the other by flowing along magnetic field lines. Is then very important for the purposes of plasma confinement to be able either to prevent the formation of tearing modes or, at least, to control their size.

7.2 Resistive MHD equations

The Magnetohydrodynamics (MHD) model [102] is one of the earliest and simplest model for fully ionized plasmas. Despite its simplicity it retains much of the important physics. In the MHD model the plasma is treated as a quasi neutral non-viscous single hydrodynamic fluid subject to the Lorentz force created by the external and self consistent electromagnetic fields. The equations that define the MHD model are:

$$\frac{d\rho_m}{dt} + \rho_m \nabla \cdot \mathbf{V} = 0; \tag{7.1}$$

$$\rho_m \frac{d\mathbf{V}}{dt} = -\nabla p + \mathbf{J} \times \mathbf{B}; \tag{7.2}$$

$$\mathbf{E} + \mathbf{V} \times \mathbf{B} = \eta \mathbf{J}; \tag{7.3}$$

$$\frac{d}{dt}\left(p\rho_m^{-\Gamma}\right) = const; \tag{7.4}$$

$$\nabla \times \mathbf{B} = \mu_0 \mathbf{J}; \tag{7.5}$$

$$\frac{\partial \mathbf{B}}{\partial t} = -\nabla \times \mathbf{E}; \tag{7.6}$$

$$\nabla \cdot \mathbf{B} = 0. \tag{7.7}$$

where ρ_m is mass density, $\mathbf{V}$ is the plasma velocity, p the pressure, $\mathbf{J}$ the current, $\mathbf{E}$ the electric field, η the plasma resistivity, μ_0 the free space permeability and Γ the exponent characterizing the plasma equation of state, (7.4). Equation (7.1) is the mass continuity equation, equation (7.2) the single fluid equation of motion and (7.3) is the so called generalized Ohm's law. Equations (7.5), (7.6), (7.7) are simply the Maxwell's equations assuming the plasma to be quasi neutral.

If we assume the plasma to be incompressible the equation of state can be replaced simply by $\rho_m = const$. As a consequence equation (7.1) reduces to $\nabla \cdot \mathbf{V} = 0$. As we mentioned before the tearing modes can exist only if we allow the plasma resistivity η to be different from zero. They will then grow on the *resistive*

time scale

$$\tau_\eta \equiv \frac{L^2 \mu_0}{\eta}$$

where L is a length characterizing the size of the plasma. This time scale is much bigger than the time scale that enters the equation of motion (7.2). For this reason we can study the dynamics of a tearing mode as a succession of plasma equilibria: adiabatic approximation. In this case we can neglect the inertial term in (7.2). We will also assume *force free* configurations for which is $\nabla p = 0$. After these consideration we can simplify the resistive MHD model to the following set of equations:

$$\nabla \cdot \mathbf{V} = 0; \tag{7.8}$$

$$\mathbf{J} \times \mathbf{B} = 0; \tag{7.9}$$

$$\frac{\partial \mathbf{B}}{\partial t} = \nabla \times (\mathbf{V} \times \mathbf{J}) + \frac{\eta}{\mu_0} \nabla^2 \mathbf{B}; \tag{7.10}$$

$$\nabla \times \mathbf{B} = \mu_0 \mathbf{J}; \tag{7.11}$$

$$\nabla \cdot \mathbf{B} = 0. \tag{7.12}$$

7.3 Tearing mode instability

Let R_0 and a be the major and minor radii respectively of a toroidal plasma. In the large aspect ratio, $R_0 \gg a$, we can map the torus to a periodic cylinder of length $L = 2\pi R_0$. Let us define the parameter

$$\beta \equiv 2\mu_0 \frac{\langle p \rangle}{\langle B^2 \rangle}$$

where the angle brackets denote volume average. In the zero β, large aspect ratio limit the plasma equilibrium is characterized by magnetic surfaces that map out (almost) concentric circles in the poloidal plane. To describe this equilibrium and perturbations around it we use the coordinates (r, θ, ϕ), where r and θ are the

polar coordinates in the poloidal plane and $\phi \equiv z/R_0$ is the simulated toroidal angle. In the limit of zero β large aspect ratio the plasma equilibrium will be $\mathbf{B}_0 = (0, B_\theta(r), B_\phi(r))$ with:

$$\nabla \times \mathbf{B}_0 = \sigma(r)\mathbf{B}_0.$$

We want to consider helical perturbations around the equilibrium. A (m, n) helical mode has $m \in \mathbb{N}$ periods in the poloidal direction, and $n \in \mathbb{N}$ periods in the toroidal direction. It will be convenient to use the poloidal angle $\xi \equiv m\theta - n\phi$. Then for a poloidal mode all the quantities will depend only on ξ and r. Let's define the unit vectors (Fig. 7.2)

$$\hat{\xi} \equiv \frac{\nabla\xi}{|\nabla\xi|}; \qquad \hat{\mathbf{n}} \equiv \hat{\mathbf{r}} \times \hat{\xi};$$

and the quantities

$$\mathcal{C}(r) \equiv \frac{1}{\sqrt{\mathrm{m}^2 + n^2\epsilon^2}}; \qquad \epsilon \equiv \frac{r}{R_0}.$$

Because $\mathbf{V}$ and $\mathbf{B}$ are divergence free, without loss of generality we can write:

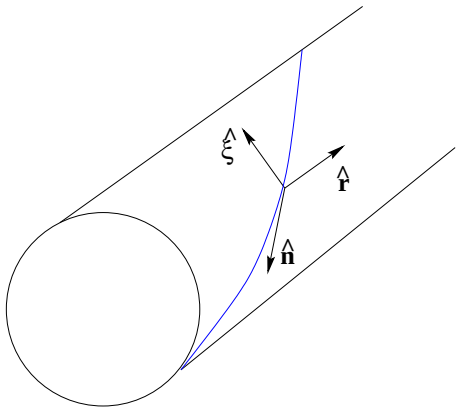

Figure 7.2: Orthonormal unit vectors used to describe a tearing mode instability.

$$
\begin{aligned}
\mathbf{B} &= \mathcal{C}(r)\nabla\psi \times \hat{\mathbf{n}} + B_{\|}\hat{\mathbf{n}} \\
\mathbf{V} &= \mathcal{C}(r)\nabla\chi \times \hat{\mathbf{n}} + V_{\|}\hat{\mathbf{n}} \\
\frac{B_{\|}}{\mathcal{C}} &= G(\psi) \\
\frac{J_{\|}}{\mathcal{C}} &= H(\psi)
\end{aligned}
$$

where G and H are functions, to be determined, only of the magnetic flux ψ.

After adding an (m, n) helical perturbation the total magnetic field will be given by

$$\mathbf{B} = \mathbf{B}_0 + \mathbf{b}^{m,n}(r)e^{i\xi},$$

and the magnetic flux by

$$\psi = \psi_0(r) + \psi_1^{m,n}(r,t)e^{i\xi}; \qquad \psi_1^{m,n}(r,t) = -irb_r^{m,n}.$$

Inserting these expressions in the resistive MHD equations (7.8)-(7.12) gives us the equations governing the dynamics of the helical mode. As a first approximation we can assume the resistivity of the plasma, η, to be zero. In this case in linear approximation, the flux function $\psi_1^{m,n}(r,t)$ satisfies the Newcomb's equation

$$\frac{d}{dr}\left[f^{m,n}\frac{d\psi_1^{m,n}}{dr}\right] - g^{m,n}\psi_1^{m,n} = 0; \tag{7.13}$$

where

$$
\begin{aligned}
f^{m,n}(r) &= \frac{r}{m^2 + n^2\epsilon^2} \\
g^{m,n}(r) &= \frac{1}{r} + f^{m,n}(r)\left[\frac{n\epsilon B_\theta + mB_\varphi}{B_*}\frac{d\sigma}{dr} + \frac{2mn\sigma}{R} - \frac{\sigma^2}{r}\right]
\end{aligned}
$$

and

$$B_* \equiv \frac{1}{N}\mathbf{B}\cdot\hat{\xi} = mB_\theta(r) - n\frac{r}{R}B_z(r).$$

For $B_* = 0$ the Newcomb's equation becomes singular. The radius r_s for which $B_*(r) = 0$ is the radius that individuates the *m/n rational surface* at which the helical perturbation is resonant with the equilibrium magnetic field. The singularity at $r = r_s$ is resolved if we relax the condition of zero resistivity. As a matter of fact terms proportional to η are negligible everywhere apart around the rational surface where they cannot be neglected. If we consider $\eta \neq 0$ in the region around r_s we will have reconnection of the field lines and the singularity will be resolved by the presence of a thin magnetic island centered around the rational surface. In order to find the dynamics of this island we first solve the Newcomb's equation away from the radius r_s requiring $b_r^{m,n}$ to be continuous across the island. We then solve the resistive MHD equations in a small region around r_s and asymptotically match the solution, *inner solution*, to the *outer solution* obtained from the Newcomb's equation.

Let us define the dimensionless quantities

$$\begin{aligned} \hat{\psi} &\equiv \frac{\psi}{\hat{\psi}_1}; \\ \mu &\equiv \frac{\hat{\psi}_1}{r_s \mathrm{B}'_*}; \\ X &\equiv \frac{1}{\mu^{1/2}} \frac{r - r_s}{r_s}. \end{aligned}$$

In terms of these dimensionless quantities the most general solution of the Newcomb's equation in the vicinity of the rational surface is written as:

$$\begin{aligned} \hat{\psi} = \; & - \left\{ \frac{X^2}{2} + \mu^{1/2}[\lambda_1(\lambda_0 - \lambda_2 + 1) - 1] \frac{X^3}{6} \right\} \\ & + \Big\{ 1 - \mu^{1/2} \ln \mu^{-1/2} \lambda_0 \lambda_1 X \\ & \quad + \mu^{1/2} \left[\lambda_0 \lambda_1 X \ln |X| + A_0 X + \frac{1}{2} \Delta' |X| \right] \\ & \quad - \mu \ln \mu^{-1/2} \lambda_0 \lambda_1 (\lambda_0 \lambda_1 - \lambda_2) \frac{X^2}{2} \Big\} \cos \xi \end{aligned} \tag{7.14}$$

Where:

$$\begin{aligned}\lambda_0 &\equiv \left(\frac{r\sigma'}{\sigma}\right)_{r_s}\\ \lambda_1 &\equiv \left(\frac{r\sigma}{r\sigma - 2\mathcal{C}^2 mn\epsilon}\right)_{r_s}\\ \lambda_2 &\equiv [\mathcal{C}^2(m^2 - n^2\epsilon^2)]_{r_s}\end{aligned}$$

For the inner region from the resistive MHD model we find the equations:

$$\frac{\partial\psi}{\partial t} = \frac{1}{r}[\chi,\psi] - \eta\left[\frac{J_\parallel}{\mathcal{C}} - \frac{J_{\parallel 0}}{\mathcal{C}}\right] \tag{7.15}$$

$$\mathbf{J} = \frac{1}{\mu_0}\nabla\times\mathbf{B}. \tag{7.16}$$

where we use the notation

$$[\chi,\psi] \equiv \frac{\partial\chi}{\partial X}\frac{\partial\psi}{\partial\xi} - \frac{\partial\psi}{\partial X}\frac{\partial\chi}{\partial\xi}.$$

Let

$$\begin{aligned}\hat{\mathrm{J}}_\parallel &\equiv \frac{\mu_0}{\mathrm{B}'_*|_{r_s}}\frac{\mathrm{J}_\parallel}{\mathcal{C}},\\ \hat{\mathrm{B}}_\parallel &\equiv \frac{1}{r_s\mathrm{B}'_*|_{r_s}}\frac{\mathrm{B}_\parallel}{\mathcal{C}},\\ \hat{\chi} &\equiv -\frac{\mu_0}{\eta}\chi\\ \hat{t} &\equiv \frac{\eta}{\mu_o r_s^2}t = \frac{t}{\tau_\eta^{(r_s)}}.\end{aligned}$$

and adopt the following expansions:

$$\begin{aligned}\hat{\psi} &= \hat{\psi}_0 + \mu^{1/2}\ln\mu^{-1/2}\hat{\psi}_1 + \mu^{1/2}\hat{\psi}_2 + \mu\ln\mu^{-1/2}\hat{\psi}_3 + O(\mu)\\ \hat{\mathrm{J}}_\parallel &= \hat{\mathrm{J}}_{\parallel 0} + \mu^{1/2}\ln\mu^{-1/2}\hat{\mathrm{J}}_{\parallel 1} + \mu^{1/2}\hat{\mathrm{J}}_{\parallel 2} + \mu\ln\mu^{-1/2}\hat{\mathrm{J}}_{\parallel 3} + O(\mu)\end{aligned}$$

If we assume

$$\hat{\psi}(r,t) = \hat{\psi}_1(r,\mu(t))$$

so that up to terms of order μ we have:

$$\frac{\partial \psi}{\partial t} = \hat{\psi}_1 \frac{d\mu}{dt}.$$

in terms of dimensionless quantities the equations (7.15), (7.16) take the form:

$$\hat{\psi}\frac{d\mu}{dt} = -\mu^{1/2}[\hat{\chi},\hat{\psi}] - (\hat{\mathrm{J}}_{\|} - \hat{\mathrm{J}}_{\|eq}) \tag{7.17}$$

$$\hat{\mathrm{J}}_{\|} = -\frac{\partial^2 \hat{\psi}}{\partial x^2} + \lambda_3[1-(1-\lambda_2)\mu^{1/2}X]\hat{\mathrm{B}}_{\|0} - \lambda_2\mu^{1/2}\frac{\partial \hat{\psi}}{\partial X} + O(\mu) \tag{7.18}$$

where

$$\lambda_3 \equiv \left(\frac{2mn}{m^2+n^2\epsilon^2}\right)_{r_s}.$$

The dimensionless equilibrium current in the vicinity of the rational surface is given by:

$$\hat{\mathrm{J}}_{\|eq} = \lambda_1 + \lambda_0\lambda_1\mu^{1/2}X + O(\mu) \tag{7.19}$$

For orders smaller than $\mu^{1/2}$ integrating the first equation across the island region we find:

$$\frac{d\mu}{dt}\int_{\infty}^{\infty}(\hat{\psi}_1)_{<\mu^{1/2}}dX = -\int_{\infty}^{\infty}(\hat{\mathrm{J}}_{\|} - \hat{\mathrm{J}}_{\|eq})_{<\mu^{1/2}}dX$$

and then using equation (7.18) and the expression for the equilibrium current (7.19) we find that up to order $\mu^{1/2}\ln\mu^{-1/2}$ is $d\mu/dt = 0$. To consider terms of order $\mu^{1/2}$ and higher we have to deal with the term $[\chi,\psi]$. To do this we introduce the *flux*

surface average defined as:

$$\langle \mathcal{Q} \rangle = \begin{cases} \dfrac{1}{2\pi} \oint \dfrac{\mathcal{Q}(\mathrm{sgn}(X), \hat{\psi}, \xi)}{\left| \frac{\partial \hat{\psi}}{\partial X} \right|_\xi} d\xi; & \hat{\psi} \leq -1 \\ \dfrac{1}{4\pi} \displaystyle\int_{-\xi_0}^{\xi_0} \dfrac{\mathcal{Q}(\mathrm{sgn}(X), \hat{\psi}, \xi) + \mathcal{Q}(-\mathrm{sgn}(X), \hat{\psi}, \xi)}{\left| \frac{\partial \hat{\psi}}{\partial X} \right|_\xi} d\xi; & \hat{\psi} \geq -1 \end{cases}$$

It is easily demonstrated that

$$\langle [\hat{\chi}, \hat{\psi}] \rangle = 0$$

irrespective of the form of χ. Using this fact and the fact that $\hat{J}_\parallel$ depends only on $\hat{\psi}$, after flux *flux averaging* equation (7.17) we find:

$$\frac{d\mu}{dt} \frac{\langle \psi \rangle}{\langle 1 \rangle} = -\hat{\mathrm{J}}_\parallel(\psi) + \frac{\langle \mathrm{J}_{\parallel eq} \rangle}{\langle 1 \rangle}. \tag{7.20}$$

where $\hat{J}_\parallel$ is given in terms of $\hat{\psi}$ by equation (7.18). Integrating this equation across the island region and asymptotically matching $\hat{\psi}$ with the outer solution (7.14) we find the equation:

$$\frac{d\mu}{dt} = \frac{\Delta'}{\Lambda_1} \mu^{1/2} - \lambda_0^2 \lambda_1^2 \mu \ln \mu^{-1/2} \tag{7.21}$$

where

$$\Lambda_1 \equiv \frac{1}{\pi} \int_0^{2\pi} d\xi \int_{-\infty}^{\infty} dX \frac{\langle \cos \xi \rangle}{\langle 1 \rangle} \cos \xi = 1.645$$

The island width w by definition is equal to $4 r_s \mu^{1/2}$ and then in term of w equation (7.21) becomes:

$$\frac{\tau_\eta^{(r_s)}}{2 r_s} \frac{dw}{dt} = \frac{\Delta'}{\Lambda_1} - \lambda_0^2 \lambda_1^2 \frac{w}{4 r_s} \ln \frac{w}{4 r_s}. \tag{7.22}$$

If we neglect the second term on the right hand side we recover the *Rutherford island evolution equation* [106]. The second term on the right hand side was first obtained heuristically in [107] and more rigorously in [108].

7.4 Tearing modes with overtones

We now want to consider the more general class of tearing modes for which is

$$\psi(r,\xi,t) = \psi_0(r) + \sum_{l=1}^{\infty} \frac{1}{l} \psi^{lm,ln}(r,t) e^{il\xi}.$$

For these modes besides the fundamental (m,n) mode, higher modes are present that have the same helicity. To find the dynamics of the magnetic island the same procedure that we have presented in the previous section can be used. Assuming

$$\begin{aligned} \psi_l &\approx \mu^{1/2} \psi_1 \hat{\psi}_l; & \hat{\psi}_l &\approx O(1) \\ \Delta\psi_l &\approx \Delta\psi_1 \Delta\hat{\psi}_l; & \Delta\hat{\psi}_l &\approx O(1) \end{aligned}$$

for the overtone amplitudes we find:

$$\frac{\psi_l}{\psi_1} = -(-1)^l l \frac{\Delta_1'}{\Delta_l'} \frac{\Lambda_l}{\Lambda_1}; \qquad l \geq 2. \tag{7.23}$$

where

$$\Delta_l' \equiv \left[r \frac{d\psi^{lm,ln}(r)}{dr} \right]_{r_{s-}}^{r_{s+}}$$

measures the gradient discontinuity at the rational surface of the $l-th$ component of the outer solution and

$$\Lambda_l \equiv \frac{1}{\pi} \int_0^{2\pi} d\xi \int_{-\infty}^{\infty} dX \frac{\langle \cos l\xi \rangle}{\langle 1 \rangle} \cos\xi.$$

Typical values of Δ_l', Λ_l are given in table 7.1. Using equation (7.23) for the magnetic flux inside the island we finally find the expression:

$$\hat{\psi}(X,\xi) = -\left(\frac{X^2}{2} - \cos\xi \right) - \frac{\Delta_1'}{\lambda_0 \lambda_1 \Lambda_1} X \cos\xi - \sum_{l=2}^{\infty} (-1)^l \frac{\Delta_1'}{\Delta_l'} \frac{\Lambda_l'}{\Lambda_1} \cos l\xi \tag{7.24}$$

l	Λ_l	Δ'_l
1	+1.6454	+2.826
2	+1.7058e-1	-5.148
3	-3.3174e-2	-10.06
4	+1.2816e-2	-14.52

Table 7.1: Values of Λ_l, Δ'_l for a $m = 2, n = 1$ tearing mode in the limit $\beta \to 0$, $\epsilon \to 0$, for an equilibrium configuration characterized by $\sigma = \sigma_0[1-(r/a)^2]^{2.768}$. For this equilibrium is $r_s = 0.778a$.

The second and third term on the right hand side are the nonlinear corrections to the profile of $\hat{\psi}$ in the island region. The second term *skews* the island chain and is generated by the current gradient. The third term is instead generated by the overtone harmonics. We see how these two terms become more important as the island become more unstable, i.e. Δ'_1 becomes bigger. In the remainder of this chapter we will treat Δ'_1 as a variable while assuming that the other parameters; listed in table 7.1 remain fixed. This treatment is justified because Δ'_1 is far more sensitive to slight local changes of the current profile than any of the other parameters. With this approach inf Fig. 7.3 we plot the island profiles, calculated using (7.24), for different values of Δ'_l in order to show the effects of the nonlinear terms.

7.5 Tearing modes coupled to helical magnetic perturbations

In this section we examine the effect of external helical perturbations, *error fields*, on the dynamics of tearing modes. In the previous section we found that a (m, n) tearing mode in general has overtone harmonics of relative amplitude

$$C_l \equiv \frac{\Delta'_1}{\Delta'_l}\frac{\Lambda'_l}{\Lambda_1}.$$

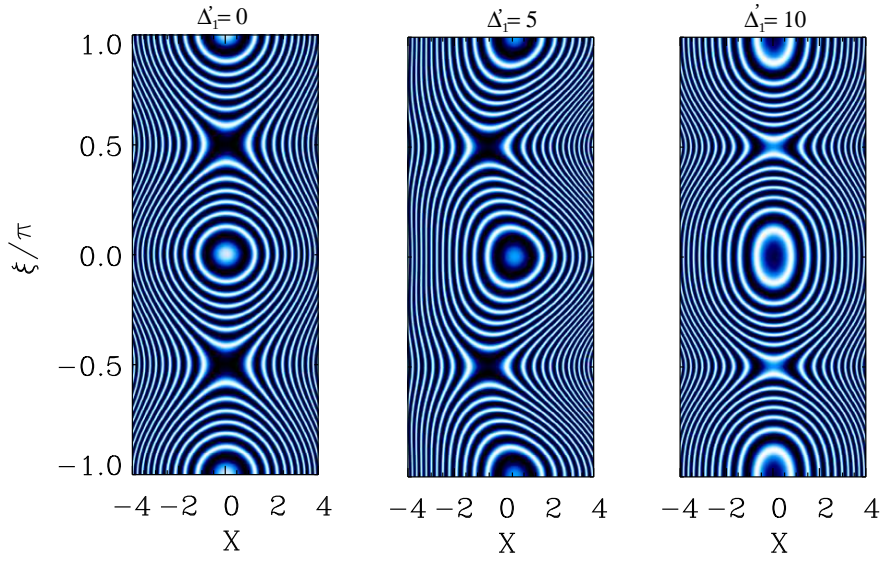

Figure 7.3: In the first panel on the left the profiles of the island flux surfaces for a saturated tearing mode characterized by $\Delta'_1 = 0$ are shown. The center panel shows the profiles of the flux surfaces for $\Delta'_1 = 5$. In this case we see that the nonlinear corrections skew the island chain. In the right panel the profiles of ψ when $\Delta'_1 = 10$ are shown. In order to enhance the effect of the overtone harmonics we have suppressed the *skew* term (second term on the right hand side of (7.24)). It can be seen that the overtone harmonics act to elongate the island flux surfaces along the ξ direction.

We expect then that a (m, n) tearing mode should also respond to an externally generated (lm, ln) magnetic perturbation. In this section we investigate the dynamics of an (m, n) magnetic island in the presence of a stationary external magnetic field that is a superposition of $l = 1$ and $l > 1$ magnetic perturbations.

In presence of an external magnetic perturbation the island evolution equation(7.22) gets modified into the following equation [109]:

$$\frac{\tau_\eta^{(r_s)}}{2r_s}\frac{dw}{dt} = \frac{\Delta'}{\Lambda_1} - \lambda_0^2\lambda_1^2\frac{w}{4r_s}\ln\frac{w}{4r_s} + \left(\frac{w_c}{w}\right)^2\cos\varphi \tag{7.25}$$

where φ is the phase difference between the tearing mode fundamental harmonic

and the (m,n) component of the external perturbation. w_c^2 is a measure of the amplitude of the (m,n) component of the error field.

The external perturbation in addition will exert an electromagnetic torque δT_ϕ on the island given by the following expression [109]:

$$\delta T_\phi = \frac{2\pi^2 R_0}{\mu_0}\frac{n}{m^2+n^2\epsilon_s^2}A_1\left[\sin\varphi + a_l\frac{\Delta_1'\Lambda_l}{\Delta_l'\Lambda_1}\sin(l\varphi-\delta_l)\right] \tag{7.26}$$

where A_1 is a constant proportional to the amplitude of the (m,n) component of the error field and a_l, δ_l are the relative amplitudes and phases of the overtone harmonics of the external perturbation. The torque δT_ϕ will try to lock the island at a specific value of the phase difference φ. To study the dynamics of the phase φ we can consider an island equation of motion that incorporates phenomenological inertia, I, and damping terms ν. For example [110]:

$$I\frac{d^2\varphi}{dt^2} + \nu\frac{d\varphi}{dt} + \delta\hat{T}_\phi = 0. \tag{7.27}$$

where $\delta\hat{T}$ is the normalized torque

$$\delta\hat{T} \equiv \delta T_\phi\left[\frac{2\pi^2 R_0}{\mu_0}\frac{n}{m^2+n^2\epsilon_s^2}A_1\right]^{-1}$$

Is then convenient to define the *potential*

$$\frac{dV}{d\varphi} = \delta\hat{T}_\phi.$$

so that (7.27) can be rewritten in the form:

$$I\frac{d^2\varphi}{dt^2} + \nu\frac{d\varphi}{dt} + \frac{dV}{d\varphi} = 0. \tag{7.28}$$

From (7.26) we have:

$$V = -\cos\varphi - \Delta_1' \sum_{l=2}^{\infty} \tilde{a}_l \cos(l\varphi - \delta_l).$$

where $\tilde{a} \equiv a_l \Lambda_l / \Delta_l' \Lambda_1$.

The island chain will lock at minima of the potential V. We see that in absence of the $l \geq 2$ component of V the island will be locked for $\varphi = 0$. From equation (7.25) we see that in this situation the effect of the error fields is the most destabilizing for the tearing mode. On the other hand if, by properly tuning the overtone components of the error fields, we manage to lock the island at a phase for which is $\cos\varphi < 0$ we obtain that the external perturbation will tend to reduce the width of the island. This can be realized for example by a potential of the form:

$$V = -\cos\varphi - \Delta_1'(-1.4612\cos 2\varphi + 0.5\cos 3\varphi), \tag{7.29}$$

shown in Fig. 7.4. For this potential at low amplitude, (small Δ_1') a resonant island chain will lock in the most *destabilizing* phase: $\varphi = 0$. However, as the chain grows to larger amplitude, the potential is modified by nonlinear effects in such a way that the minimum slowly moves until it is located in a *stabilizing* phase. This situation is illustrated in Fig. 7.5. We see that the island width w grows up to $t/\tau \approx 100$, at which point the island amplitude is big enough that the minimum of V has rotated to a stabilizing phase so that the error field term in (7.25) becomes stabilizing reducing w.

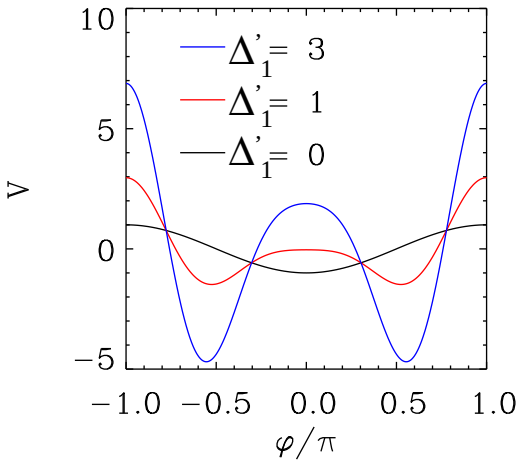

Figure 7.4: An example of potential V, Eq. (7.29), for which a large amplitude island locks in a stabilizing phase.

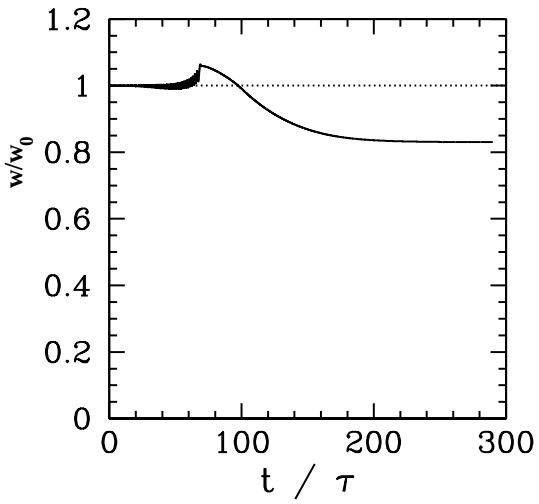

Figure 7.5: Normalized width of a 2/1 magnetic island in presence of a magnetic perturbation characterized by the potential V given by (7.29). w_0 is the width of the unperturbed island.

Bibliography

[1] S.Q. Murphy, J. P. Eisenstein, G. S. Boebinger, L. N. Pfeiffer, and K. W. West. *Phys. Rev. Lett.*, 72:728, 1994.

[2] I. B. Spielman, J. P. Eisenstein, L. N. Pfeiffer, and K. W. West. *Phys. Rev. Lett*, 84:5808, 2000.

[3] D. C Tsui, H. L. Stormer, and A. C. Gossard. *Phys. Rev. Lett.*, 48:1559, 1982.

[4] K. Von Klitzing, G. Dorda, and Pepper M. *Phys. Rev. Lett.*, 45:494, 1980.

[5] A. H. MacDonald. Introduction to the physics of quantum hall regime. In E Akkermans, G Montambaux, J L Pichard, and J Zinn-Justin, editors, *Mesoscopic Quantum Physics*. 1994.

[6] S. M. Girvin. The quantum hall effect: Novel excitations and broken symmetries. In A. Comtet, T. Jolicoeur, S. Ouvry, and F. David, editors, *Topological Aspects of Low Dimensional Systems, Les Houches Summer School*. 1998.

[7] R. E. Prange and Girvin S. M., editors. *The Quantum Hall Effect*. Springer-Verlag, 1990.

[8] S. M. Girvin and A.H. MacDonald. In S. Das Sarma and A. Pinczuk, editors, *Perspecitive in Quantum Hall effects*.

[9] Y. N. Joglekar and A. H. MacDonald. *Phys. Rev. Lett.*, 87:196802–1, 2001.

[10] A. O. Caldeira and A. J. Leggett. *Ann. Phys.*, 149:374, 1983.

[11] E. H. Hall. *American Journal of Mathematics*, 2:287, 1879.

[12] P. Drude. *Annalen der Physik*, 1:369, 1900.

[13] A. H. MacDonald. Introduction to the physics of quantum hall regime. In E Akkermans, G Montambaux, J L Pichard, and J Zinn-Justin, editors, *Mesoscopic Quantum Physics*. 1994.

[14] B. I. Halperin. *Helv. Phys. Acta*, 56:75, 1983.

[15] A. A. Burkov and A. H. MacDonald. *Phys. Rev. B*, 66:115320, 2002.

[16] B. I. Halperin, P. A Lee, and N. Read. *Phys. Rev. B*, 47:7312, 1993.

[17] J. P. Eisenstein and A. H. MacDonald. *Nature*, 432:691, 2004.

[18] J. König, M. C. Bonsager, and A. H. MacDonald. Dissipationless spin transport in thin film ferromagnets. *Phys. Rev. Lett.*, 87:187202, 2001.

[19] R Ferrari. *Int. J. Mod. Phys.*, 9:3333, 1995.

[20] E. I. Rashba, L. E. Zhukov, and L. E. Efros. *Phys. Rev. B*, 55:5306, 1997.

[21] A. M. Perelomov. *Teor. Mat. Fiz.*, 6:213, 1971.

[22] D. J. Thouless. *J. Phys.: Solid State Phys.*, 17:L325, 1984.

[23] J. Schwinger. In L Biedenharm and H. Van Dam, editors, *Quantum Theory of Angular Momentum*. Academic, New York, 1965.

[24] A. Auerbach. Springer-Verlag, 1994.

[25] K. Moon, H. Mori, Kun Yang, S. M. Girvin, and A. H. MacDonald. *Phys. Rev. B*, 51:5138, 1995.

[26] D. J. Gross. *Nucl. Phys. B*, 132:439, 1979.

[27] I. Afflelck. *Phys. Rev. Lett.*, 56:408, 1986.

[28] S. L. Sondhi, A. Kardhele, S. A. Kivelson, and E. H. Rezayi. *Phys. Rev. B*, 47:16419, 1993.

[29] D. H. Lee and C. L. Kane. *Phys. Rev. Lett*, 64:1313, 1990.

[30] T. H. R. Skyrme. *Proc. Royal Soc.*, A262:233, 1961.

[31] A. Patani, M. Schlindwein, and Q. Shafi. *J. Phys. Math. Gen*, 9:1513, 1976.

[32] S. Rapsch, J. T. Chalker, and D. K. K. Lee. *Phys. Rev. Lett.*, 88:036801, 2002.

[33] D. K. K. Lee, S. Rapsch, and J. T. Chalker. *Phys. Rev. B*, 67:195322, 2003.

[34] C. W. Gardiner. *Handbook of stochastic methods for physics, chemistry, and the natural sciences*. Springer-Verlag, 1990.

[35] J. M. Kosterlitz and D. J. Thouless. *J. Phys. C*, 6:1181, 1973.

[36] J. M. Kosterlitz. *J. Phys. C*, 7:1046, 1974.

[37] L. Benfatto, A. Toschi, and Caprara S. *Phys. Rev. B*, 69:184510, 2004.

[38] M. Klomfass, U.M. Heller, and H. Flyvbjerg. *Nucl. Phys. B*, 360:264, 1991.

[39] M. E. Fisher, M. N. Barber, and Jasnow D. *Phys. Rev. A*, 8:1111, 1973.

[40] I. B. Spielman, J. P. Eisenstein, L. N. Pfeiffer, and K. W. West. *Phys. Rev. Lett*, 87:036803, 2001.

[41] M. Kellogg, J. P. Eisenstein, L. N. Pfeiffer, and K. W. West. *Phys. Rev. Lett*, 90:246801, 2003.

[42] M. Kellogg, J. P. Eisenstein, L. N. Pfeiffer, and K. W. West. *Phys. Rev. Lett*, 93:036801, 2004.

[43] M. M. Fogler and Wilczek F. *Phys. Rev. Lett*, 86:1833, 2001.

[44] L. Balents and Radzihovsky L. *Phys. Rev. Lett*, 86:1825, 2001.

[45] Y. N. Joglekar and A. H. MacDonald. Unpublished.

[46] M. Abolfath, L. Radzihovsky, and A.H. MacDonald. *Phys. Rev. B*, 68:155318, 2003.

[47] Y.N. Joglekar and A.H. MacDonald. *Phys. Rev. B*, 64:155315, 2001.

[48] R. Landauer. *Z. Phys. B*, 32:217, 1987.

[49] M. Büttiker. *IBM J. Res. Dev.*, 32, 1988.

[50] H.U. Baranger and A.D Stone. *Phys. Rev. B*, 40, 1989.

[51] Supriyo Datta. *Electronic Transport in Mesoscopic Systems*. Cambridge University Press, 1995.

[52] Y. Ohno and H. Sakaki. *Surf. Sci.*, 362:142, 1996.

[53] D Yoshioka and A. H. MacDonald. *Phys. Rev. B*, 53:R16168, 1996.

[54] H. Fertig. *Phys. Rev. B*, 40:1087, 1989.

[55] X. G. Wen and A. Zee. *Phys. Rev. Lett.*, 69:1811, 1992.

[56] D. J. Landau. *Physiz. Z. Sowjetunion*, 2:46, 1932.

[57] C. Zener. *Proc. Roy. Soc. Lond. A*, 137:696, 1932.

[58] Jun Hu and A. H. MacDonald. *Phys. Rev. B*, 46:12554, 1992.

[59] Y. M. Ivanchenko and L. A. Zil'berman. *JETP*, 8:113, 196.

[60] V. Ambegaokar and B. I. Halperin. *Phys. Rev. Lett.*, 22:1364, 1969.

[61] J. C. Slonczewski. *J. Magn. Mag. Mat.*, 159:L1, 1996.

[62] L. Berger. *Phys. Rev. B*, 54:9353, 1996.

[63] M. Tsoi and *et. al. Phys. Rev. Lett.*, 80:4281, 1998.

[64] M. Tsoi and *et. al. Nature*, 406:46, 2000.

[65] J. Z. Sun. *J. Magg. Man. Mat.*, 202:157, 1999.

[66] A. S. Nunez and A. H. MacDonald. *cond-mat/0403710*, 2003.

[67] C. Kittel and E. Abrahams. *Reviews of Modern Physics*, 25:233, 1953.

[68] C. Kittel and A. H. Mitchell. Ferromagnetic relaxation and gyromagnetic anomalies in metals. *Phys. Rev.*, 101:1611, 1956.

[69] M. Sparks. *Ferromagnetic Relaxation Theory*. McGraw Hill, 1964.

[70] E. A. Turov. In S V Vonsovskii, editor, *Ferromagnetic Resonance*. 1966.

[71] W. F. Brown. *Phys. Rev.*, 130:1677, 1963.

[72] D. A. Garanin. *Phys. Rev. B*, 55:3050, 1997.

[73] N. Smith. *J. Appl. Phys.*, 90:5768, 2001.

[74] J. L. García Palacios and et al. *PRB*, 58:14937, 1998.

[75] Ulrich Weiss. *Quantum Dissipative Systems*. World Scientific, 1999.

[76] A. Rebei and G.J. Parker. *Phys. Rev. B*, 67:104434, 2003.

[77] C. Kittel. *Reviews of Modern Physics*, 21:541, 1949.

[78] E. W. Lee. *Rep. Progr. Phys.*, 18:184, 1955.

[79] L. D. Landau and E. M. Lifshitz. *Theory of Elasticity.* Pergamon Press, 1986.

[80] P. Hanggi. In L. Schimansky-Geier and Th. Pöschel, editors, *Stochastic Dynamics*, volume 484 of *Lecture Notes in Physics*. Springer, 1997.

[81] R. M. Bozorth. *Ferromagnetism.* Van Nostrand, 1951.

[82] H. Chen, P. De Gasperis, and R. Marcelli. *IEEE Transactions on Magnetics*, 29:3013, 1993.

[83] M. Covington and et al. *Phys. Rev. Lett.*, 89:237202, 2002.

[84] J. Sinova, T. Jungwirth, X. Liu, Y. Sasaki, J. K. Furdyna, W. A. Atkinson, and A. H. Macdonald. *Phys. Rev. B*, 69(8), 2004.

[85] Y. Tserkovnyak, G. A. Fiete, and B. I. Halperin. *Appl. Phys. Lett.*, 84:5234, 2004.

[86] B. Heinrich, D. Fraitová, and V. Kamberský. *Phys. Stat. Sol.*, 23:501, 1967.

[87] V. Kamberský. *Can. J. Phys.*, 48:2906, 1970.

[88] L. Berger. *Journal of physics and chemistry of solids*, 38(12):1321 – 1326, 1977.

[89] S. M. Bhagat and L. L. Hirst. *Phys. Rev.*, 151:401, 1966.

[90] S. M. Bhagat and P. Lubitz. *Phys. Rev. B*, 10:179, 1974.

[91] B. Heinrich, D. J. Meredith, and J. F. Cochran. *J. Appl. Phys.*, 50:7726, 1979.

[92] J. M. Rudd, J. F. Myrtle, J. F. Cochran, and B. Heinrich. *J. Appl. Phys.*, 57:3693, 1985.

[93] V. Korenman and R. E. Prange. *Phys. Rev. B*, 6:2769, 1972.

[94] V. Korenman. *Phys. Rev. B*, 9:3147, 1974.

[95] J. Kunes and V. Kambersky. *Physical Review B*, 65(21), 2002.

[96] J. Kunes and V. Kambersky. *Phys. Rev. B*, 68(1):019901, 2003.

[97] S. Ingvarsson, L. Ritchie, X.Y. Liu, G. Xiao, J.C. Slonczewski, P.L. Trouilloud, and R.H. Koch. *Physical Review B*, 66(21), 2002.

[98] Y. Tserkovnyak, A. Brataas, and G.E.W. Bauer. *Physical Review Letters*, 88(11), 2002.

[99] E. Simanek and Heinrich B. *Phys. Rev. B*, 67:144418, 2003.

[100] E. Simanek. *Phys. Rev. B*, 68:224403, 2003.

[101] A. Rebei and M. Simionato. `cond-mat/0412510`.

[102] R. J. Goldston and P.H. Rutherford. *Introduction to plasma physics*. IOP, 1995.

[103] R. D. Hazeltine and J.D. Meiss. *Plasma confinemetn*. Addison Wesley, 1992.

[104] J. A. Wesson. *Nucl. Fus.*, 18:87, 1978.

[105] R. Carrera, J.D. Hazeltine, and M. Kotschenreuther. *Phys. Fluids*, 29:899, 1986.

[106] P. H. Rutherford. *Phys. Fluids*, 16:1903, 1973.

[107] R. B. White and et al. *Phys. Fluids*, 20:800, 1977.

[108] A. Thyagarja. *Phys. Fluids*, 24:1716, 1981.

[109] R. Fitzpatrick. *Phys. Plasmas*, 6:1168, 1999.

[110] R. Fitzpatrick and F. L. Waelbrock. *Phys. Plasmas*, 7:4983, 2000.

Vita

Enrico Rossi was born in Turin, Italy on September 2, 1972, the son of Mario Rossi and Vannamaria Crivello. After earning a joint B.A. and M.S. degree in Physics Engineering from the Polytechnic of Turin in January 1999 he began his graduate studies at the University of Texas at Austin.

Permanent Address: 3517 N. Hills Dr. Apt E204
Austin TX 78731

This dissertation was typeset with LaTeX 2_ε[1] by the author.

[1] LaTeX 2_ε is an extension of LaTeX. LaTeX is a collection of macros for TeX. TeX is a trademark of the American Mathematical Society. The macros used in formatting this dissertation were written by Dinesh Das, Department of Computer Sciences, The University of Texas at Austin, and extended by Bert Kay, James A. Bednar, and Ayman El-Khashab.